Power Quality Issues and Feasibility Study in a DC Residential Renewable Energy System

By

Miguel Angel Rodríguez Otero

A thesis submitted in partial fulfillment of the requirements for the degree of

MASTER OF SCIENCE
in
ELECTRICAL ENGINEERING

UNIVERSITY OF PUERTO RICO
MAYAGÜEZ CAMPUS
2008

Approved by:

Efraín O'Neill-Carrillo, Ph.D. President, Graduate Committee	Date
Eduardo I. Ortiz-Rivera, Ph.D. Member, Graduate Committee	Date
Miguel Vélez-Reyes, Ph.D. Member, Graduate Committee	Date
Iván Baigés, Ph.D. Representative of Graduate Studies	Date
Isidoro Couvertier, Ph.D. Chairperson of the Department	Date

ABSTRACT

This research work aims to study power quality issues and the feasibility of a DC residence. The evaluated residence is in the area of Mayaguez, PR. Feasibility studies includes the design of a hybrid power system to supply a stand-alone residence, analysis of current AC home appliances and an adaptation of appliances to be supplied by DC power, a wiring analysis and an economic analysis. Power quality issues are to be conducted in the DC bus and at the point of common coupling with the utility grid. DC ripple, transients and flicker are studied at the DC bus; power factor, displacement factor, harmonics and THD is measured at loads that incorporate BLDC motors. Feasibility results show that though lower power consumption is achieved, low power appliances are feasible; high power loads are not suitable for low voltage DC supply. Concerning the wiring analysis, there was a reduction in cable size for the air conditioning units, the removal of the cable for the water heater, and, the addition of a circuit to supply the microwave. Simulations show that the most relevant power quality issues are DC ripple and noise, one associated with another. BLDC motors, one of the DC appliances, produce DC current ripple, along with DC/DC converters, which in turn produces noise and slight degradation of the motor performance. Finally, the economic analysis results show that, although no option considered has a positive net present value, there is a significant difference in the total system costs and in the payback period when considering a DC residence, as compared to an AC residence.

RESUMEN

El siguiente trabajo de investigación se enfoca en estudiar problemas de calidad de potencia y estudiar la viabilidad para una residencia DC. La residencia a evaluar se encuentra situada en el área de Mayagüez, PR. Entre los estudios de viabilidad realizados se encuentra el diseño de un sistema renovable hibrido para una casa que opera de modo independiente a la utilidad, análisis de los enseres del hogar y como estos se pueden adaptar para poder suplir dichas cargas con potencia DC, análisis de cableado y un análisis económico. Los problemas de calidad de potencia serán estudiados en la barra de la casa DC, y en el punto de acoplamiento mutuo al interconectar la residencia con la red. Rizado, transitorios y parpadeos serán estudiados en la barra DC; el factor de potencia, factor de desplazamiento, distorsión harmónica total y un análisis harmónico será realizado en las cargas las cuales usan motores DC sin escobillas. Resultados del análisis de viabilidad muestran que aunque se logra disminuir el consumo de potencia de las cargas, las mismas son viables para aplicaciones de baja potencia; las cargas que manejan alta potencia no son recomendadas para ser suplidas con potencia DC. En términos del análisis del cableado, la diferencia reside en la disminución del cable que alimenta el aire acondicionado, la eliminación del circuito dedicado para el calentador de agua, y la adición de un circuito dedicado para el microondas. Resultados de simulación muestran que el problema más crucial de calidad de potencia lo es el rizado DC y el ruido, uno asociado con el otro. Los motores DC sin escobillas producen rizado en la corriente DC, al igual que los convertidores DC/DC, los cuales producen rizado y ruido. Esto produce degradación del desempeño del motor.

Finalmente, el resultado del análisis económico demuestra que, aunque no se obtuvo un valor presente positivo para ninguna de las opciones evaluadas, hay una diferencia significativa en el costo total del sistema y en el tiempo de recobro al considerarse una residencia DC, en comparación con una residencia AC.

.

To the glory of God and all Light Beings

And to my mother, the engineer specialized in life, and the mastermind behind all my achievements. My success is thanks to you…

ACKNOWLEDGEMENTS

First of all, I want to thank God and the Angels for letting me live up to this day and time. You are the only ones who know what I have been through; I deeply thank you for your assistance at all moments. Without you, this thesis would not have been possible.

I want to start expressing a sincere acknowledgement to my advisor, Dr. Efrain O'Neill-Carrillo, for believing in me and giving me the opportunity to continue graduate studies at UPRM. He has transcended the limits of the student-professor relationship in order to become a humanitarian person; I truly consider him a friend. I express my sincere thanks to him for letting me conduct research under his supervision and guidance.

I would like to thank Dr. Miguel Velez-Reyes and Dr. Eduardo Ortiz-Rivera for serving as members of my graduate committee.

I would like to thank my mother, for always encouraging me to keep achieving my dreams; all my achievements are thanks to your unconditional support and love.

A million thanks to Mrs. Maribel Feliciano and Mrs. Sandra Montalvo, for having so much patience with me and for all their professionalism and guidance during my graduate term.

This research work was primarily supported by the NSF ERC program under grant EEC-9731677.

TABLE OF CONTENTS

TABLE LIST

Tables **Page**

FIGURE LIST

Figures **Page**

1 INTRODUCTION

1.1 Motivation

Environmental concerns pose strong requirements on electricity production, which is responsible for a major portion of carbon dioxide (CO_2) and other harmful emissions. By increasing the use of renewable energy sources to produce electricity, emissions can be reduced. Inefficient use of electricity, e.g., power losses, also contributes to emissions: for one kWh utilized, more than one kWh has to be produced, with consequent release of CO_2 if the energy comes from fossil fuels [1].

DC systems are already implemented on various applications such as electric ships, telecommunications, and transmission and distribution systems. DC systems are considered in electric ships in order to eliminate problems in the AC grid, including harmonics, phase synchronization, frequency control, oscillations and waveform distortion, among others [2]; in distribution systems, High Voltage Direct Current (HVDC) is utilized due to the reduction of losses as a result of the absence of reactive power [3].

In some works, AC appliances have been powered with DC sources as a way to reduce electricity consumption and reducing harmful emissions. Most appliances are able to work internally with DC power; they contain an input transformer and a rectifier to obtain the proper dc operating voltage. When the appliance is in stand-by mode, the transformer absorbs a small open-circuit current that creates stand-by losses. The total domestic power consumption of consumer electronic equipment in stand-by mode in the United States has been estimated to around 36 TWh/year and it is predicted to increase to 62 TWh/year in 2010

[1]. Available work on DC residences performed very simple analysis concerning the modeling of powering current home appliances with DC power. Other work in the area did not perform detailed analysis to determine which stages can be removed, altered, or replaced due to the shift from the AC input to the DC input. Thus, models for DC home loads do not exist in order to conduct power quality/reliability studies for a DC residence.

DC distribution systems are being considered in this thesis for residential applications, since most home appliances internally work with DC power. A DC powered residence will eliminate the transformer/rectifier stages, completely eliminating standby losses. Reported advantages of a DC residence also include improved efficiency, reduction of EMI, and reduced losses due to the absence of reactive power.

Due to the penetration of Renewable Energy Systems (RES) into the utility grid, various states in US, including Puerto Rico, agreed to pay a fixed rate to any RES users who inject power into the utility grid [4]. This rate was usually the avoided cost rate, lower than what the same companies charge consumers for each KWh. Nevertheless, net metering measures have been approved in which the purchase rate of injected power equals the rate at which the consumed power is charged. This makes RES even more attractive to users, since both the present value of the system and the recovery time will decrease. The interconnection of a DC residence to the utility grid will also be considered in this thesis.

1.2 Objectives:

The objectives of this research work are presented below:

- Implement dynamic models that represent the behavior of PV and wind systems under real environmental conditions.
- Simulation of converters / inverters to ensure proper operation of the renewable energy sources.
- Simulate techniques to control the renewable sources to work in a desired operation point (range).
- Analysis and modeling of DC home appliances.
- Conduct a feasibility study on a DC residence with the models of DC home appliances.
- Conduct power quality studies on the DC side (DC bus) and on the utility grid, after the residential system is connected.

1.3 Contributions

Though a feasibility analysis for a DC distribution systems has been conducted in [3], DC home appliance modeling and sustainability has been presented in [5], no work presents either electrical models that adapt current AC appliances for a DC residence, nor an integrated study where electrical issues are combined with feasibility studies. The models developed in [5] are developed by applying a DC voltage to a series of household appliances, which in turn produces linear models for various loads. Though these models accurately predict the transient and steady state behavior of the loads under study, the work does not addresses the analysis of appliances, neither recent advances in power electronics are taken

into account to develop more efficient models of DC home appliances. Moreover, in order to use these models, experimental data taken from measurements must be available, which is difficult to obtain. A similar research as the one done in [5] is being done at the Center for Power Electronics Systems (CPES); but a two-bus configuration is proposed, in where low-power loads are fed from 48V, and high-powered loads are to be fed from a 325V bus.
Also, the studies available focus on the viability of shifting from AC to DC, but no study addresses the electrical issues of shifting appliances from AC power to DC power, in terms of power quality/system reliability.

In order to support current and future work research in CPES on dc-based power systems for residences, a proper analysis of how to integrate current AC home appliances into a DC residence will be presented in this thesis. The contribution of this work is to provide a comprehensive analysis of a DC residence; the principles of operation of the most used appliances will be studied, and based on this, models powered up by DC will be proposed. The comprehensive analysis will take into account the detailed models of both renewable energy systems (RES) and DC loads. Power quality issues will be studied for two scenarios: the first considers the residence as a standalone system (meaning that the grid is not available), and PQ will be studied at the DC bus; the second scenario includes the interconnection of the stand alone residence to the utility grid, in order to study PQ at the Point of Common Coupling (PCC).

Also, a feasibility study will be conducted covering major areas such as a hybrid system sizing, a wiring analysis, and an economic analysis. Furthermore, net metering will be considered since the approval of law #114 that allows RES users to qualify for net metering

in Puerto Rico; but the power flow considered will be exclusively from the RES residence into the grid (any excess power produced will be injected to the grid).

This work will support future research efforts in CPES on dc-based power systems for residences.

1.4 Outline of Thesis

The necessary theoretical background is presented in Chapter 2. Chapter 3 presents the mathematical models for the different systems considered. Chapter 4 presents the results of the different cases evaluated along with proper system sizing, wiring analysis and an economical analysis. Chapter 5 present the conclusions along with future work.

2 THEORETICAL BACKGROUND

This chapter reviews literature concerning the modeling of Renewable Energy Systems (RES), including Photovoltaic (PV) systems and Wind Energy Conversion Systems (WECS). The presented reviews cover different DC/DC converters and their applications (section 2.1), the renewable energies to be used in this research along with the proper control techniques (section 2.2 – section 2.4), storage elements (section 2.5), different RES configurations (section 2.6), interconnection to the utility grid (section 2.7), a review on current home appliances (section 2.8), a comparison between the differences between AC and DC residences (section 2.9), operation principles, modeling and control of Brushless DC (BLDC) motors (section 2.10), DC distribution system literature (section 2.11), power quality indexes (section 2.12), and electromagnetic interference (EMI) (section 2.13).

2.1 DC/DC Converters

DC/DC converters are used to provide a regulated output from an unregulated input. Depending on the topology, converters can be used to increase, decrease and/or reverse the voltage polarity at the output. A transformer is used when galvanic isolation is needed between the source and the load. For higher power applications (500W or more), basic circuit configurations can be modified to incorporate the half-bridge (two power switches) or full-bridge (4 power switches) configurations [6].

The most popular topologies are the boost converter, which provides an output voltage that will always be higher than the input voltage; the buck converter, which is the opposite of the boost topology, providing lower output voltages; and the buck-boost converter, which is a

combination of the buck and boost topologies. Each topology can be modified with the half-bridge or full-bridge configurations. The flyback converter topology is the same as the buck-boost converter, but an isolation transformer is included; as a result, flyback converters are very popular for low-power applications such as laptop computers and LCD TV's.

2.2 Distributed Power Systems (DPS)

2.2.1 Power System Architectures

The evolution of power architectures began with the centralized architecture. This type of architecture concentrates all the power processing technology into a single stage from the front end through the conversion stages [69]. It converts the line voltage to the number of DC voltages needed in the system and buses each voltage to the appropriate load. It is a very cost-effective architecture, since it does not consumes precious board real estate at the point of load with the power conversion function [70].

Centralized power works well in many respects, but the most obvious problem is how to distribute high power with low output voltages. This system often fails to provide adequate performance for new generations of electronic equipment.

In comparison, the modular architecture features multiple power conversion stages, usually located far away from the loads. Voltages and currents can be combined to meet high power demand from loads [69].

2.2.2 Distributed Energy Resources (DER)

Distributed power systems are becoming increasingly popular due to the architecture's many advantages, including the ability to provide a better point of load voltage regulation,

increased power density, reduced harmonics and EMI and reliability and suitability for modular system design [69]. Distributed energy resources differ from centralized energy resources in several aspects: Distributed energy resources are small, modular, and come in sizes that range in capacity from kilowatts to megawatts. They comprise various technologies that can be located on-site or nearby the location where the energy is used, including PV systems, fuel cells, wind turbines and energy storage systems, among others. This provides the opportunity for greater local control and more efficient waste heat utilization to boost efficiency and lower emissions associated with environmental issues [69-70].

Though distributed power architectures are complex and specialized, most are derived from five main basic configurations, presented below:

1. Paralleling- A single high power supply is replaced with a group of paralleled lower power modules, trying to increase system reliability.
2. Cascading - An intermediate bus voltage is developed with each interconnection. This architecture is employed, for example, in appliances using electric drives in order to provide power factor correction and reduced power quality issues to the utility.
3. Stacking – Allows combining of the outputs of several converters to obtain different levels of voltage/current.
4. Source Splitting – Allows the use of separate power sources to supply a common load for applications such as battery backup, feeding separate phases or multiple buses
5. Load splitting – Separate load converters are used to supply different loads for distributed power, regulation.

2.3 Photovoltaic Modules (PVM's)

PV is best known as a method for generating solar power by using solar cells packaged in photovoltaic modules, often electrically connected in multiples as solar photovoltaic arrays to convert energy from the sun into electricity [7]. Commercial efficiencies for PV modules range between 15 % and 18 %. Depending on the material built, PV modules can be more or less efficient. Reducing efficiency means increasing the number of solar modules in order to supply a fixed load demand. Maximum Power Point Tracking (MPPT) algorithms have been developed in order to increase module efficiency and decrease the overall system cost.

Depending on the load demand and the battery bank voltage, arrays may be formed in order to properly match the system voltage and provide the load demand. PV modules connected in series provide a higher voltage, and connecting the modules in parallel provides higher currents.

2.3.1 *PV System*

The PV system is composed of the PV network and a regulator (DC/DC converter). The DC/DC converter is used in order to perform different functions: it regulates the PV output, provides isolation between the sources and loads, and properly matches the system voltages. Figure 1 shows the proper PV system configuration:

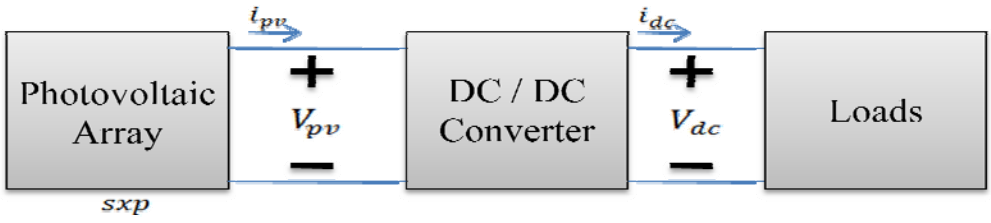

Figure 1. PV system.

Where “s” is the PV modules connected in series, and “p” is the number of PV modules connected in parallel.

2.4 Maximum Power Point Tracking (MPPT) for PV systems

For PV systems, there exists a characteristic curve, the I-V curve that depends on the value of solar irradiation and temperature. This means that, there exists an I-V curve for each value of solar irradiation and temperature. In order to maximize the PVM efficiency, the operating point must be shifted to the optimal values of both voltage and current in order to produce the maximum power. The maximum power is calculated by multiplying the optimal current I_{op} by the optimal voltage, V_{op}. Figure 2 clearly illustrates this concept.

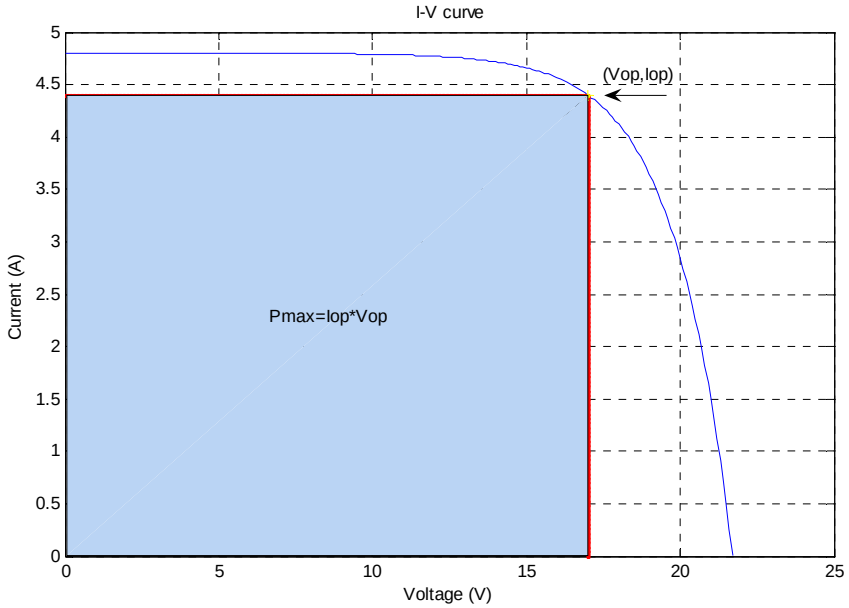

Figure 2. I-V curve for a PV panel showing the optimal operating point

This point though is a maximum, will vary depending on the solar irradiation and temperature values. If the irradiation or temperature values decrease, the maximum power will decrease. If the values of solar irradiation and/or temperature increase, then the

maximum power will increase. The MPPT control effectively finds this operating point, in order to extract the maximum power at any time.

There are various techniques available to obtain the maximum power from a PV array: the Perturb and Observe (P&O) and the Incremental Conductance (IC) methods are two of the most commonly used methods to extract the maximum power of a PV array. The P&O method involves a perturbation in the duty cycle of the dc/dc converter, which perturbs the operating point of the PV array(voltage and current).The power is measured, and, if the actual power increases, the perturbation should be kept constant; if there is a decrease in power, then the perturbation must be decreased. The process is repeated periodically until the MPP is reached. After finding the MPP, the system oscillates around that point. This is clearly a disadvantage of this method; though the oscillations can be reduced by reducing the perturbation size, but the control becomes slow [8].

The IC method is based on the knowledge that the slope of the PV array power curve is zero at the MPP, positive on the left of the MPP, and negative on the right. The P-V curve for a single PVM is presented below in order to clarify this concept in figure 3 [8]:

$$\begin{cases} \dfrac{dP}{dV} = 0 \; at \; MPP \\ \dfrac{dP}{dV} > 0 \; Left \; MPP \\ \dfrac{dP}{dV} < 0 \; Right \; MPP \end{cases} \tag{2.3-1}$$

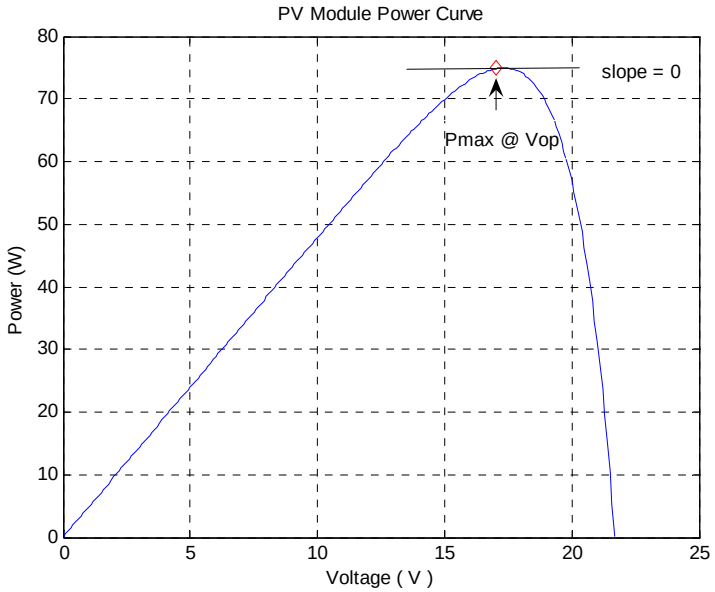

Figure 3. Power curve showing the slope on the maximum point.

Considering that

$$\frac{dP}{dV} = \frac{d(IV)}{dV} = I + V\frac{dI}{dV} \cong I + V\frac{\Delta I}{\Delta V} \tag{2.3-2}$$

The IC of a solar array can be controlled in order to operate the system in this point. That is,

$$\begin{cases} \dfrac{\Delta I}{\Delta V} = -\dfrac{I}{V} \; at\ MPP \\ \dfrac{\Delta I}{\Delta V} > -\dfrac{I}{V} \; Left\ MPP \\ \dfrac{\Delta I}{\Delta V} < -\dfrac{I}{V} \; Right\ MPP \end{cases} \tag{2.3-3}$$

Equation 2.3-3 means that the Maximum Power Point (MPP) can be tracked by comparing the instantaneous conductance to the incremental conductance. Once the MPP is reached, the operation of the PV array is maintained at this point, unless a change in ΔI is noted, indicating a change in atmospheric conditions at the MPP. The algorithm decrements or increments the reference voltage, V_{ref} to track the new MPP. The increment size

determines how fast the MPP is tracked. Fast tracking can be achieved with bigger increments, but the system might not operate exactly at the MPP, but instead it will oscillate about it.

A less obvious, but effective way of performing the IC method is to create an error signal, consisting of the sum of the instantaneous and the incremental conductance. Since it is known that, at the MPP, the slope of the power curve must be zero, then a simple PI controller can be used to drive e, the error signal, to zero [8].

Compared to the P&O or the IC methods, a much simpler MPPT control technique for both PV and Wind systems is presented in [9-10]. For the PV system, a linear relationship is suggested between the maximum voltage and the open circuit voltage, as well as for the short circuit current and the maximum current.

2.5 Wind Energy Conversion Systems (WECS)

The purpose of WECS is to extract the power from the wind and convert it to electric power. Wind turbines can be separated into two types, based on the axis in which the turbine rotates. They are classified into the horizontal axis type and the vertical axis type.

Wind Turbine can be operated at fixed speeds or variable speed operation. Fixed speed wind turbines can produce 8% to 15% less energy output as compared to their variable speed counterparts. However, variable speed wind turbines allow control techniques to extract the maximum power from the wind turbine by maximizing the power coefficient, while reducing mechanical fatigue and power fluctuations at the utility grid [11].

2.5.1 *WECS System*

The principal elements of typical WECS are the wind turbine, an electrical generator, which is typically an induction motor or a permanent magnet synchronous generators (PMSG), a rectifier (three-phase or single-phase, depending on the output of the generator) and a DC/DC converter to regulate the DC output and to match the system voltage with the voltage at the battery bank, as shown in Figure 4.

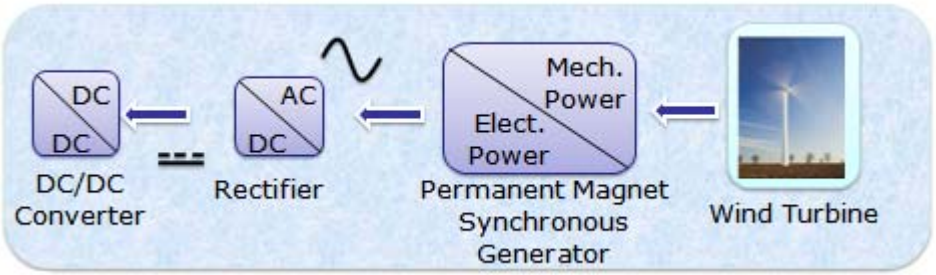

Figure 4. WECS system components.

2.6 Sliding Mode Control (SMC)

Sliding Mode involves a discontinuous control action, whose primary function is to switch between two distinctively different system structures (or components) such that a new type of system motion, called sliding mode, exists in a manifold [12]. First, a control law that constrains the motion of the system to the manifold (surface) is defined; then, in the reaching phase, trajectories that start away of the manifold start moving towards it; finally, in the sliding phase, after the system reaches the manifold in a finite time, the motion is confined to the manifold.

Advantages of this control scheme include excellent system performance, while at the same time the system becomes insensible to parameter variations, and rejects disturbances

completely [13]. A disadvantage of this control is that it suffers from chattering, or oscillations around the sliding manifold. Switching non-idealities, which are usually neglected, are the main cause. [12] Chattering produces low control accuracy, high heat losses in electrical circuits, and might excite unmodeled high frequency dynamics, which degrades the performance of the system and may lead to system instability [13].

2.6.1 *SMC in WECS*

Valenciaga presents in [14] a SMC technique focused on the wind energy conversion system (WECS), in order to supply continuous power to the loads. The SMC is designed to operate in two regions: power regulation (when the climate conditions suffice) and maximum power point tracking (when the climate conditions are not enough to provide the demanded power by the loads).

A SMC for a renewable system where PV and wind systems are combined is presented in [15]. The objective here is to design a supervisor control is in order for the system to operate in three operating modes; the system will shift between operation modes depending on the load power demand.

2.7 Batteries

A battery is an electrochemical device that converts chemical energy into electricity, by means of a galvanic cell. Batteries, in a RES, provide a way of energy storage for later use. Also, batteries are able to supply loads such as motors and pumps intermittently, due to the fact that they are capable of discharging rapidly to yield more current than the charging sources (PV or Wind Turbine).

Deep cycle batteries are the most recommended to use with a RES and for marine applications, due to the ability to deliver low currents for longer periods of time. The most commonly-used batteries for RES are the Valve Regulated Lead Acid (VRLA) Batteries.

When using lead-acid batteries for RES, the system is designed in a way that the battery bank will never discharge more than 20-40% (maintaining a state of charge of 80-60%) in order to preserve battery life. A single battery will have a useful life of 5 years, depending on various factors, such as storage temperature and rate of charge and/or discharge, among others. Completely discharging a battery can reduce its effective life or damage it.

2.8 Renewable Energy Systems (RES) Configurations

RES can be classified in various categories, depending on their configuration and accessibility to the utility grid.

- ***Stand Alone:*** The utility grid is not available, or connection to the grid is not possible or needed. The system must be able to supply the total power demand, comprised of the power demand plus the battery charging requirements. Users who do not have access to, or are completely independent from the utility grid usually choose this configuration.
- ***Grid Interconnected.*** This configuration allows users to keep the utility grid as a second back-up source for the power demand. When the RES is unable to supply the present power demand, the utility grid works as a back-up source, supplying the whole or part of the power demand (comprised of the load and battery charging requirements). An advantage of this configuration in residential applications is the

possibility to inject any excess power produced by the RES into the utility grid, alleviating electricity costs and lowering the present cost of the whole system.

2.9 Interconnection

2.9.1 *Connecting to the utility grid*

In order to connect to the utility grid, with present RES configurations, a DC/AC inverter is needed, since current residential loads are fed by AC power. The inverter must comply with IEEE standards of harmonic distortion, power factor and electromagnetic interference [16-17]. Though some inverters are configured for unidirectional power flow (from the grid to the loads), modern inverters must allow bidirectional power flow, due to the fact that users can inject any excess power generated by RES into the grid.

2.9.2 *Net Metering*

Net Metering allows owners of renewable energy technologies, whom are connected to the utility grid, the injection of any excess power produced by the RES t back to the utility. This proves to be an essential incentive to motivate more people to invest in RES, due to the fact that the price per KWh of generated power will equal the price at which the utility sells power to their users [4]. Canada, Japan, Germany and more than 40 states from the United States of America are already offering Net Metering to customers with RES. Furthermore, law # 114, approved in 2007 in Puerto Rico, which demands that the electric power authority must establish a Net Metering program [4].

In order for residential users to qualify for this service, the system overall capacity must not exceed 20 KVA. Furthermore, the interconnected system must not generate any stability or power quality problems at the PCC.

2.10 Operating Characteristics of Home Appliances

2.10.1 *Appliances with Motors*

Many different types of motors are used in most home appliances. Mixers, vacuum cleaners, automatic gates, garage doors, dishwashers, ventilation fans, cloth washers and cloth dryers, among other appliances, are examples of loads that incorporate the use of a single phase AC motor. Motors produced for home applications vary up to 1hp, and their efficiency is often very low, often less than 50% [18]. The most commonly used single-phase motor for those appliances is the universal motor, because of the high speeds and capability of operating with AC and DC voltages. Cloth washers, cloth dryers, and old refrigerators usually incorporate a single phase induction motor, between capacitor start and capacitor run motors [3].

2.10.2 *TV's*

With the implementation of digital television, Liquid Crystal Display (LCD) and Plasma TV's are rapidly replacing televisions which employ Cathode Ray Tubes (CRTs) [19]. While plasmas are mostly being manufactured now, they demand more power than LCDs. Furthermore, aside from the fact that Plasma TV's are heavy, their operating life is nearly 5 years, which is half compared to the present CTR, which is 10 years [19].

LCD's exhibit a long operating life, because its operation depends on the backlight, which gradually deteriorates and the user does not notice until the degradation is extreme [19]. The backlight, commonly a cold cathode fluorescent lamp (CCFL), is used in LCD TV's, laptop computers and cellular phones because of their small size, high efficiency, and long operating life [20].

Current LCD power supplies are composed of the regular transformer/rectifier stage followed by a Power Factor Correction (PFC) stage, which is typically a boost DC/DC converter working in discontinuous conduction mode (DCM). The DC bus voltage after both stages above mentioned is around 380-400V; this voltage needs to be lowered further in order to operate the inverter needed for the CCFL, which is from 8-20V. Since the CCFL needs a sinusoidal voltage, a transformer must be used to provide the high voltage level. Also, a standby voltage of 5V must be derived from the bus. A flyback DC/DC converter is used to lower the voltages to the desired levels. The actual LCD TV power supply AC configuration schematic is shown in figure 5 [21-22]:

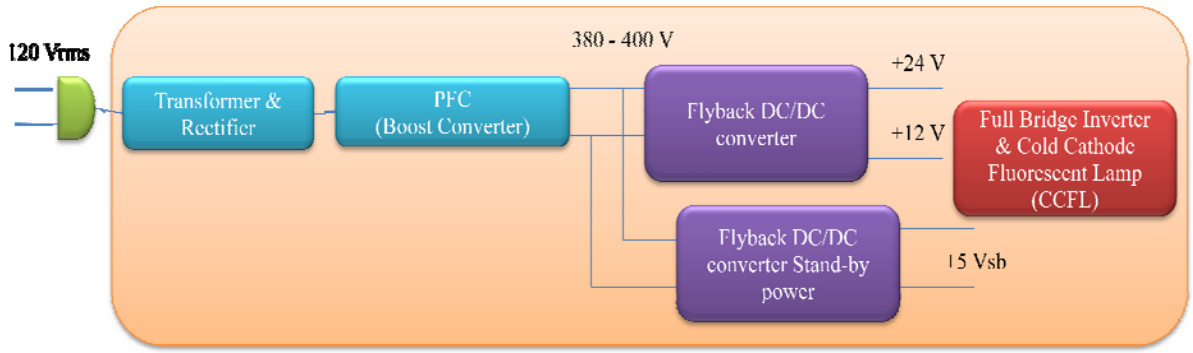

Figure 5. LCD TV schematic diagram.

2.10.3 *Laptop Computers*

Laptop computers are expected to oversell desktop computers in the near future [23], due to their low power consumption and portability. Laptop computers use microprocessors, which have greatly improved their performance, but at the same time, their current consumption has also increased. Mobile Pentium microprocessors can consume around 50-60A due to the high clock frequency [23].

The current power management architecture for a laptop computer is shown in figure 6. An internal switch inside the laptop computer controls the flow of power to the internal circuitry. The switch allows the mains to supply the power (when available), or the batteries to supply power (when the mains is unavailable). Normally, the bus voltage of the distribution system varies between 19.5V when the wall adaptor is connected and 14.8V when the laptop is running with battery power. The bus voltage range will be from 10.8V to 16.8V, depending on the configuration and number of cells in the battery [23, 25]. Voltage Regulators (DC/DC converters) are connected to the distribution bus to supply different voltages for different loads inside the computer, including the microprocessor. The main voltages to be supplied are 5V, 3.3V, and 1.5V / 60A (CPU).

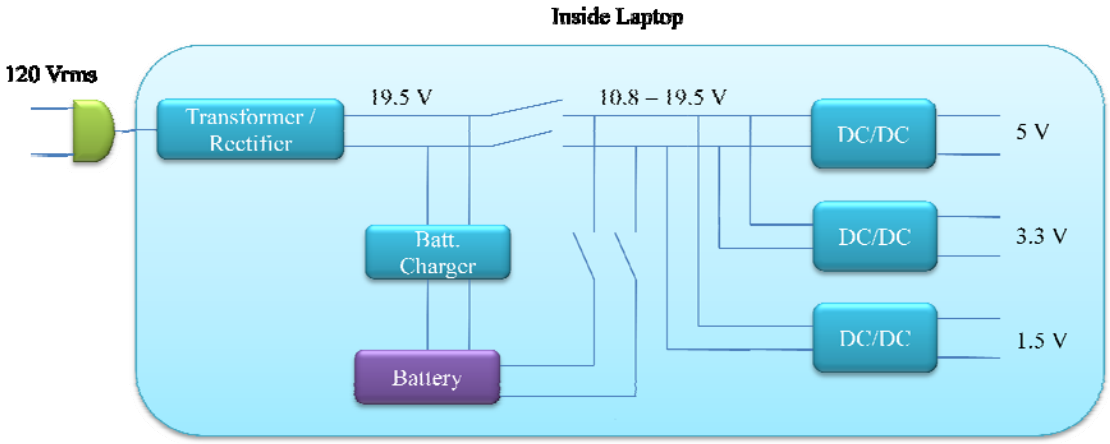

Figure 6. Conventional laptop power management architecture [24]

2.10.4 *Microwave Oven*

All microwaves have two power supplies and two independent circuits. The low voltage section is composed of the printed circuit board, and the high voltage section is composed of the magnetron, or the component responsible for generating the microwave energy to cook the food. The high-voltage components accomplish this by stepping up the AC line voltage to high voltage, which is then changed to an even higher DC voltage. This DC power is then converted to the radio frequency energy that cooks the food [26]. (Last phrase used with permission from the author [26]).

In the low voltage section, the solid state circuitry controls the cycling of the magnetron tube, and is in charge of the microwave clock, the touch pad and its many options. Since the printed circuit controls the power sent to the magnetron, a relay interconnects the low voltage section with the high voltage section. Otherwise, both parts are independent. In the high voltage section, a fuse and a high voltage transformer elevates the voltage up to the thousand volts in order to operate the magnetron tube.

As soon as the microwave is started, a fan automatically starts operating in order to cool down the magnetron. Beneath the food on many units is a second stirring device. Two small motors operate both the fan and a spindle that turns the food dish [27]. A simplified schematic diagram showing the high voltage section is shown in figure 7 below:

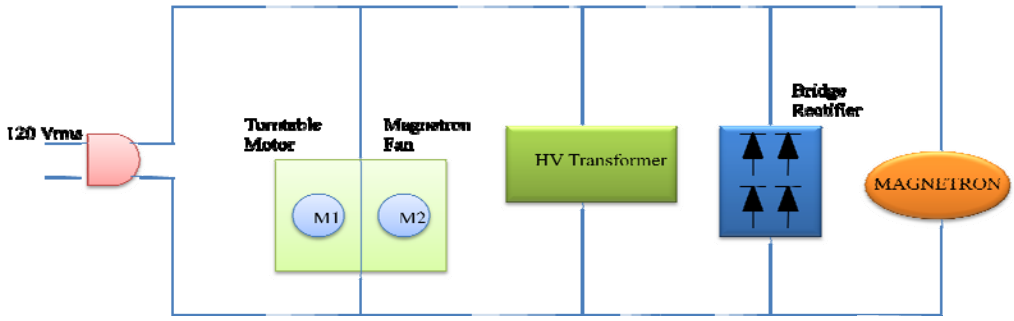

Figure 7. Microwave AC Schematic.

2.11 AC vs. DC Home Appliances

Most of today's household appliances are capable of working with DC power [1, 18]. In order to properly operate appliances in today's residences, a conversion stage (composed of a transformer/rectifier) is used to provide the correct DC voltage. Appliances with transformers are responsible for stand-by losses, due to the absorption of small currents in stand-by mode. Furthermore, rectifiers are responsible for generating EMI [28].

In order to solve these issues, a DC/DC converter is included in recent appliances; it is included after the rectifier/transformer stage. The duty cycle of the converter can be controlled to obtain unity power factor at the mains, while at the same time reducing system harmonics [28]. However, introducing this stage further decreases efficiency, and increases overall costs due to the added components for the converter and for compliance with EMI standards.

The concept of a DC residence will address all the issues above mentioned. The conversion stage can be removed, increasing efficiency and decreasing the number of components needed for each appliance. Furthermore, the absence of reactive power lowers the current needed to transfer the same amount of power [19]. Though some appliances might need a DC/DC converter to properly adjust the DC voltage needed for the appliance, harmonics and power factor issues are eliminated. Furthermore, with advances in power electronics technology, motor driver devices are being considered to replace actual motors in home appliances. Now, the use of three-phase induction and synchronous motors in DC applications is becoming attractive, due to the fact that such motors exhibit greater efficiencies and higher power densities than the actual motors used for appliances. Brushless DC motors, which are Permanent Magnet Synchronous Motors (PMSM), are being considered because of the high power density, high torque and efficiency.

2.12 Brushless DC Motors (BLDC motors)

As stated in section 2.9, BLDC motors are rapidly replacing single phase motors and motors with brushes, due to the advances in power electronics technology. BLDC motors are composed of a PMSM, coupled to a drive. The drive, composed of a DC to three-phase inverter, allows the motor to be fed by a DC voltage [29, 31]. Three phase motors are the most popular and widely used, but configurations of single-phase and 2-phase are available.

BLDC motors are electronically commutated; to rotate the BLDC motor, rotor position information is needed in order to energize the stator windings in a sequence. This information is obtained through Hall Effect sensors or encoders, which are embedded into the

stator. Whenever the rotor magnetic poles pass near the Hall sensors, they give a high or low signal, indicating the N or S pole is passing near the sensors. Based on the combination of these three Hall sensor signals, the exact sequence of commutation can be determined.

There are two types of stator windings variants: trapezoidal and sinusoidal motors. The trapezoidal motor produces trapezoidal back electromotive forces (EMF) and phase currents, while the sinusoidal motor's back EMF and phase currents are sinusoidal. As a result, the torque output from a sinusoidal contains less ripple than that the trapezoidal motor torque. For motors with sinusoidal excitations, encoders and resolvers can be used as position detectors, but such are too expensive for home applications as well as making the system bulky. As a result, sensorless estimation of rotor position is suggested for BLDC motors in home appliances [32].

Advantages of Brushless DC Motors:

- Less maintenance, due to absence of brushes.
- Longer life.
- Operation at all speeds with rated load.
- High efficiency (no voltage drop across brushes)
- High output power
- Reduced Frame size due to superior thermal characteristics.
- Low rotor inertia / improved dynamic response.
- Higher speed Range
- Low generation of electrical noise.

Disadvantages of BLDC motors:

- Complex and expensive control
- Permanent magnets increase building costs
- Control is always required to keep the motor running.

BLDC motors have excellent performance in applications that have frequent starts and stops and frequent reversals of rotation when the motor is loaded. Reversals and changes in rotation demands more torque than the rated torque. This requirement comes for a brief period, especially when the motor starts from a standstill and during acceleration. During this period, extra torque is required to overcome the inertia of the load and the rotor itself.

2.12.1 *Sinusoidal Pulse Width Modulation (SPWM)*

SPWM, as the name implies, uses a sinusoidal signal to produce the PWM signal. The sinusoidal wave is compared with the carrier wave to produce a square wave, which will be used to drive the MOSFET gates of the inverter. As a result, the output voltage of the inverter will still be a square wave, but the wave will be shaped very similar to a sinusoidal wave. This reduces total harmonic distortion (THD) while increasing the Displacement Factor (improving power factor). Figure 8 below shows the principle of SPWM, where a set of three phase balanced sine waves are compared to a triangular carrier waveform.

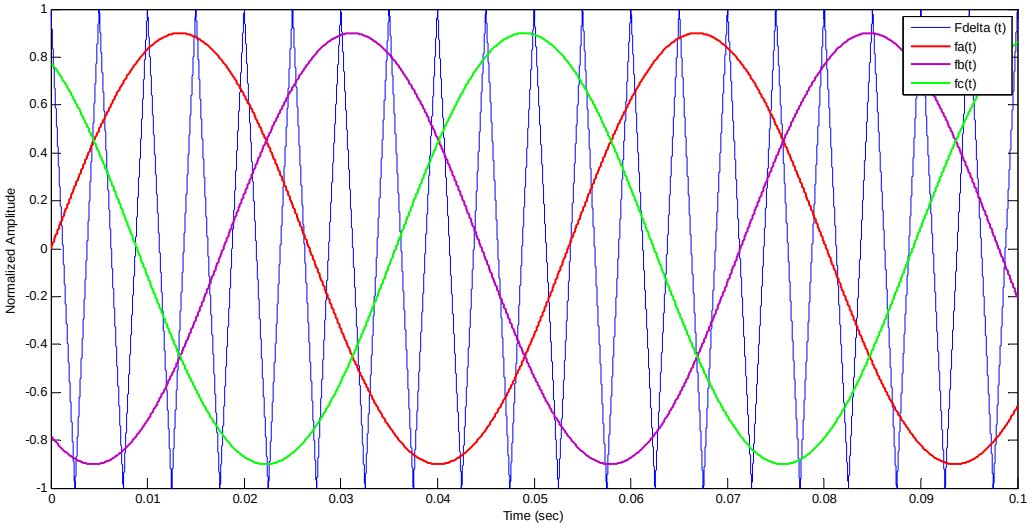

Figure 8. Principle of Operation of SPWM.

2.13 Feasibility Analysis

One of the same contributions of this research is to develop a feasibility analysis for a DC Residential Distribution system. Various studies shall be conducted, in order to find out if the viability of the DC residence:

1. Load estimation – An estimation based on the load profile in a residence is necessary to develop the correct RES configuration to supply all load demand.
2. RES sizing – This study will provide the configuration of a RES system based on load profile in order to supply all load demand.
3. DC Loads Modeling – An analysis that will determine if actual home appliances are suitable to be powered up with DC power.
4. Wiring Analysis – Based on the modeling of appliances supplied with DC power, a wiring analysis must be done in order to see and compare the

advantages/disadvantages with an actual residence supplied by AC power. This analysis involves the calculation of wire impedances, for which a residence configuration is needed.

5. Economic Analysis – An Economic analysis will demonstrate the feasibility of the DC residence, compared to an actual one. The Present Value and recovery time will be determined.

Figure 9 below shows the residence configuration to be considered in this analysis is presented. The information for the residence configuration was provided by Dr. Agustin Irizarry, professor of the University of Puerto Rico, Mayaguez Campus [33]. Results for steps 1, 2 and 4 will be presented in Chapter 3. For more information about load estimation and RES sizing, refer to sections 4.1.1 and appendix D.

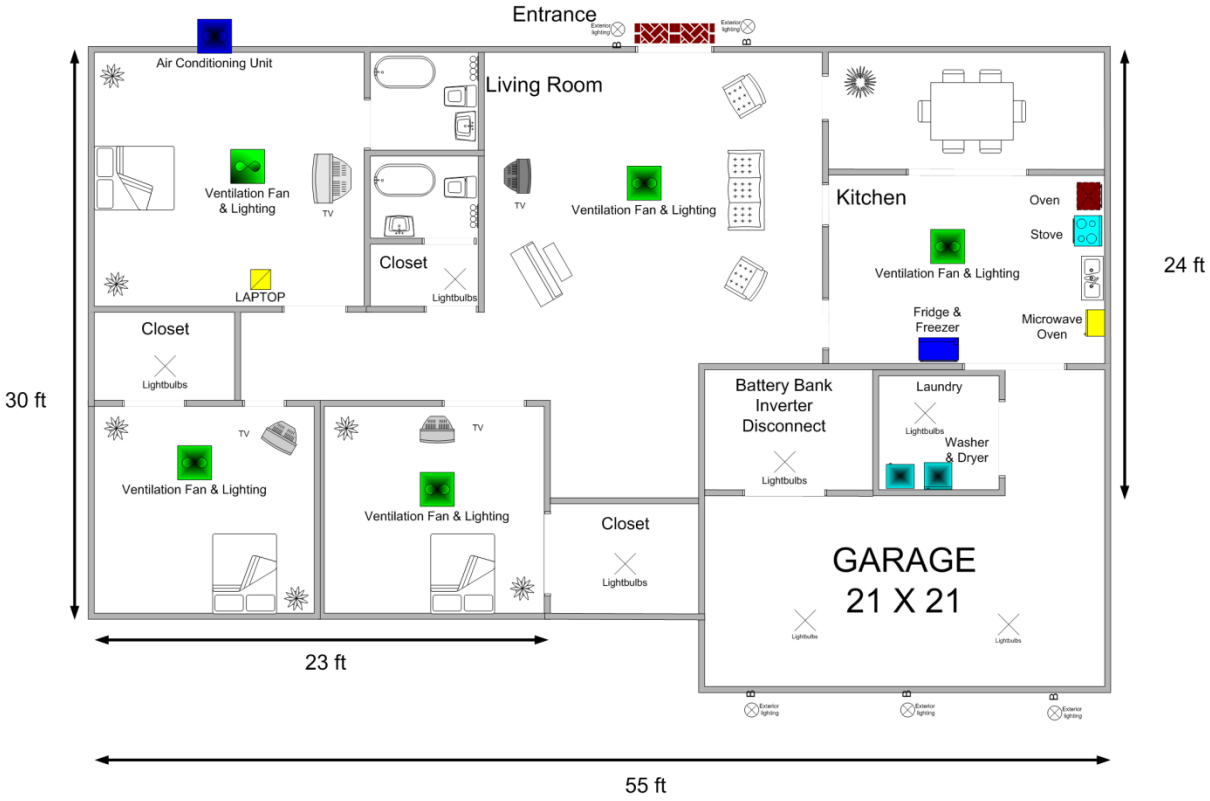

Figure 9. DC Residence Configuration to be considered [33]

2.14 Power Quality

Recently, the penetration of nonlinear loads and power electronic devices into the utility grid is becoming a major source degradation of electric power quality due to:

- Transients – undesirable momentary deviation from the supply voltage or load current.
- Interruptions – Reductions in the supply voltage or load current for not longer than one minute.

- Harmonics – periodic sinusoidal distortions of the supply voltage and/or current due to a non-linear load. Waveforms contain periodic distortions of a sinusoidal nature, and are usually integer multiples of the fundamental supply frequency.
- Sags – Reduction of the waveform RMS magnitude; the event lasts for more than half a cycle, and up to one minute.
- Swells - Increase in the waveform RMS magnitude; the event lasts for more than half a cycle, and up to one minute.
- Flicker – Small voltage variations on electrical lighting equipment. Usually in the frequency of 1-30 Hz.

Such disturbances distort the power system waveforms, producing further problems with customers and highly-sensitive loads.

When interconnected to the utility grid, high penetration of inverters at the PCC can generate higher than expected distortion levels, due to the fact that each inverter generates small amounts of 11th, 13th, 23rd, and 25th harmonic currents. When these currents are combined with background voltage distortion, higher than expected total distortion on the feeders results [34]. A high penetration of wind turbines in the utility grid may produce unwanted variations at the PCC and possible light flicker [35].

BLDC motors, compared to Switched Reluctance Motors (SRM), exhibit less active power consumption and less THD when studied at no load and partial load conditions; power factor and reactive power consumption increases with partial loading for the BLDC motor [36].

2.14.1 Interconnection Issues

When interconnecting the RES system to the utility grid, the following IEEE standards (and power quality indexes) must be met:

- IEEE 519 – Establishes flicker and voltage variation limits when synchronizing the user inverter with the utility grid. Also limits the voltage and current THD to 5% of the voltage value at the fundamental frequency [16].
- IEEE 1547 – Acceptable limits for current THD, power factor, frequency and voltage range for a grid interconnected PV system are established. The standard applies to the point of common coupling between the loads and the utility grid. Establishes the specifications and technical requirements for interconnection and system testing [17].

2.15 Electromagnetic Interference (EMI)

The recent advance in semiconductor devices and large scale integration has dramatically reduced the size of electronic equipment while increasing the probability for electromagnetic interference between the different systems and subsystems. The Federal Communications Commission (FCC) is in charge of regulating the use of radio communications and controlling EMI in the United States. The International Special Committee on Radio Interference (CISPR) regulates the international community. Though the CISPR is no regulator authority, their standards have been adopted by most European nations [37]. Figure 10 below shows the noise limits for the FCC and the CISPR. Class B is the most relevant limit in this work, since it addresses residential environments electronic equipment. Conducted emissions are typically studied at a frequency range between 0.15 and 30MHz,

and involve noise between the power lines and ground (Common-Mode, CM) or between power conductors (Differential-Mode, DM).

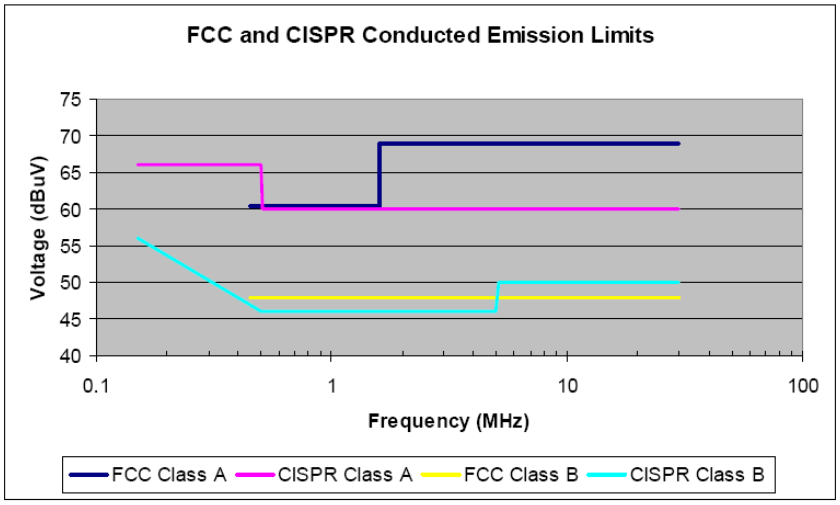

Figure 10. FCC and CISPR conducted emissions limits.

DM Conducted Emissions will be addressed in this work; radiated emissions, which are studied at frequencies greater than 30 MHz, are out of the scope of this study.

2.15.1 EMI and DC/DC Converters

RES studied in this work, namely PV systems and WECS, produce unregulated outputs; therefore, regulators must be interconnected in order to ensure nearly regulated outputs. In most applications, DC-DC converters are chosen to perform the proper regulation, with the addition of an increase/decrease in voltage. However, DC-DC converters generate current-related interference at their inputs, and voltage related interference at their outputs. The conducted input EMI noise generally comprises reflected ripples, in which the input current noise of a DC/DC converter interacts with the source impedance of the supply voltage,

significantly polluting the main voltage source [38]. Buck converter topologies generate noise at the input currents due to the semiconductor switch in series with the input power line [38].

Differential mode emissions include the basic switching current waveform and its harmonics as well as periodic current "spikes" at the switching frequencies. These spikes are generally coincident with the turn-on of a power semiconductor switch. Common mode emissions consist of periodic current spikes through chassis ground caused by rapidly switched voltage across parasitic capacitances. Sources of parasitic capacitance include transformer inter-winding capacitance, transistor case-to-chassis capacitance and stray capacitance associated with the physical layout. Figure 11 shows the different types of conducted noise in a DC/DC converter.

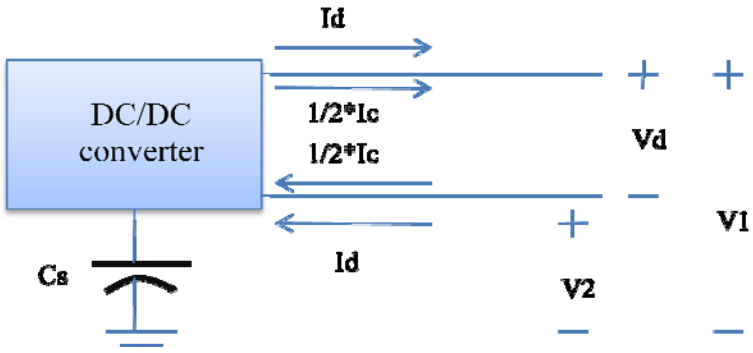

Figure 11 . EMI in a DC/DC converter

$$\begin{cases} V_d = V_1 - V_2 \\ I_d = \dfrac{I_1 - I_2}{2} \\ V_c = \dfrac{V_1 + V_2}{2} \\ I_c = I_1 + I_2 \end{cases} \quad (2.12.1\text{-}1)$$

Where V_d is the differential mode voltage; I_d is the differential-mode current; V_c is the common-mode voltage; and I_c is the common-mode current. For simulation purposes, only the differential mode voltage EMI will be studied. Common-mode emissions, which consists of periodic current spikes through chassis ground due to parasitic capacitances, is out of the scope of this study.

2.15.2 Measuring Conducted Noise (EMI)

A standard load impedance must be created at the measurement point. Commonly called a line impedance stabilization network (LISN), it must be placed between the mains and the source [37]. The LISN establishes a standard profile of load impedance toward the EMI source and filters out high frequency disturbances on the mains. At the same time, the system must not be affected by this impedance. A 50Ω/50μH LISN is commonly used. Figure 12 below shows the LISN used to measure noise [39].

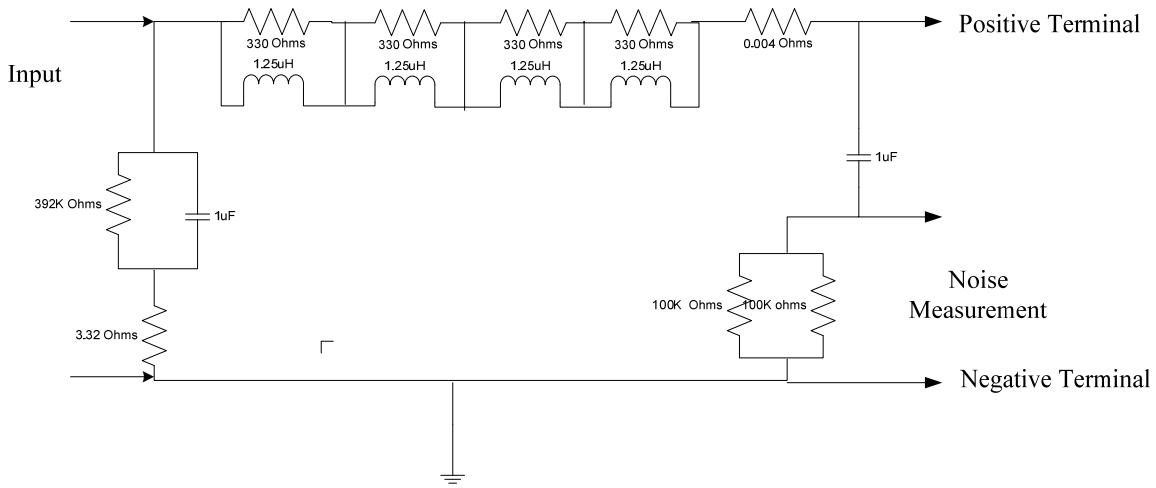

Figure 12. LISN model.

3 SIMULATION MODELS

3.1 DC/DC Converters Modeling

3.1.1 *Boost Converter*

Boost converters can produce an output voltage that will always be higher than the input voltage. It is considered to properly match the PV voltage with the battery voltage. The converter topology is presented in figure 13.

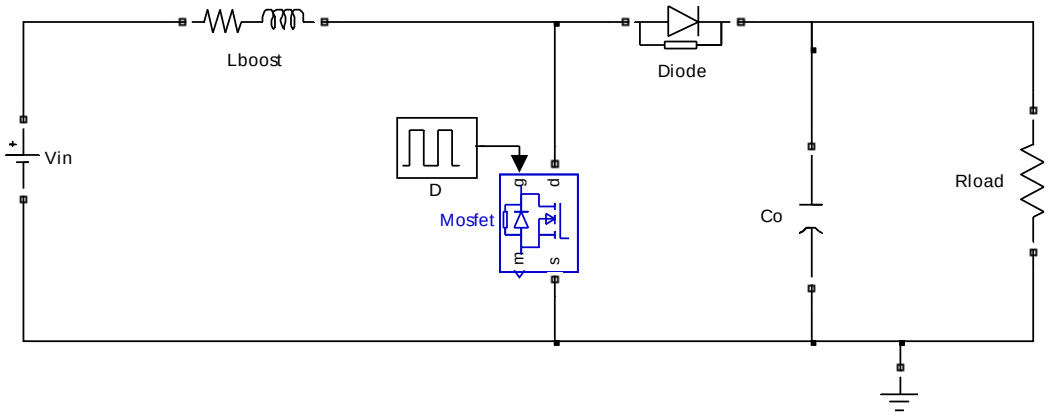

Figure 13 . Boost Converter Topology.

3.1.2 *Synchronous Buck Converter*

Synchronous Buck converters are derived from the buck converters, which produce an output voltage which will always be lower than the input voltage. Synchronous buck converters present a higher efficiency due to the fact that the diode is replaced by another MOSFET/switch. Figure 14 shows the topology of the Synchronous Buck converter implemented in Simulink.

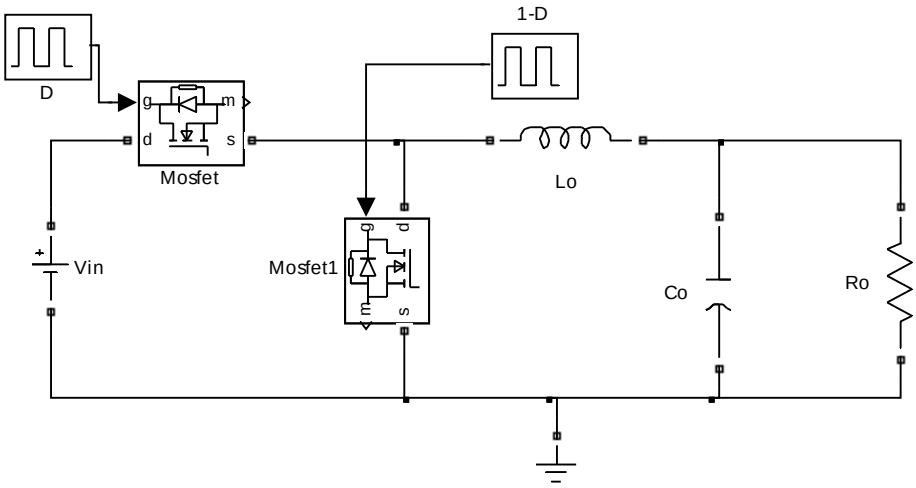

Figure 14. Synchronous Buck Converter topology.

3.1.3 *Flyback DC/DC Converters*

Flyback converters are derived from the buck-boost converter topologies. Flyback converters include a transformer, which serves as galvanic isolation between the source and the loads. They are used for low-power applications such as laptop battery chargers, computer monitors and LCD televisions.

This converter will be used when modeling DC appliances such as the Microwave Oven. The flyback average model is presented in figure 15 [40]:

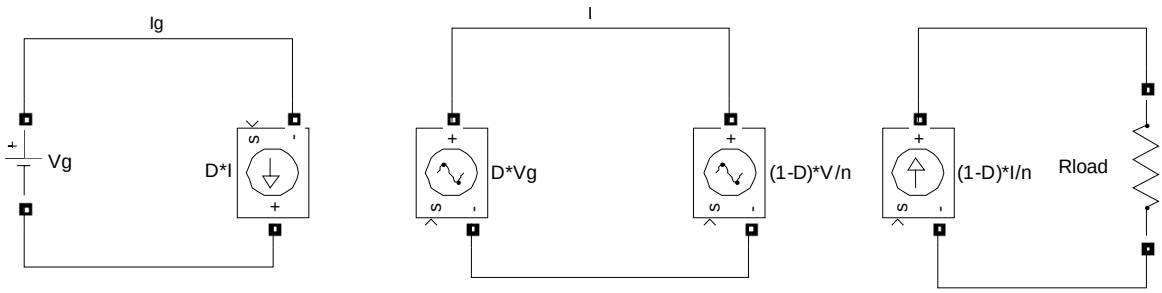

Figure 15. Flyback converter average model.

Where V_g is the input voltage; I_g is the input current; D is the duty cycle, n is the transformer turns ratio, R is the load resistance value, V is the output voltage.

$$D' = 1 - D, \qquad 0 < D < 1 \tag{3.1.3-1}$$

$$n = \frac{N_1}{N_2} \tag{3.1.3-2}$$

The Simulink model of the flyback converter representing the magnetron supply of the microwave is presented in figure 16.

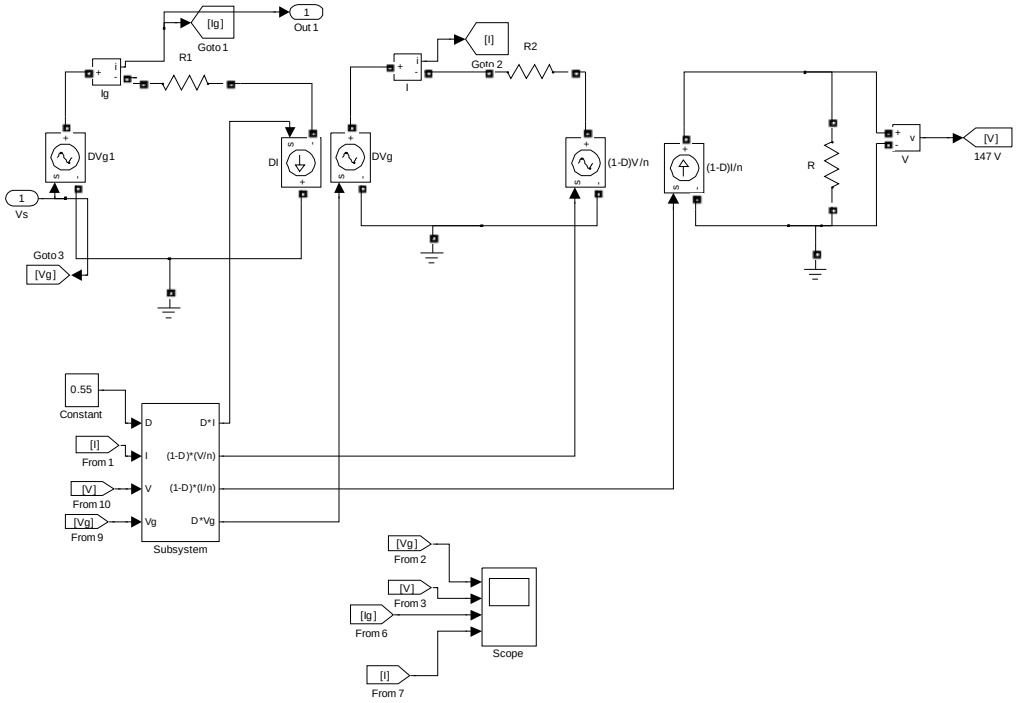

Figure 16. Flyback converter model in Simulink.

3.1.4 *Full Bridge DC/DC Converter*

The Full Bridge converter configuration is used for applications of high power (usually higher than 500W). The topology considered here is a boost converter, which will be needed to increase the battery voltage (of 48V) to the voltage and current levels needed by the BLDC motor of the Cloth Washer and Cloth Dryer. The schematic is presented in figure 17[41]:

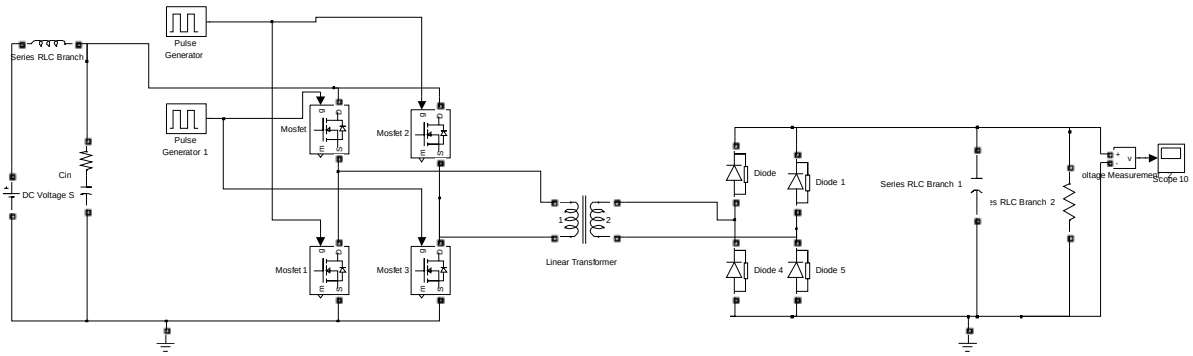

Figure 17. Full Bridge DC/DC Converter Topology

3.1.5 *Single Phase Full Bridge Inverter*

A Single Phase Full Bridge inverter is considered for interconnecting the utility grid with the RES residence, and to supply power to the cold cathode fluorescent light (CCFL) found in laptop computers and LCD TV's. The average model, derived from the state variable equations of the system, will be used to implement the inverter in Simulink for both the laptop computer and the LCD TV. The system equations, in state variable form, are expressed below [42]:

$$\begin{bmatrix} i_L \\ \dot{v}_C \end{bmatrix} = \begin{bmatrix} \frac{-R_L}{L} & -\frac{1}{L} \\ \frac{1}{C\left(1+\frac{R_C}{Z}\right)} & -\frac{1}{ZC\left(1+\frac{R_C}{Z}\right)} \end{bmatrix} \begin{bmatrix} i_L \\ v_C \end{bmatrix} + \begin{bmatrix} \frac{D_R}{L} \\ 0 \end{bmatrix} v_{DC} \quad (3.1.5\text{-}1)$$

Where D_R is the duty cycle; Z is the load impedance; L and C are connected in series as the output filter; and R_L and R_C are the small resistance values associated with the output inductor and capacitor, respectively. The average model of the inverter is presented in figure 18.

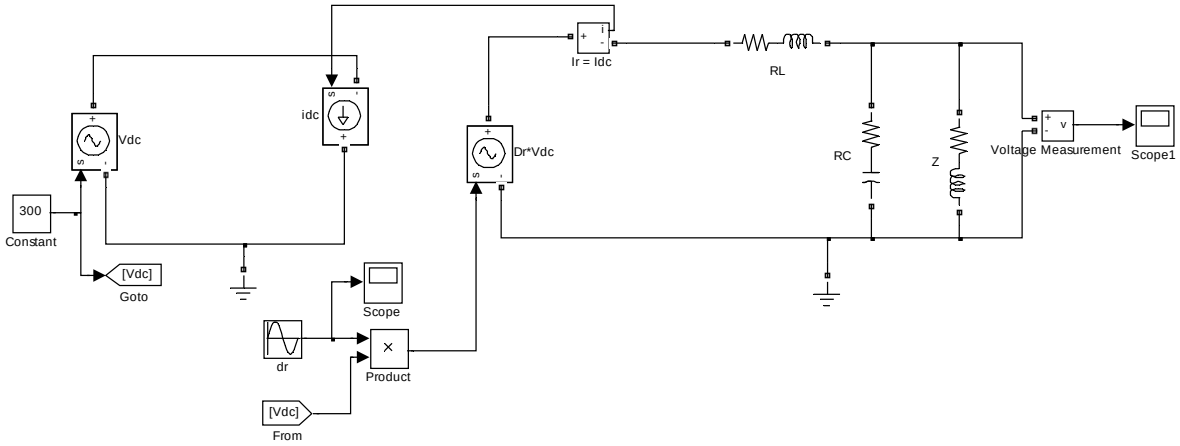

Figure 18. Full Bridge Inverter average model in Simulink.

The circuit topology considered for interconnection of the RES to the utility grid is shown in figure 19. The topology chosen in this research for this purpose is the Voltage Source Inverter (VSI), since the PV modules behave as a voltage source [17]. For this configuration, the input voltage must be greater than the peak value of the output voltage value. That is,

$$V_{in} > \sqrt{2}V_{out-RMS} \quad (3.1.5\text{-}2)$$

Again, the FB dc converter topology presented in figure 17 is necessary to properly increase the battery voltage level from 48V to the desired DC value, which is 450V in this case.

The inverter topology considered is a split phase, meaning that the inverter has a dual 120V output that can be joined to produce a 240V output. This topology was chosen since it is available commercially by Xantrex (model XW 6048 Grid tie) [43], and this eliminates need of a 120V/240V transformer to increase the output voltage to the appropriate level to match the voltage of the utility grid. Figure 19 below presents the VSI grid-connected inverter.

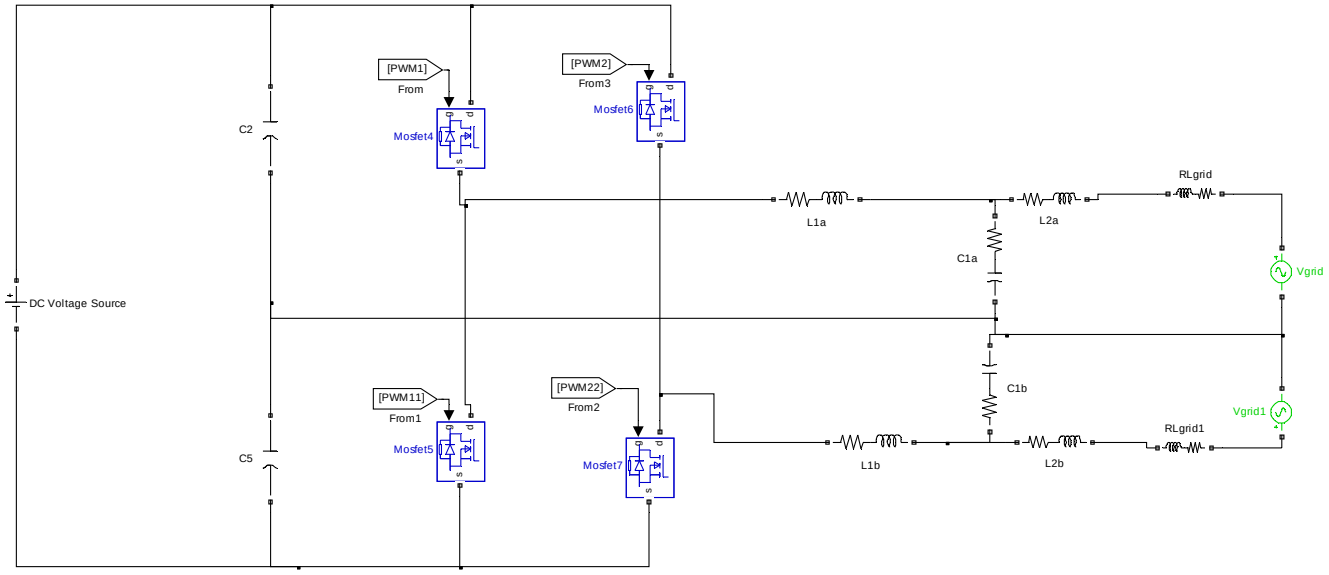

Figure 19. VSI Split Phase Inverter, connected to the Grid by a LCL filter.

3.2 PV System Modeling

The dynamic mathematical model of the photovoltaic module used in this work has been proposed by Ortiz-Rivera [7]. This model is very practical for distributed power generation, since all of the parameters needed to conduct simulations are readily available from the manufacturer's data sheets. The model is presented below:

$$I(V) = \frac{I_x}{1 - e^{-\left(\frac{1}{b}\right)}}\left[\, 1 - e^{\left(\frac{V}{bV_x} - \frac{1}{b}\right)} \,\right] \tag{3.2-1}$$

Where V is the panel voltage; b is the characteristic constant; I_x is the short circuit current at any given value of solar irradiation E_i and temperature T, which can be calculated when the voltage, V is zero; and V_x is the open circuit voltage at any given E_i and T, and it is the voltage of operation for the PVM when the current, I is zero. The expression for the short circuit current is presented below:

$$I_x = p\left(\frac{E_i}{E_{iN}}\right)[\, I_{sc} + TCi\,(T - T_N)\,] \tag{3.2-2}$$

p is the the number of PVM's connected in parallel is denoted by p; E_i is actual value of solar irradiation, while E_{iN} is the nominal value, 1000 W/m^2; I_{sc} is the short circuit current; TCi is the temperature coefficient of the short circuit current; and T is the actual value of temperature (in°C), while T_N is the nominal value, 25°C. The expression for V_x is presented below:

$$V_x = s\left(\frac{E_i}{E_{iN}}\right)TCv\,(T - T_N) + s\big(V_{max} - (V_{max} - V_{min})\big)e^{\left(\frac{E_i}{E_{iN}}\ln\left(\frac{V_{max} - V_{oc}}{V_{max} - V_{min}}\right)\right)} \tag{3.2-3}$$

The number of PVM's connected in series is denoted by s; V_{oc} is the open-circuit voltage; $V_{\max}$ is the open-circuit voltage at more than 1,200 W/m^2; $V_{\min}$ is the open-circuit voltage at

less than 200 W/m^2; and *TCv* is the temperature coefficient of V_{oc}. The expression of the dynamic PV system is given below:

$$\frac{\partial V}{\partial t} = \frac{1}{C_x}[I(V) - I_i] = \frac{I_x}{C_x}\left[\frac{\left[1 - e^{\left(\frac{V}{bV_x} - \frac{1}{b}\right)}\right]}{1 - e^{\left(-\frac{1}{b}\right)}} - I_i\right] \tag{3.2-4}$$

Figure 20 presents a diagram of the dynamic PV model; figure 21 presents the boost DC/DC converter.

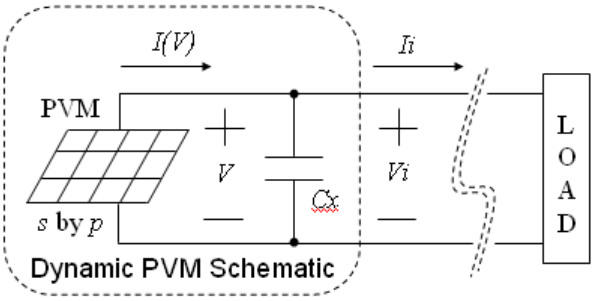

Figure 20. PV dynamic model [7].Used with permission from the author.

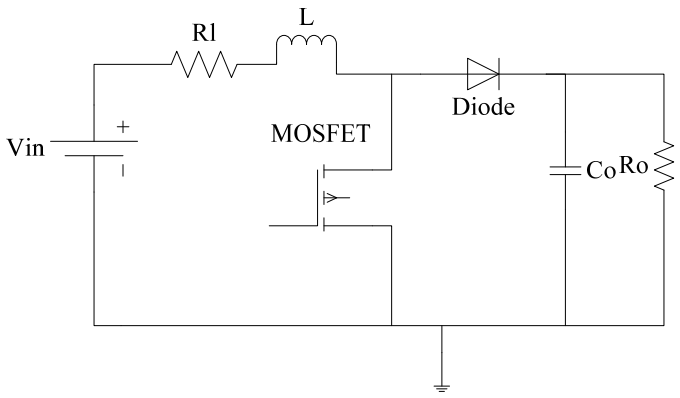

Figure 21. DC/DC Boost converter topology.

Where v_{in} is the input converter voltage, which, in this case, is the PVM voltage; i_l is the input inductor current, which, in this case, is the PVM output current, i_{pv} ; The output

voltage v_c is equal to the battery bank voltage, v_b. R_L is the equivalent series resistance (ESR) for the inductor. C_o is the output capacitor, $R_o$is the output resistor, and s corresponds to the value of the switch, which can be 0 or 1. In order to implement the DC/DC converter in Simulink, the SimPowerSystems toolbox was used. The module chosen is the Kyocera KD205GX-LP [44]; Table 1 presents the parameters used in simulations for the PV module.

Parameters	***Values***
Module Power	205 W
Open Circuit Voltage V_{OC}	33.2 V
Short Circuit Current I_{SC}	8.36 A
Voltage @ Maximum Power V_{OP}	26.6 V
Current @ Maximum Power I_{OP}	7.71 A
Constant b	0.0778
Temperature Coefficient of V_{OC}, TC_v	-0.120 V/°C
Temperature coefficient of I_{SC}, TC_i	0.00502 A/°C

Table 1. PV module parameters.

Figure 22 presents the MATLAB/SIMULINK simulation model of the PVM and the SimPowerSystems model for the Boost DC/DC converter.

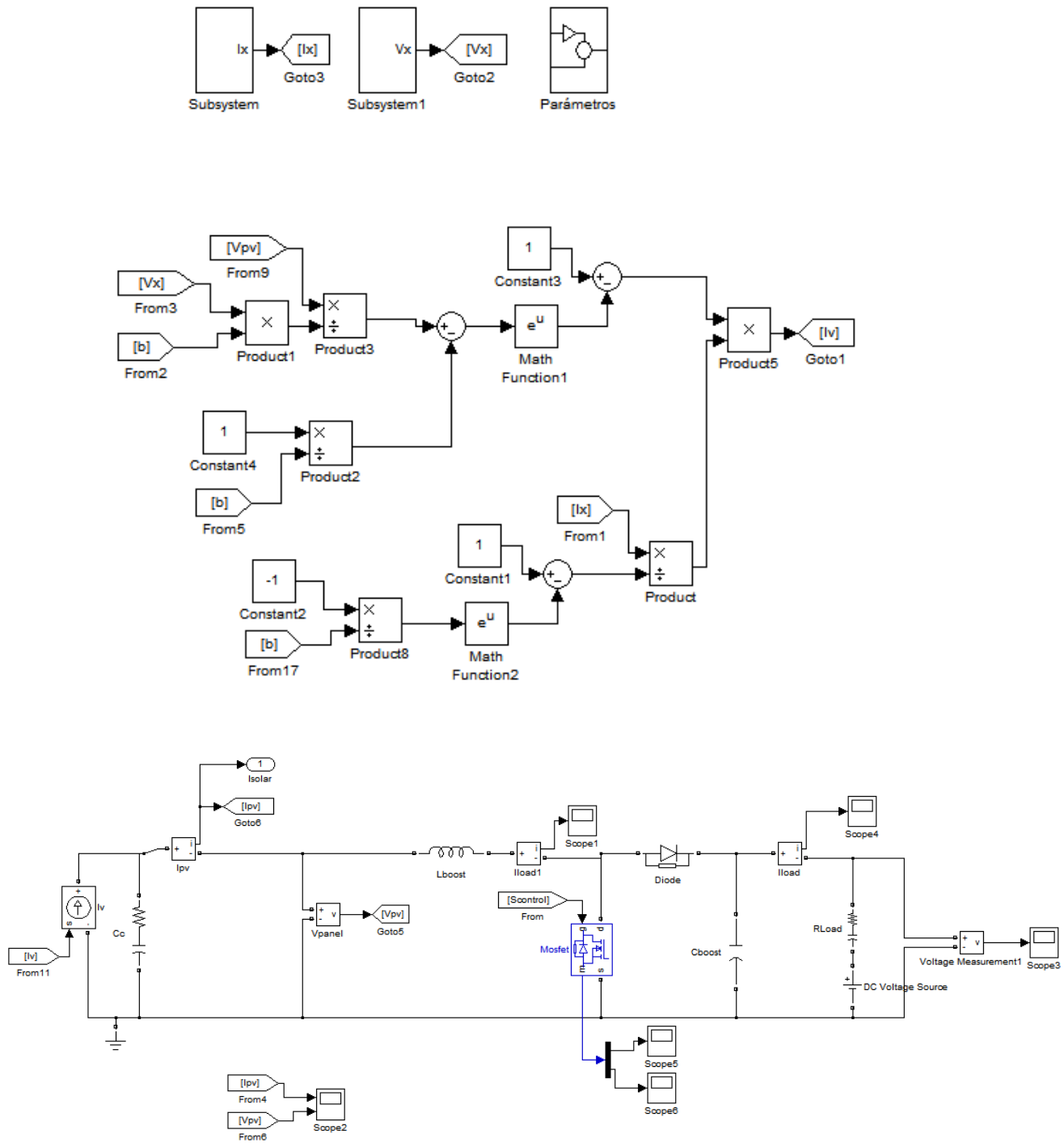

Figure 22. Dynamic PV system in Simulink.

3.3 PVM control: Maximum Power Point Tracking (MPPT)

The IC method requires actual measurements of the current operating point of the PV system (both voltage and current); the PVM model given by Ortiz [7] provides the respective expressions for the instantaneous and incremental conductance (shown below):

$$\frac{I}{V} = \frac{I_x\left(1 - e^{\left(\frac{V}{bV_x} - \frac{1}{b}\right)}\right)}{V\left(1 - e^{-\frac{1}{b}}\right)} \tag{3.3-1}$$

$$\frac{\partial I}{\partial V} = \frac{-I_x\left(e^{\left(\frac{V}{bV_x} - \frac{1}{b}\right)}\right)}{bV_x\left(1 - e^{-\frac{1}{b}}\right)} \tag{3.3-2}$$

The results from both expressions are added to obtain the error signal, C, which is corrected by the PI controller, and then compared to the triangular carrier wave in order to perform the Pulse Width Modulation (PWM) technique to properly operate the DC/DC converter. That is,

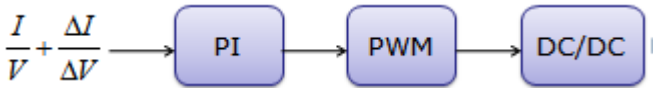

Figure 23. Block diagram for implementing the IC method.

Where

$$e = \frac{I}{V} + \frac{\Delta I}{\Delta V} \tag{3.3-3}$$

Figure 24 depicts the implementation of the IC method in Simulink:

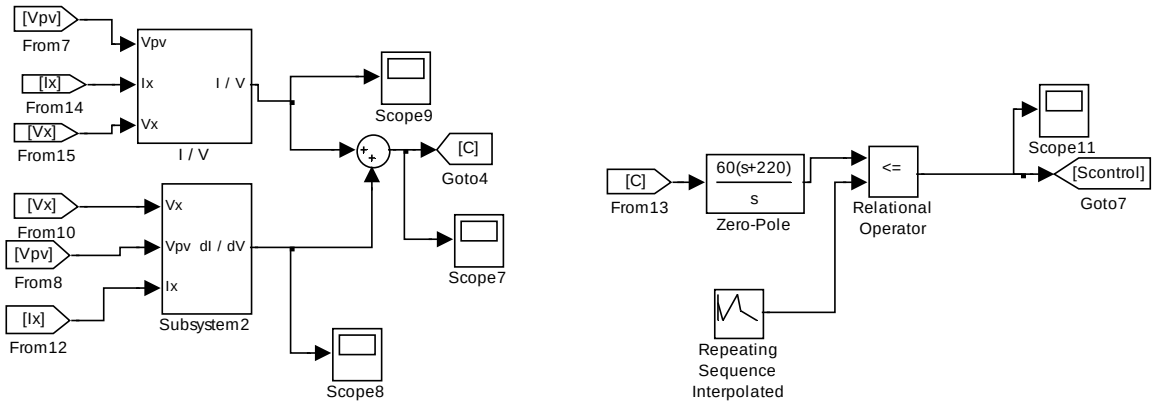

Figure 24. IC algorithm built in Simulink.

3.4 WECS Modeling

The wind turbine model used in this work was proposed in [14] by Valenciaga et al. The Wind turbine is coupled to a PMSG, which converts the mechanical power produced by the turbine into Electrical Power. Since the generator has a three-phase output, a rectifier and a DC/DC converter is required, to integrate this subsystem to the battery bank.

The mechanical power generated by a turbine is proportional to the air density (ρ), the power coefficient of the rotor (C_p), the cube of the wind speed (v), and the swept area (A):

$$P_t = \frac{1}{2} C_p(\lambda) \rho A v^3 \tag{3.4-1}$$

The power coefficient, C_P (λ), depends upon the aerodynamics of the rotor blades, the blades angle, and the wind velocity; the expression that determines the tip-speed ratio, λ ,is given by:

$$\lambda = \frac{r\omega_m}{v} \tag{3.4-2}$$

Where r is the blade length, ω_m is the angular shaft speed and v is the wind velocity in m/s.

The power coefficient is obtained by inserting the result of equation 3.4-2 into the expression below [45]:

$$C_p(\lambda) = -0.0006\lambda^5 + 0.0104\lambda^4 - 0.0602\lambda^3 + 0.146\lambda^2 - 0.108\lambda + 0.043 \quad (3.4\text{-}3)$$

The wind turbine torque is given by:

$$T_t = \frac{P_t}{\omega_m} = \frac{1}{2}\frac{C_p(\lambda)}{\lambda}\rho A r v^2 \quad (3.4\text{-}4)$$

The expression of the electrical angular speed, corresponding to the minimum shaft speed below which the system is unable to generate is given by:

$$\omega_{e\,lim} = \frac{V_s}{\phi_m} \quad (3.4\text{-}5)$$

Where ϕ_m is the flux linked by the stator windings, and V_s is the line voltage of the PMSG. The PMSG dynamic model of the system, referred to the *d-q* rotor reference frame, is presented below:

$$\dot{\imath_q} = -\frac{R_s}{L} i_q - \omega_e i_d + \frac{\omega_e \phi_m}{L} - \frac{\pi v_b i_q u_x}{3\sqrt{3}L\sqrt{i_q^2 + i_d^2}} \quad (3.4\text{-}6)$$

$$\dot{\imath_d} = -\frac{R_s}{L} i_d + \omega_e i_q - \frac{\pi v_b i_d u_x}{3\sqrt{3}L\sqrt{i_q^2 + i_d^2}} \quad (3.4\text{-}7)$$

$$T_e = \frac{3}{2}\frac{P}{2} P\left(\phi_m i_q + \left(L_d - L_q\right) i_q i_d\right) \quad (3.4\text{-}8)$$

$$\dot{\omega}_e = \frac{P}{2J}(T_t - T_e) \quad (3.4\text{-}9)$$

$$\omega_m = \frac{P}{2}\omega_e \quad (3.4\text{-}10)$$

The expression for the torque is proportional to the difference of the inductances of the direct and quadrature axes. Presuming that the air gap in the PMSG is smooth, the quadrature axis inductance equals the direct axis inductance ($L_d = L_q$), further simplifying equation 3.4-8. i_q and i_d are, respectively, the quadrature current and the direct current; L and R_s are the per phase inductance and resistance of the stator windings; P is the PMSG number of poles; J is the inertia of the rotating parts; $\phi_m$is the flux linked by the stator windings; and u_x is the control signal.

The voltage V_s is externally imposed by the DC/DC converter as a function of the duty cycle, and is described by:

$$V_s = \frac{\pi v_b}{3\sqrt{3}} u_x \tag{3.4-11}$$

Where v_b is the voltage of the battery bank. If we assume an ideal static conversion, the output current of the WECS can be determined by:

$$i_w = \frac{\pi}{2\sqrt{3}} \sqrt{i_q^2 + i_d^2} u_x \tag{3.4-12}$$

Figure 25 shows the WECS model in MATLAB-Simulink.

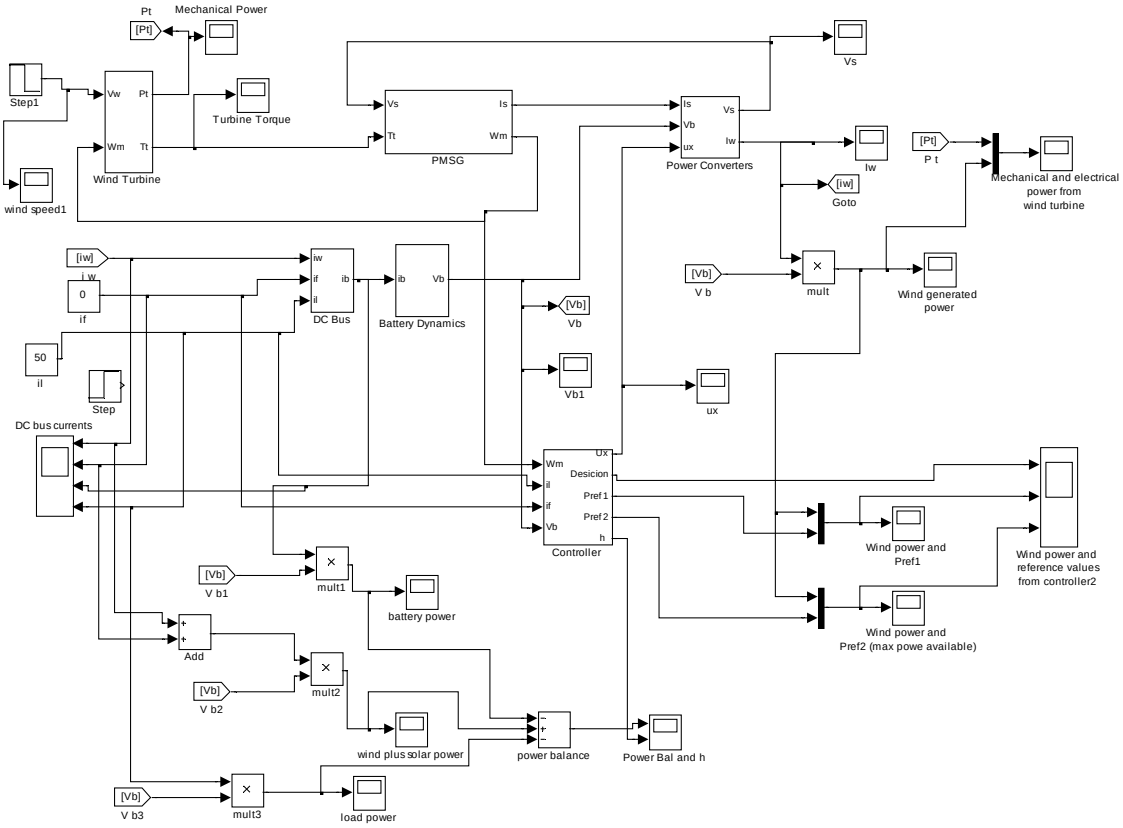

Figure 25. WECS model in MATLAB / Simulink.

Table 2 shows the parameters used for the WECS in MATLAB/Simulink.

Parameters	***Values***
PMSG Power Rating	3 KW
Stator Resistance	0.3676 Ω
Quadrature axis Inductance L_Q	3.55mH
Permanent Magnet Flux	0.2867Wb
Inertia	7.856 Kg m^2
Wind Turbine Radius	1.525m

Table 2. WECS Simulation Parameters.

The Whisper 500 wind WECS is commercially available on the market with a 3KW / 48V output [71], which will be chosen for the RES design later on.

3.5 WECS control: Sliding Mode Control (SMC)

The main objective of the SMC is to control the power produced by the wind subsystem into the DC bus to complement that injected by the PV system and to satisfy the power demand [14]. To accomplish this, two operation modes are defined: power regulation load (in case the Wind turbine is able to supply the power demand) and MPPT (when the wind power is not enough to supply the power demand).

3.5.1 *First Operation Mode*

In the first mode, the wind turbine is capable of supplying the power demanded by loads. The power reference is:

$$P_{ref1} = V_b\left(i_L + i_{bref} - i_{solar}\right) \tag{3.5.1-1}$$

Where V_b is the DC bus voltage, i_L is the load current, i_{bref} is and i_{solar} is the output PV current.

In order to regulate the power produced by the wind turbine, the system must follow the power reference P_{ref1}. To accomplish this objective, the sliding surface $h_1$is defined, in terms of currents on the battery bank.

$$h_1 = P_{ref1} - P_w \tag{3.5.1-2}$$

Where

$$P_w = V_b i_o = T_e \omega_m \tag{3.5.1-3}$$

In order to satisfy the control objective, the sliding surface $h_1 = 0$.

Equation 3.5.1-2 introduces the switching control signal into the sliding surface; by doing this, an unwanted deviation is produced in the electromagnetic torque and a high ripple on the current of the DC/DC converter. To avoid this problem, an integrator has been added to the input μ_x, turning the control signal into a new state variable; the integrator input signal *w* becomes the new input to the system. As a result, the algebraic dependence between the input of the system and the sliding surface is broken. The dynamic model of the extended system is shown below:

$$\dot{x} = \begin{bmatrix} \dot{\omega}_e \\ \dot{u}_x \end{bmatrix} = \begin{bmatrix} f_1(x) \\ f_2(x) \end{bmatrix} + \begin{bmatrix} g_1(x) \\ g_2(x) \end{bmatrix} w \tag{3.5.1-4}$$

$$\dot{x} = \begin{bmatrix} \dot{\omega}_e \\ \dot{u}_x \end{bmatrix} = \begin{bmatrix} \dot{\omega}_e \\ \dot{u}_x \end{bmatrix} = \begin{bmatrix} \frac{P}{2J}(T_t - T_{elin}) \\ 0 \end{bmatrix} + \begin{bmatrix} 0 \\ 1 \end{bmatrix} w \tag{3.5.1-5}$$

Where T_{elin} is the electrical torque of PMSG, which is given by

$$T_{elin} = K(\omega_e - \omega_{elim}) \tag{3.5.1-6}$$

The switched control law is

$$w = \begin{cases} w^+ = -\dfrac{1}{L_g h_1(x)} \left[\dfrac{\partial h_1}{\partial x^T} P(x) \dfrac{\partial h_1}{\partial x} \right] \; if \; h_1 \geq 0 \\ w^- = -\dfrac{1}{L_g h_1(x)} \left[\dfrac{\partial h_1}{\partial x^T} N(x) \dfrac{\partial h_1}{\partial x} \right] \; if \; h_1 \leq 0 \end{cases} \tag{3.5.1-7}$$

$$w = \begin{cases} w_1^+ = \dfrac{-|f_1(x)|}{4} \left[\dfrac{-18L^2\phi_m^2 u_x \omega_e + 2\pi\sqrt{3}L^2 u_x^2 \phi_m v_b}{\sqrt{3D}\phi_m R_s + 9\phi_m^2 R_s^2 - 36C + 10B - 2A} + 1 \right]^2 \\ w_1^- = \dfrac{|f_1(x)|}{4} \left[\dfrac{18L^2\phi_m^2 u_x \omega_e + 2\pi\sqrt{3}L^2 u_x^2 \phi_m v_b}{\sqrt{3D}\phi_m R_s + 9\phi_m^2 R_s^2 - 36C + 10B - 2A} + 1 \right]^2 \end{cases} \tag{3.5.1-8}$$

Where

$$A = \pi^2 L^2 v_b^2 u_x^2 \tag{3.5.1-9}$$

$$B = \pi\sqrt{3} L^2 \phi_m v_b \omega_e u_x \tag{3.5.1-10}$$

$$C = L^2 \phi_m^2 \omega_e^2 \tag{3.5.1-11}$$

$$D = 27\phi_m^2 R_s^2 - 108C + 24B - 4A \tag{3.5.1-12}$$

3.5.2 *Second Operation Mode*

The second operation mode, MPPT, occurs when the wind power is not enough to satisfy the total demand (The system is not able to operate on the sliding surface h_1). In this case, the power reference is proportional to the optimum power extracted by the turbine.

$$P_{ref2} = K_{opt} \omega_m^3 \tag{3.5.2-1}$$

Where

$$K_{opt} = \frac{C_t(\lambda_{opt}) \rho A R^3}{2\lambda_{opt}^2} \tag{3.5.2-2}$$

λ_{opt} is the optimum tip speed ratio that will produce the maximum value of the power coefficient $C_p(\lambda_{opt})$.

A second sliding surface, h_2, is incorporated to extract the maximum power available from the wind turbine. The proposed sliding surface is:

$$h_2 = P_{ref2} - P_w \tag{3.5.2-3}$$

$$w = \begin{cases} w_2^+ > 0 & if \quad h_2 \geq 0 \\ w_2^- < 0 & if \quad h_2 < 0 \end{cases} \tag{3.5.2-4}$$

For simplicity w_2^+ and w_2^- are assumed to be constants.

3.5.3 *Boundary between Operation Modes*

The boundary between the operation modes of the wind subsystem is given by the angular shaft speed of the boundary point; it is obtained by equaling the power references of both operation modes:

$$V_b\left(i_L + I_{bref} - I_{solar}\right) = K_{opt}{\omega_{m\,SW}}^3 \tag{3.5.3-1}$$

Resulting in the following function for the delimiting electrical angular speed:

$$\omega_{m\,SW} = \sqrt[3]{\frac{V_b\left(i_L + I_{bref} - I_{solar}\right)}{K_{opt}}} \tag{3.5.3-2}$$

Figure 26 shows the operation points of both sliding surfaces. The controller will operate on any of the two operation modes by comparing the measured speed with the boundary speed, $\omega_{m\,SW}$:

$$\begin{cases} \omega_m \geq \omega_{m\,SW} \rightarrow Power\ Regulation \\ \omega_m \leq \omega_{m\,SW} \rightarrow MPPT \end{cases} \tag{3.5.3-3}$$

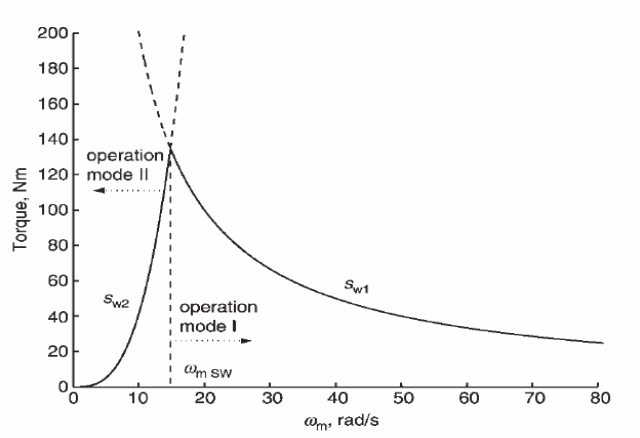

Figure 26. Boundary between operating modes [14].
(Used with explicit permission from the authors)

3.5.4 *Battery Modeling*

The battery model to be studied represents a simplified model of a lead acid battery. This model is presented in [14, 45], and consists of the main battery bank voltage with an RC network in series. This model has been modified in order to introduce losses associated with wire resistance.

$$v_b = E_b + (R_{wire} + R_b)\left(\frac{\pi}{2\sqrt{3}}\sqrt{i_q^2 + i_d^2} + i_{solar} - i_{loads}\right) + v_c \tag{3.5.4-1}$$

Where R_{wire} is the resistance due to the wiring configuration; R_b is the battery internal resistance; and E_b is the nominal battery bank voltage. The capacitor voltage is defined as follows:

$$\dot{V}_c = \frac{1}{C_b}\left(\left(\frac{\pi}{2\sqrt{3}}\sqrt{i_q^2 + i_d^2}\right)u_x + I_{solar} - I_{load}\right) \tag{3.5.4-2}$$

Table 3 presents the parameters used in the simulation for the battery bank [14].

Parameters	***Values***
Battery Bank Nominal Voltage	48V
Wire Impedance	0.0128 Ω
Capacitance	180,000 F
Battery Internal Resistance	14 mΩ

Table 3. Battery Bank Parameters.

The battery chosen in this research is a Deka 8A8D LTP AGM, 12 volt 245 Ah, commercially available [71]. This will be considered later on for further analysis.

3.6 BLDC Modeling

The Brushless DC motor model to be utilized in this work is referred to the *d-q* reference frame, with SPWM control [30-31]. The motor model in the stationary (ABC) reference frame is presented in matrix form below [31]:

$$\begin{bmatrix} V_{as} \\ V_{bs} \\ V_{cs} \end{bmatrix} = \begin{bmatrix} R_{xs} & 0 & 0 \\ 0 & R_s & 0 \\ 0 & 0 & R_s \end{bmatrix} \begin{bmatrix} i_{as} \\ i_{bs} \\ i_{cs} \end{bmatrix} + \begin{bmatrix} \dot{\lambda_{as}} \\ \dot{\lambda_{bs}} \\ \dot{\lambda_{cs}} \end{bmatrix} \tag{3.6-1}$$

Where V_{as} is the phase voltage, R_s is the stator resistance, i_{as} is the phase current and λ_{as} is the flux linkage. $\dot{\lambda_{as}}$ denotes the derivative of the flux linkage, that is:

$$\dot{\lambda_{as}} = \frac{d(\lambda_{as})}{dt} \tag{3.6-2}$$

The phase voltages are balanced (each voltage is shifted 120° from one another) and must have the same frequency, which depends on ω_r. The expression for the flux linkages is described below:

$$\begin{bmatrix}\lambda_{as}\\ \lambda_{bs}\\ \lambda_{cs}\end{bmatrix} = \begin{bmatrix}L_{aa} & L_{ab} & L_{ac}\\ L_{ba} & L_{bb} & L_{bc}\\ L_{ca} & L_{cb} & L_{cc}\end{bmatrix}\begin{bmatrix}i_{as}\\ i_{bs}\\ i_{cs}\end{bmatrix} + \begin{bmatrix}\lambda_m \sin(\theta_r)\\ \lambda_m \sin\left(\theta_r - \frac{2\pi}{3}\right)\\ \lambda_m \sin\left(\theta_r + \frac{2\pi}{3}\right)\end{bmatrix} \quad (3.6\text{-}3)$$

Where λ_m is the amplitude of the flux linkage established by the permanent magnet as viewed from the stator phase winding, and θ_r denotes the electrical angle between the magnetic axis of phase a and q axis relative to the fixed rotor reference frame. $L_{ab}, L_{bc}\ and\ L_{ca}$ are the mutual inductances, and $L_{aa}, L_{bb}\ and\ L_{cc}$ are the self inductaces. The expression for the electromagnetic torque can be expressed in terms of the motor variables:

$$T_{em} = P[2L_b[\alpha \sin 2(\theta_r) + \beta \cos 2(\theta_r)] + \lambda_m(\gamma \cos(\theta_r)) + (\delta \sin(\theta_r))] \quad (3.6\text{-}4)$$

$$\alpha = \left(i_{as} - \frac{{i_{bs}}^2}{2} - \frac{{i_{cs}}^2}{2} - i_{as}\, i_{bs} - i_{as} i_{cs} + 2 i_{bs} i_{cs}\right) \quad (3.6\text{-}5)$$

$$\beta = \frac{\sqrt{3}}{2}\left(i_{as} - \frac{{i_{bs}}^2}{2} - \frac{{i_{cs}}^2}{2} - i_{as}\, i_{bs} - i_{as} i_{cs} + 2 i_{bs} i_{cs}\right) \quad (3.6\text{-}6)$$

$$\gamma = \left[i_{as} - \frac{i_{bs}}{2} - \frac{i_{cs}}{2}\right] \quad (3.6\text{-}7)$$

$$\delta = \frac{\sqrt{3}}{2}(\, i_{bs} - i_{cs}\,) \quad (3.6\text{-}8)$$

The torque expression now includes the new variable,P, which takes into account the number of pole pairs of the motor. The expression for the electrical speed of the motor is:

$$\dot{\omega}_e = \frac{P(T_{em} - T_l - B\omega_r)}{J} \quad (3.6\text{-}9)$$

Where T_{em} is the electromagnetic torque T_l is the load torque and the $B\omega_r$ expression takes into account losses due to the mechanical friction. This term is mostly neglected, since the

friction coefficient B is usually low. J is the motor inertia. Note that, contrary to the wind turbine-PMSG, the electrical speed imposes the frequency of the voltage sources at the inverter [31]. That is,

$$\omega_e = \omega_r \tag{3.6-10}$$

The system's equations can be transformed from the ABC stationary reference frame to the *d-q* reference frame by means of Park's Transformation (see appendix B for more information). Applying the transformation to the system equations, the *d-q* equivalent system equations are as follows:

$$V_q = \iota_q \omega_r \lambda_m L_q \dot{} + R_s \iota_q + \omega_r L_d \iota_d \tag{3.6-11}$$

$$V_d = \iota_d L_d + \dot{R}_s \iota_d - \omega_r L_q \iota_q \tag{3.6-12}$$

$$T_{em} = \frac{3}{2} P\left[\left(L_d - L_q\right) i_q i_d + \lambda_m i_q\right] \tag{3.6-13}$$

The dynamics of the system does not depend on the reference frame at which the system is modeled; as a result, the equation corresponding to the motor speed is the same.

In order to model the three phase SMPW inverter [31], three 3-phase time dependent square-waves must be used to control the inverter switches. This is achieved by are made by comparing the 3-phase reference sinusoidal waves with a single high frequency triangular carrier wave (see figure 27). The 3-phase reference sinusoidal waves are given by

$$f_a = M \cos(\theta_e) \tag{3.6-14}$$

$$f_b = M \cos\left(\theta_e - \frac{2\pi}{3}\right) \tag{3.6-15}$$

$$f_c = M \cos\left(\theta_e + \frac{2\pi}{3}\right) \tag{3.6-16}$$

Where M is the modulation index of the inverter, defined as:

$$M = \frac{Sine\ Wave\ Amplitude}{Carrier\ Wave\ Amplitude}, 0 \leq M \leq 1 \tag{3.6-18}$$

The modulation index must be limited between a range of values in order to operate the system in a linear region; if the modulation index is out of the boundaries established, the inverter operate in a non-linear region, further complicating control issues.

The inverter pole voltages V_{ao}, V_{bo}, V_{co} are given by:

$$\begin{cases} V_{io} = \frac{V_{dc}}{2}\ if\ f_i(t) > F_\Delta(t) \\ V_{io} = -\frac{V_{dc}}{2}\ if\ f_i(t) < F_\Delta(t) \end{cases} \tag{3.6-19}$$

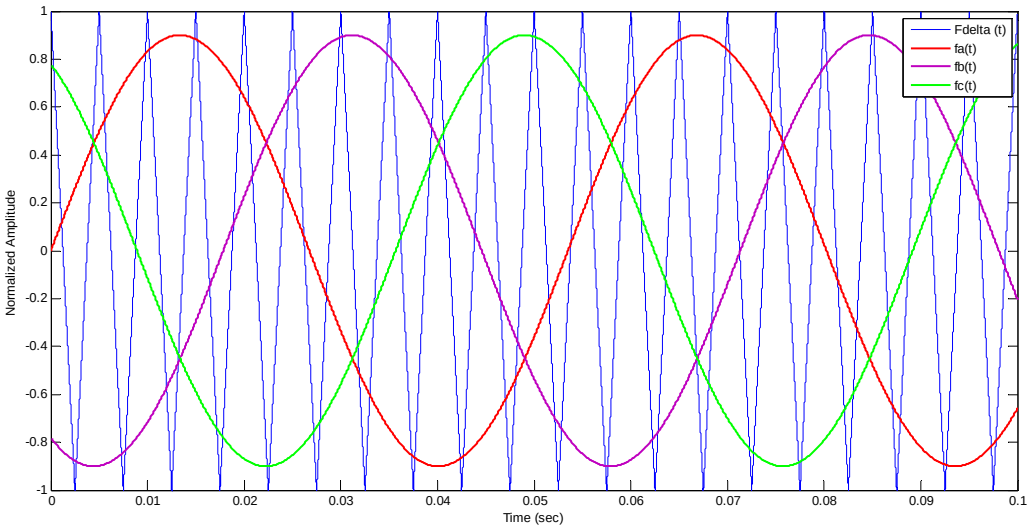

Figure 27. SPWM operation

Then, the motor phase voltages V_{as}, V_{bs}, V_{cs} are given by:

$$V_{as} = \frac{1}{3}(2V_{ao} - V_{bo} - V_{co}) \tag{3.6-20}$$

$$V_{bs} = \frac{1}{3}(2V_{bo} - V_{ao} - V_{co}) \quad (3.6\text{-}21)$$

$$V_{cs} = \frac{1}{3}(2V_{co} - V_{ao} - V_{co}) \quad (3.6\text{-}22)$$

The torque-current relationship is linear; then, the input current can be calculated as follows:

$$T = KI \quad (3.6\text{-}23)$$

Where K is the torque constant.

The output power of the motor is described by the following expression:

$$P_{out} = T_{load}\omega_e \quad (3.6\text{-}24)$$

Table 4 presents the parameters used in the simulations to represent various types of DC rotating loads. The parameters used for the Cloth Washer are presented in the first column, while the parameters for all the other rotating loads are presented in column 2.

BLDC motors Parameters	***Cloth Washer Values***	***Rotating Loads Values***	***Air Conditioner***
Number of Poles	48	4	2
Stator Resistance	4.6 Ω	988.9 mΩ	0.16 Ω
Quadrature / Direct axis Inductances	32mH	2.72mH	0.7mH
Permanent Magnet Flux	0.0152Wb	0.0562350Wb	0.025Wb
Inertia	0.05 Kg m^2	15.17μ Kg m^2	24.4483 μ Kg m^2
Torque Constant	35/6	0.34	0.15

Table 4. BLDC motor parameters for the Cloth Washer and other motor loads.

The BLDC model built in Simulink is presented in figure 28:

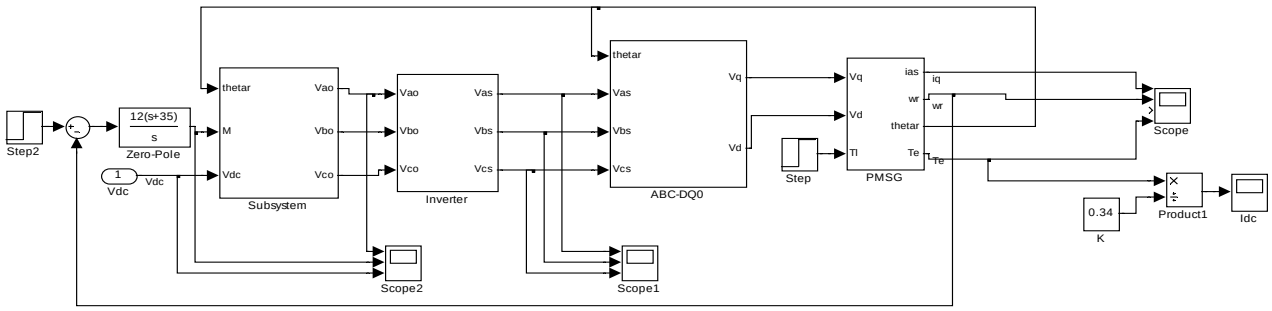

Figure 28. Brushless DC motor model in Simulink.

3.7 DC Home Appliances Modeling

Commercially, most appliances are readily available with an input voltage of 12 and 24V. Because of the low voltage, such appliances demand a high current (following ohm's law). In this study, unless otherwise stated, the following assumption is made:

- All appliances will operate at a voltage of 48V. Power ratings for the considered appliances can be found in section 4.1.1.

There are various reasons for why the battery bank voltage has been chosen to be 48V. First, DC voltages lower than 48V have proven to eliminate the risk of electric shocks or electrocution to the user(s). Second, compared to appliances with low voltage ratings (12V), increasing the input voltage decreases the current, which in turn decreases feeder losses. Also, it is assumed that in a near future, the market for DC appliances will be so high that they will be manufactured at higher levels due to the advantages above explained.

3.7.1 *Resistive Loads*

Current AC home appliances that are considered as resistive loads (heaters) include Stoves, Ovens, Dryers, Toasters, and Lighting. These loads can be effectively modeled as a resistance.

In the case of lighting, a new alternative for a DC house is to use light emitting diodes (LEDs) [18]. LEDs in the future will provide a better alternative than DC fluorescent lighting. Advantages of LEDs over Fluorescent lighting are as follows:

- LEDs operate better with DC voltages containing small ripple.
- They are rugged; there is no filament or glass envelope.
- They are easily mass-produced (meaning low costs).
- Instantaneous ON and OFF states (reduced losses).
- They have an operating life of 100,000 hours.
- LEDs do not produce any kind of EMI.
- LEDs do not produce any flicker.

3.7.2 *Appliances with Motors*

With advances in power electronics technology, motor driver devices are being considered to replace actual motors in home appliances that incorporate motors. Now, the use of three-phase induction and synchronous motors in DC applications is becoming attractive, due to the fact that such motors exhibit greater efficiencies and higher power densities than

the actual motors used for appliances. The PMSG has been considered because of the high power density, high torque, and the absence of brushes.

Loads in which a BLDC motor drive can be incorporated, and that will be considered in this study, are enumerated below:

1. Cloth Washer

For oscillating basket washers, the motor should cover wide operating ranges; High torque and low speeds are demanded for washing cycles, while lower torque and higher speeds are required in spinning cycles [32]. Figure 29 below shows the torque vs. speed requirements during both washing and spinning cycles.

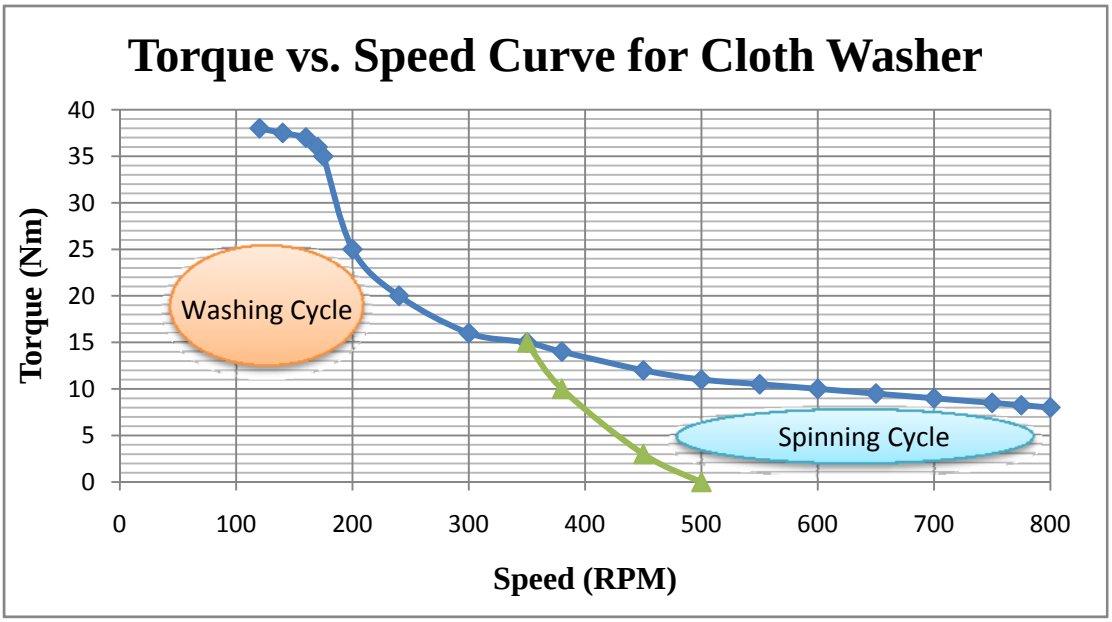

Figure 29. Torque and speed requirements for a Cloth Washer.

Cloth Washers with BLDC motors are commercially available by Fisher and Paykel [46]. The washers available are powered from a single-phase outlet, meaning that there are two

possible schematics: the possibility of a rectification stage followed by the DC to three phase inverter or the possibility of a single phase to three phase AC-AC converter. The washer considered here is fed by DC voltage, which is inverted to a three phase voltage. In order for the motor to provide high torques, the motor must be fed with a high voltage. Since the voltage is in a three-phase configuration, the DC input voltage must be higher than 100V [32]. As a result, a DC/DC converter must be used in order to increase the battery voltage up to the required input voltage. A Full Bridge (FB) DC converter will be used, as a coupling device between the battery bank and the appliance itself. The schematic of the Cloth washer appliance is presented in figure 30 below:

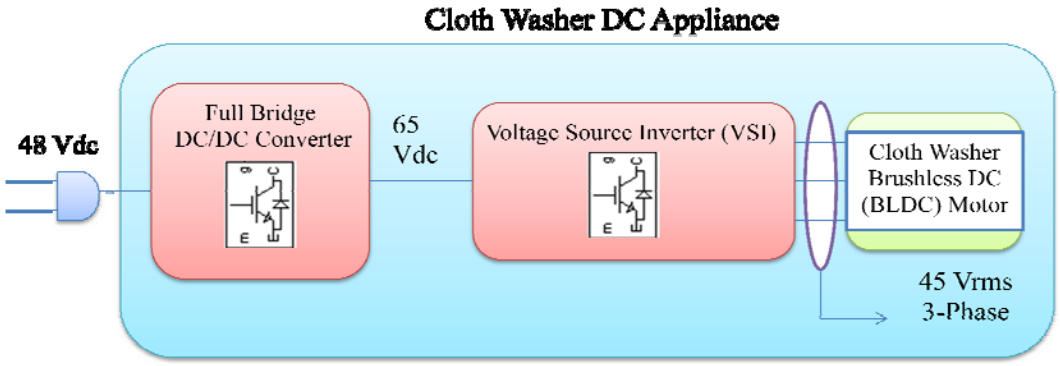

Figure 30. Colth Washer appliance schematic.

The FB DC/DC converter topology used has been modeled in Simulink with the aid of the SymPowerSystems toolbox. Figure 31 depicts the converter, and Figure 32 presents the BLDC motor:

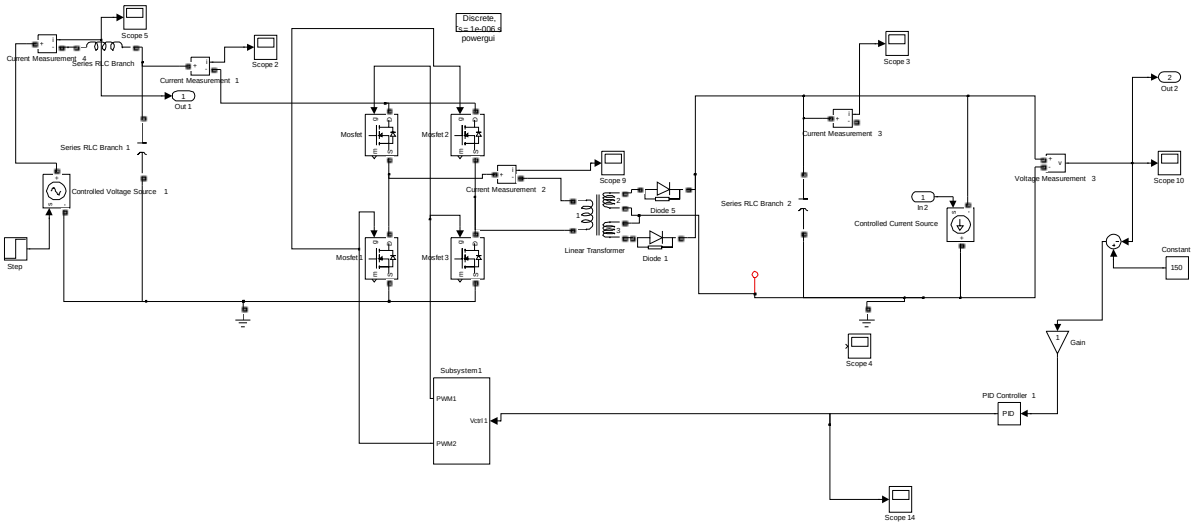

Figure 31 FB DC Converter Model in Simulink for the Washer.

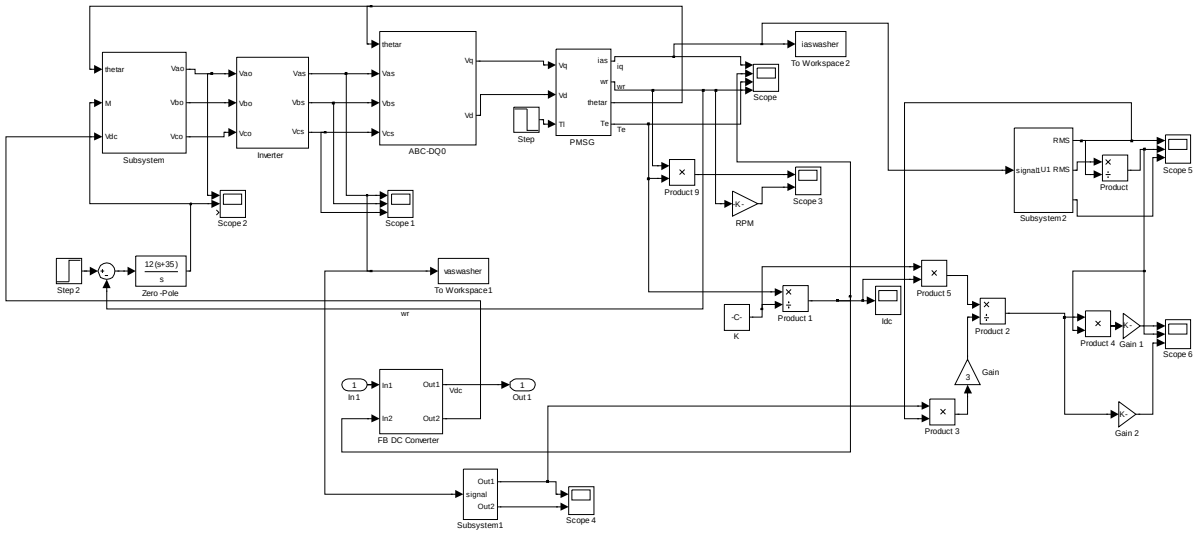

Figure 32. Cloth Washer Appliance model developed in Simulink.

Figure 31, which increases the battery voltage up to the levels needed for the Cloth Washer, is inside block “subsystem 4” in figure 32.

2. Cloth Dryer

Commercially available cloth dryers are replacing single phase motors with an induction drive. For example, Fisher and Paykel's "smart load" brand of dryers incorporate induction drives [47]. However, the use of induction drives present various disadvantages, as compared to a PMSM. Rotor slip is always present, meaning that the motor will never reach synchronism, and at the same time, rotor losses will always be higher due to the fact that they depend of the slip. Another disadvantage of induction motors is that they are manufactured to operated at a rated frequency; operating these motors at different frequencies means increased iron losses and the possibility of thermal breakdown of the motor [48]. Furthermore, the control of induction motors is more complicated than the control of a BLDC motor. For those reasons, a BLDC motor is proposed here, and most important, it is viable.

The Spin-X dryer is a new type of dryer available commercially which incorporated the drive technology [49]. The developers claim that two minutes in this spin dryer will save 30 minutes on a regular cloth dryer [49]. This is due to the high spinning speed of this dryer, which is a rated 3300 rpm. As with the cloth washer, a FB dc/dc converter stage is considered to supply the power needed by the motor drive.

3. Air Conditioner Units (AC units)

Air conditioners operating with a DC input voltage are commercially available by the DCAIRCO Company [50]. These units incorporate the use of BLDC motors. Air conditioners are available with input voltages of 12 and 24V, as well as with various

cooling levels. The ratings of the AC unit considered are 9000 BTU/h (equivalent to 3000 W).

4. Freezers & Fridges

Freezer and fridges are one of the most popular appliances that are available commercially with DC input power, and for various applications. Freezers and Fridges with DC inputs are manufactured separately, as well as together. SunFrost and SunDanzer are two of the most common brands available, with voltage inputs of 12V and 24V. A SunDanzer Freezer/Fridge will be considered for simulation purposes [51]. Model DCR225 is the fridge, and DCF225 is the freezer.

5. Ceiling Fans

Ceiling fans, as an AC appliance, operates with a single phase induction motor, specifically a universal motor. Panasonic has released the WhisperGreen ceiling fans for bathrooms, with an integrated BLDC motor [52].

Table 5 shows the different torque requirements for the motor to supply the rated appliance power.

Appliance	***Torque (N-m)***
Cloth Washer	35 (Washing Cycle) 10 (Spinning Cycle)
Cloth Dryer	1
Air Conditioning Unit	2.2
Freezer / Fridge	0.35
Ceiling Fan	0.35

Table 5. Torque requirements for rotating loads.

3.7.3 *TV's*

In order to operate an LCD with DC power, the transformer/rectifier can be eliminated. The Boost PFC can be replaced by a synchronous buck converter to lower the 48V input voltage to the 24V desired level. This allows the removal of the flyback converter, and a direct connection to the inverter. The inverter/transformer stage for the CCFL does not need to be changed. The flyback standby stage needs to be modified to manage an input voltage of 24V (from the bus). Figure 33 shows the proposed LCD TV schematic supplied by DC power.

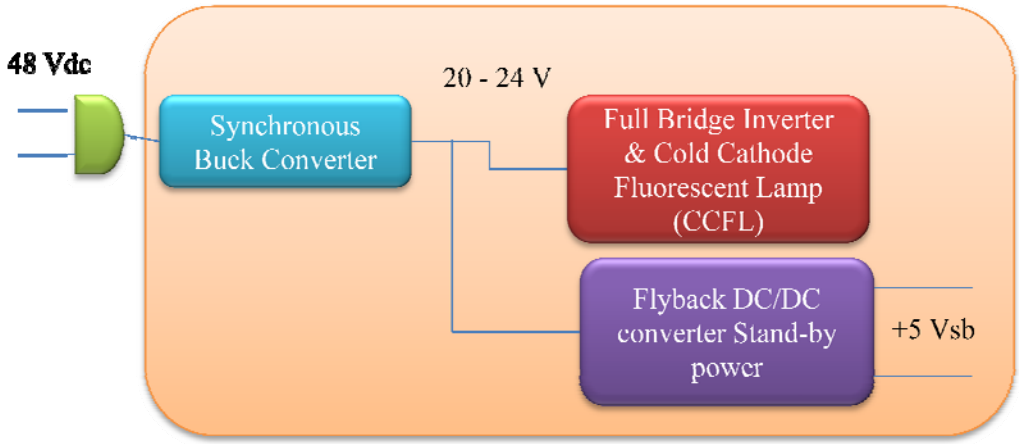

Figure 33. LCD TV schematic diagram supplied with DC power.

Figure 34 shows the Simulink schematic of the LCD TV.

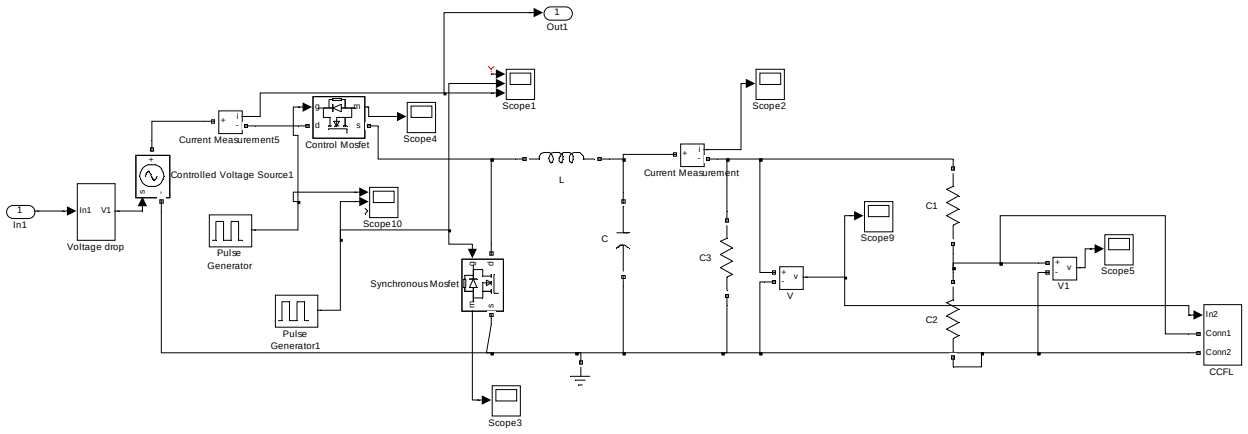

Figure 34. LCD TV Simulink Model.

The Synchronous buck lowers the 48V battery voltage into 24V. From the 24V output, a voltage divider is used to obtain the 20V necessary to power up the inverter for the CCFL. The lamp ratings are 560Vrms, 7.5mA, at a frequency of 55 KHz [53]. Figure 35 shows the inverter/transformer needed to power the CCFL.

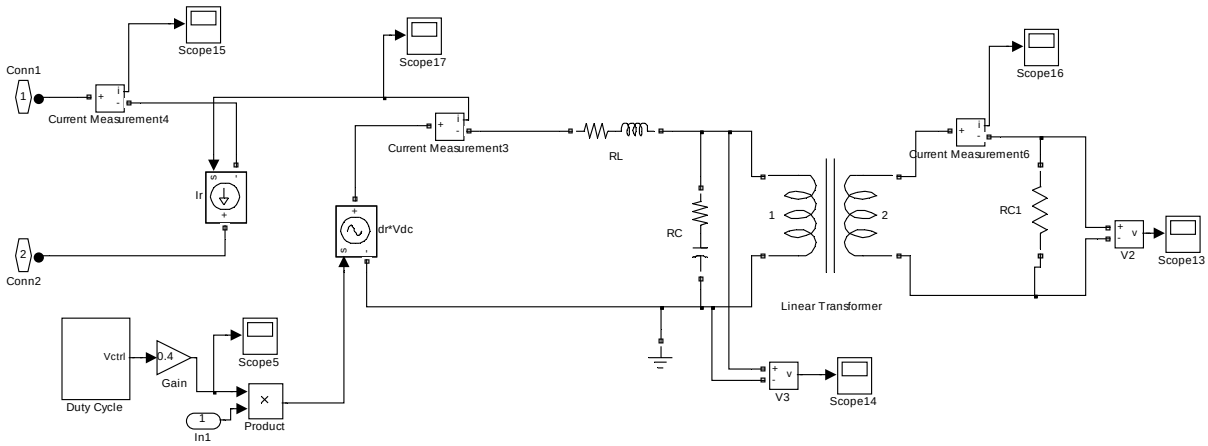

Figure 35. Full Bridge Inverter/Transformer configuration for the CCFL.

3.7.4 *Laptop Computer*

Considering that the laptop computer is capable of running with DC power when removing the transformer/rectifier stages, a Synchronous Buck converter will be utilized to

model the step down DC/DC converters needed in the computer [54]. The proposed DC schematic is presented in figure 36:

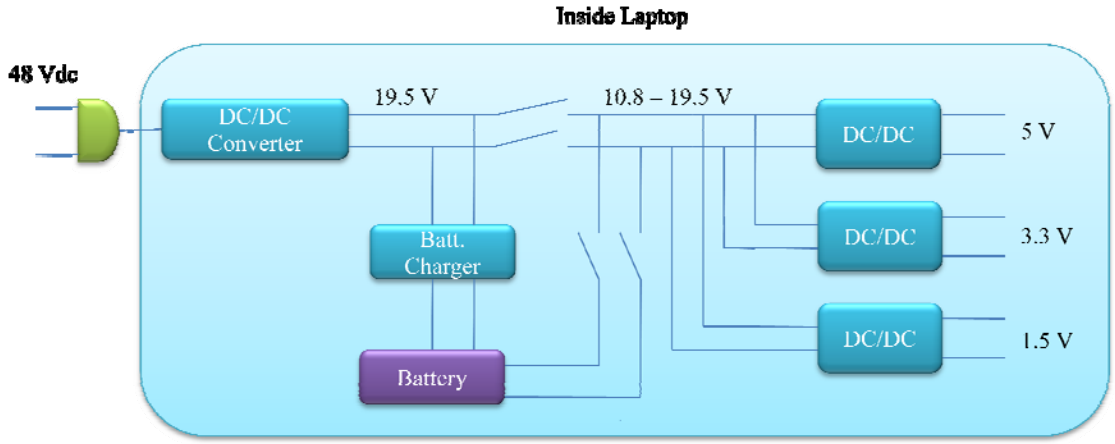

Figure 36. Proposed Laptop power management schematic.

Figure 37 below shows the computer simulation schematic in Simulink:

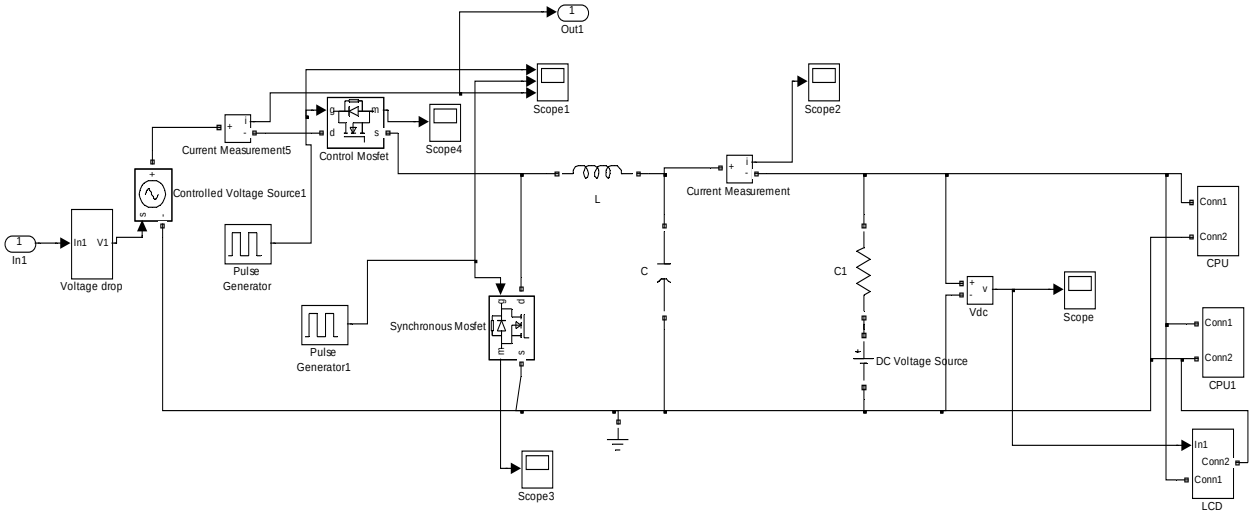

Figure 37. Laptop Computer Simulink Model.

The battery charger considered is a Dell 90W AC adapter with the following specifications:

- 100-240 V_{RMS} , 1.5A input
- 19.5V_{DC}, 4.62A output

The buck converter serves as a step down to match the input voltage with the laptop battery voltage, which is 19.5V. The CPU block contains 2 synchronous buck converters in parallel, in order to supply the total CPU current demand of 60A.The converters supplying the CPU must have a switching frequency of 250 KHz or higher. The CCFL operates at 300-400 V_{rms}, 5-6 mA**,** in the 25-50 KHz frequency range.

3.7.5 *Microwave Oven*

In order to operate a microwave with DC power, the transformer/rectifier stages can be removed. Furthermore, the high-voltage transformer can be replaced with two flyback DC/DC converters in parallel, which is suitable for providing appliances with higher voltages. The microwave considered was once available, with ratings of 12V_{DC} , 700W, 65A. This microwave included an inverter in order to supply power to the appliance. However, it is no longer being manufactured [55-56]. The proposed model of the DC microwave oven is presented in figure 38:

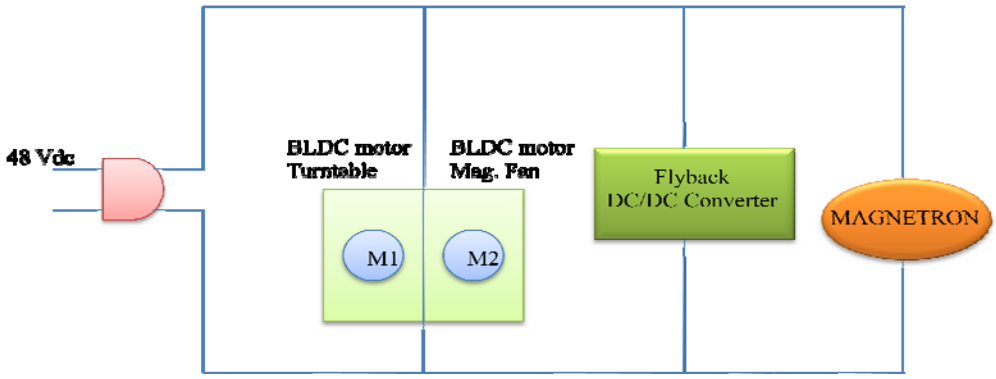

Figure 38. Microwave schematic supplied by DC power.

The Simulink diagram for the microwave is presented in figure 39 below:

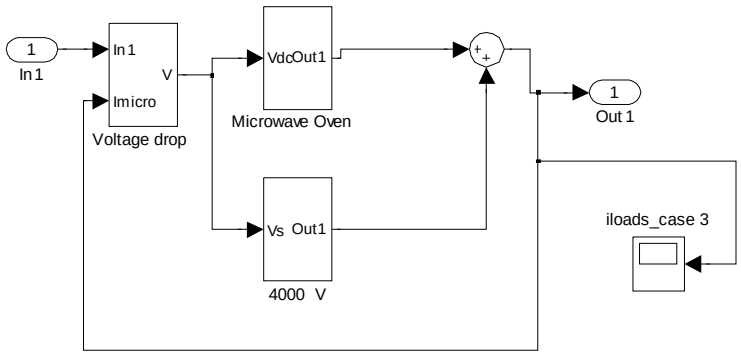

Figure 39. Microwave simulation model.

The microwave oven block contains two DC motors, which are considered to be BLDC motors. The second block contains a high-voltage transformer. The transformer has been modeled as a flyback DC/DC converter with a resistive load. The magnetron is rated at 4000V, 300mA. The parameters for both brushless DC motors used on the microwave are shown below:

1. Turntable Motor – 5.8RPM, 2.8W

2. Magnetron Cooling Motor – 3000RPM

3.8 *Power Quality*

The power quality indexes to be studied are enumerated as follows:

The common definition of displacement power factor (DPF), often confused with power factor, can be defined as

$$dpf = \cos\theta \tag{3.8-1}$$

For a three-phase circuit [57]:

$$pf = \frac{P}{3(Vrms_{\phi})(Irms_{\phi})} \tag{3.8-2}$$

Where θ is the angle between the phasors of voltage and current for both cases. In a three phase circuit, the power factor is inversely proportional to the RMS phase voltage and current.

The Total Harmonic Distortion (THD) is a measure that indicates the percentage of deviation from a Sine wave. This is defined for both voltages and currents [57]:

$$THD = \sqrt{\frac{{V_2}^2 + {V_3}^2 + {V_4}^2 + \cdots + {V_n}^2}{{V_1}^2}} * 100 = \sqrt{\frac{{V_{rms}}^2 - {V_1}^2}{{V_1}^2}} * 100 \tag{3.8-3}$$

Where $V_2, V_3, \ldots, V_n$ are the voltage harmonic components, V_1 is the fundamental component, and V_{rms} is the RMS value of the voltage or current.

When considering harmonics, a reduction in power factor due to non sinusoidal properties of the current arises. This is another definition for DPF [57]:

$$DPF = \frac{I_{1,rms}}{I_{rms}} \tag{3.8-4}$$

In terms of the total harmonic distortion (THD), the displacement factor can be also defined as [57]:

$$DPF = \sqrt{\frac{1}{1 + (THD)^2}} \tag{3.8-5}$$

As a result, the true power factor (TPF) to be studied, is [57]:

$$TPF = DPF \cos\theta \tag{3.8-6}$$

3.9 EMI

In order to properly measure EMI, the voltage measured through the LISN must be changed to the dB scale, and plotted in a frequency scale. In order to change from the voltage scale to the dB scale, the following formula is employed [37]:

$$U_{m(dBV)} = 20\log\left(\frac{U_2}{U_1}\right) \tag{3.9-1}$$

In EMC measurements, 1μV is more commonly used as a reference voltage. As a result,

$$1\mu V = 10^{-6}V = 0\ dB\mu V = -120dBV \tag{3.9-2}$$

In order to convert the voltage from the dBV system to the $dB\mu V$ [37]:

$$U_{m(dB\mu V)} = U_{m(dBV)} + 120 \tag{3.9-3}$$

3.10 Grid Modeling

The grid will be modeled as a voltage source, in series with an RL impedance [58]. The grid nominal voltage is 240V, which is the voltage available for all residences. The split phase inverter being considered eliminates the need of a transformer, which reduces the total grid inductance [43, 58]. Moreover, in order to prevent increases in AC voltage that

surpasses the limit of 110% of the nominal voltage, the grid impedance value at the PCC must be maintained a low value. By limiting the value of the total impedance to less than 1.25Ω, AC voltage levels will comply with the limits, while at the same time maintaining higher system efficiency [59]. Table 6 shows the parameters used for the inverter filter/grid impedance used in the simulation [60]. Figure 19 shows the Inverter connected to the utility grid by means of the LCL filter.

Component	*Value*
R_{L1}	0.2Ω
L_1	2mH
R_{C1}	5Ω
C_1	5μF
R_{L2}	0.1Ω
L_2	1e-3
R_{GRID}	0.5Ω
L_{GRID}	44.6μH

Table 6. Values of the LCL filter and Grid Impedance.

3.11 Inverter Control

In order for the inverter to supply any excess power into the utility grid, the inverter output voltage must be controlled both in magnitude and in phase [41]. By making the inverter output voltage slightly higher than the voltage of the utility grid, the power flow will be from the inverter into the utility [71]. Furthermore, the voltage control of the inverter also synchronizes the inverter output voltage with the utility grid's voltage, providing an integrated phase locked loop. Since the scope of this thesis is to inject excess power from the renewable system into the grid at all times, the output voltage control was implemented in simulation. The VSI inverter output voltage control is chosen to be unipolar PWM due to the

reduction in output voltage ripple component [41]. The unipolar PWM control implemented in Simulink is shown in figure 41, which is the content of the subsystem box in figure 40.

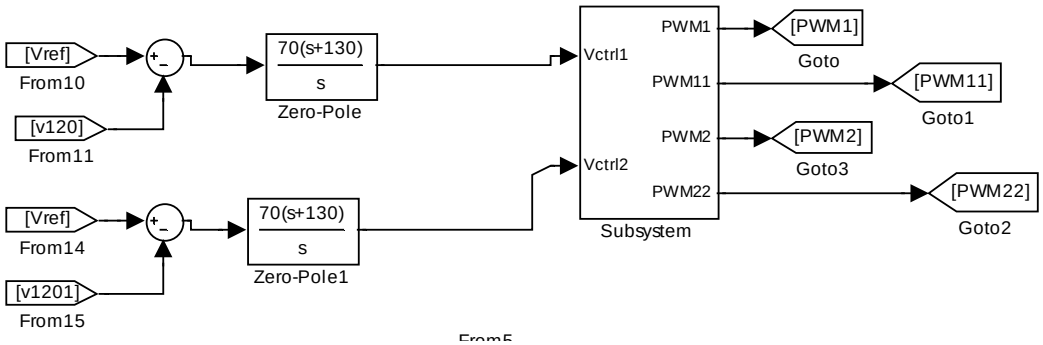

Figure 40. Inverter control loop.

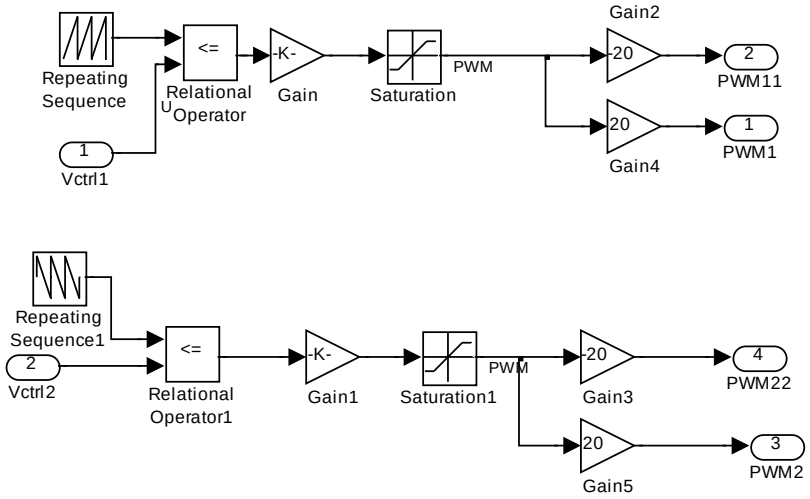

Figure 41. Unipolar PWM for Inverter switching.

4 ANALYSIS OF RESULTS

4.1 DC Distribution System

4.1.1 *Load Estimation*

Table 7 presents the different appliances analyzed, their ratings, the quantity present at the evaluated residence, and the number of hours per week that the appliance will be used. Table 8 shows the different phantom loads that are considered, along with their ratings. Phantom loads (P.L.) are being considered in this analysis in order to recreate as much as possible a real-life scenario.

DC Appliance	*Power (W)*	*Current (A)*	*Quantity*	*Hours / week*
Cloth Washer	620	13	1	2
Cloth Dryer	470	9.9	1	1
Microwave Oven	700	14	1	1
Stove	1425	29.68	1	7
Oven	120	2.5	1	1
Hair Dryer	168	3.5	1	2
Laptop Computer	110	2.5	1	30
Freezer/Fridge	120	1.2	1	168
AC Unit	670	13.96	1	25
Lighting	13	0.027	20	35
Ceiling Fan	25	0.15	5	42
LCD TV	168	3.5	4	21

Table 7. DC Appliance information used in RES sizing analysis.

Phantom Load	*Power (W)*	*Quantity*	*Hours / week*
Digital Clocks	1	2	168
Radio Clock	3.4	1	168
LCD TV	0.4	4	168
Microwave Oven	8	1	168
Laptop computer	3.4	1	168
LaserJet Printer	1	1	168

Table 8. Phantom Loads considered in the RES sizing analysis.

The information in Table 7 is obtained from [32, 49, 50-51, 61-65], and all appliances above listed are assumed to be in standby mode all 7 days of the week, during the times they are not operated. Information from table 8 is obtained from [66].

Three scenarios will be evaluated: In case I, PL are considered. All the necessary information is provided in table 7. For case II, PL are not considered, since it is assumed that the family has taken proper care in eliminating loads that consume power when no one is present at the residence. Finally, using the same appliance profile as in table 7, for an AC residence with energy star appliances, the equivalent AC monthly consumption of a residence composed of 4 family members was determined to be 450KWh/month; this is considered in order to compare an actual AC residence with the proposed DC residence.

Scenario	*Consumption (KWh/month)*
Case I	310
Case II	280
AC Residence	450

Table 9. Estimated Residential Monthly Power Consumption.

4.1.2 RES Sizing

Results for the RES system sizing are presented below. This analysis has been done considering the estimated monthly power consumption information in table 8. Also, the analysis has been done considering that the PV system will be considered as the primary, or top priority, source of power capable to supply 75% of the total monthly demand. The wind system will supply the other 25% of the monthly demand.

This results presented are computed taking into account that the worst-case scenario for solar irradiation is in the month of December. The solar irradiation and wind velocity data available is for the city of Aguadilla, PR. The data is presented in Appendix C. Wind velocity measurements are available from 2002 to 2004 (2 year period). However, most of the data is unreliable due to the fact that for some months, measurements were not taken properly. The data for the month of December from 2002 to 2004 was averaged, and an average hourly value of the wind velocity is the value that is presented in the Appendix C. Table 10 presents the results for the system sizing. The following assumptions have been considered before sizing the system:

1. All equipment will have a nominal voltage of 48V, except batteries (12V) and PV Modules (24V).
2. Only 1 wind turbine is allowed to be installed in a residence.
3. Batteries chosen are 245 Ah.

	Stand Alone		*Grid Interconnection*		
System Components	***Case I***	***Case II***	***Case I***	***Case II***	***AC Residence***
PV Array	22	22	22	22	34
Parallel modules	11	11	11	11	17
Series modules	2	2	2	2	2
Wind Turbine(s)	1	1	1	1	1
Wind Turbine(s) Tower(s)	1	1	1	1	1
Solar Water Heater	1	1	1	1	1
Battery Bank Array	28	28	28	28	40
Batteries in Parallel	7	7	7	7	20
Batteries in Series	4	4	4	4	2
AC Conduit Box (ACCB)	0	0	2	2	2
DC Conduit Box (DCCB)	0	0	2	2	2
Inverters	0	0	2	2	2
Disconnect	1	1	1	1	1
Junction Box	2	2	2	2	3
MPPT Charge Controllers	3	3	3	3	4
PV Ground Fault Protection	1	1	1	1	1
60A DC Breaker (CD60DC)	6	6	6	6	8

Table 10. System Components for all Scenarios.

Evaluating an AC residence vs. a DC residence, the reduction of load power consumption as compared to AC loads lowers the daily value of DC current needed to supply the power demand. Furthermore, the removal of inverters along with their respective equipment (AC and DC Conduit Boxes) in the DC residence reduces the overall system cost, for the stand alone scenarios. Since the value of current needed per day on the DC residence is lower, as a result, the number of solar panel, batteries and charge controllers needed also decreases. For Case I, a 3.14 KWh per week was computed; in this analysis, the consideration of phantom

loads does not reduces system components, as shown in table 10. Supplying loads with DC power, as considered in scenarios I and II proves to be the best scenario, with a reduction in 36 PV panels, 44 batteries and 3 charge controller (as compared to the AC residence).

For the Net metering analysis, in order to properly compare a DC residence to an AC residence connected to the utility grid, batteries will not be removed neither from the DC nor the AC residence. Furthermore, there is no change in the design of the RES system, except for the addition of an inverter with the AC and DC conduit boxes, in order to properly interconnect the residence with the utility grid.

4.1.3 Wiring Analysis

Table 11 shows the comparison in wiring for both a DC and an AC residence. Wire impedance calculations are shown in Table 12. Impedance data has been obtained from tables 11 and 12 from [67].

Residential Circuit / Load	***AC Wiring / Breaker***	***DC Wiring / Breaker***
Circuit: Oven & Stove	2 # 8 AWG, 50A / 2 pole	2 # 8 AWG, 50Adc
Circuit: Lightning	2 # 12 AWG, 20A / 1 pole	2 # 12 AWG, 20Adc
Circuit: Laundry	2 # 12 AWG, 20A / 1 pole	2 # 10 AWG, 30Adc
Circuit: Air Conditioner	2 # 10 AWG, 30A / 1 pole	2 # 12 AWG, 30Adc
Circuit: Water Heater	2 # 10 AWG, 30A / 2 pole	SOLAR HEATER
Circuit: Appliances	2 # 12 AWG, 20A / 1pole	2 # 12 AWG, 20Adc
Circuit: Microwave	Included in Appliances	2 # 12 AWG, 30Adc

Table 11. Comparison between AC and DC wiring

Results from table 11 show though there is no visible difference when wiring most circuits the current flowing through the DC circuits is equal or higher than the current that flows in an AC circuit. For the Stove/Oven, the DC current in the feeder is 30A, compared to the RMS value of the current in an AC circuit which is 40A. In the laundry circuit, though

the washer motor current is 6A, the FB converter draws an amount of 13A, which is a high value, compared to actual AC washer current consumption, which is around 11A. The same happens with the dryer, which draws a current of 10A from the battery bank. The only evident reduction in circuit wiring is in the case of the AC unit, which goes from #10AWG to #12AWG. The reduction in wire increases feeder resistance, but since the current also decreases, the feeder losses are not really affected. Also, the dedicated circuit for the water heater can be removed in the DC residence, since a solar water heater is considered. Finally, the other notable difference in system wiring is with the microwave. The microwave studied here consumes 12A, for which it deserves its own circuit. In an AC residence, it is included in the appliances circuit. Needless to say, decreases in current consumption also decrease the feeder total losses.

Table 12 below shows the calculated impedance values for the different appliances. The Impedance values, the distance from the battery bank to the appliance, and the equivalent impedance are presented. The distance shown on column 2 does not reflects the ***real*** distance from the battery bank to the appliance; in DC systems, the impedance must be multiplied by a factor of two to take into account the return path.

DC Circuit / Load	*Impedance Value Ω/Kft*	*Distance from Batteries* ft*	*Equivalent Impedance Ω**
Battery Bank	0.0608 + j0.041	2	0.0243e-3
Circuit: Lightning	N/A	N/A	N/A
Circuit: Laundry	1.21 + j0.050	18	0.0436
Circuit: Air Conditioner	1.93 + j0.054	17	0.0411
Circuit: Water Heater	N/A	N/A	N/A
Circuit: Appliances Freezer & Fridge	1.93 + j0.054	21	0.0811
Circuit: Appliances Ceiling Fan Room 1	1.93 + j0.054	17	0.0656
Circuit: Appliances Ceiling Fan Room 2	1.93 + j0.054	29	0.1119
Circuit: Appliances Ceiling Fan Master Room	1.93 + j0.054	35	0.1351
Circuit: Appliances Oven & Stove	0.764 + j0.052	24	0.0367
Circuit: Appliances TV	1.93 + j0.054	11	0.0425
Circuit: Microwave	1.93 + j0.054	24	0.0926

Table 12. Wiring and Equivalent Resistance Results.

4.2 Simulation Results

Simulation results for a Stand Alone and a Grid Interconnected DC residence are presented. Different case studies will be presented; under each case, transient and steady state simulations will be presented. Transient studies will include responses from the appliances, as well as for the system. Steady state simulations will present the sliding surfaces in which the system is operating, along with the turbine's behavior (power coefficient). Matlab and Simulink will be used to conduct simulations; tools such as SimPowerSystems and powergui will be used as an aid to construct converter topologies, measuring THD and doing harmonic analyses on various waveforms.

4.2.1 Case I

4.2.1.1 Transient Simulations

It is assumed that there is no one during the daytime at the residence. The only loads present in the system are the Fridge/Freezer, and PL. Simulation is conducted to represent the system's response from 12:00pm to 5:00pm. The values for solar irradiation, temperature and wind velocities are shown in Appendix C and correspond to the time at which the simulation is conducted to study the system's response (12:00pm-5:00pm). A 5A load is considered to represent the phantom loads being active.

Results:

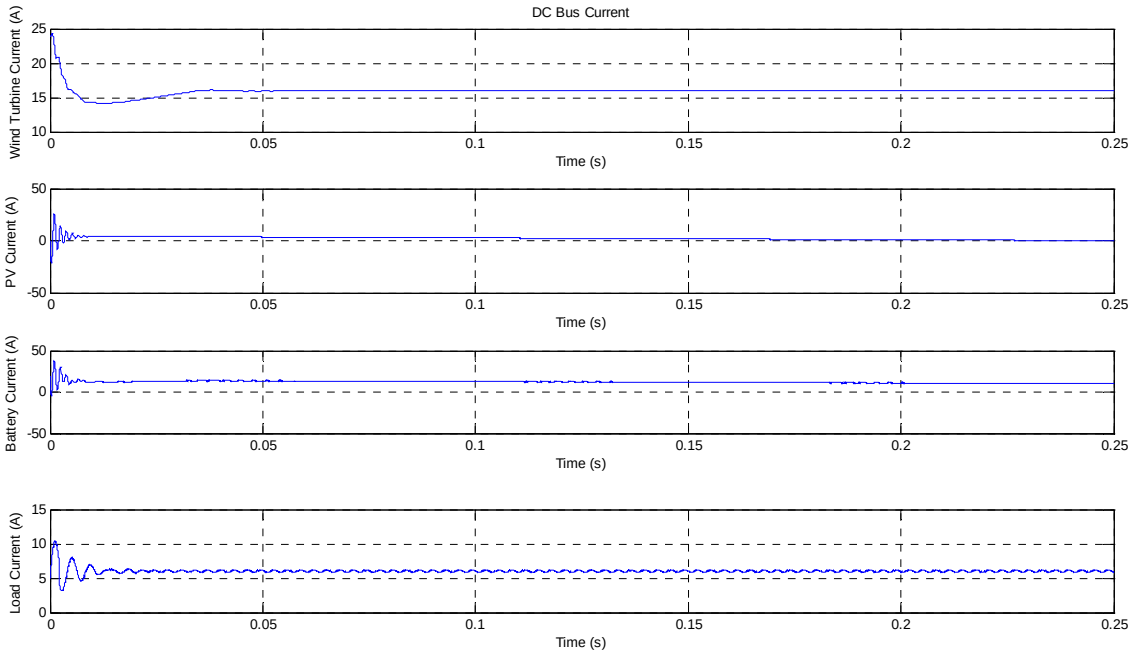

Figure 42. DC Bus currents

Figure 42 shows the DC bus currents. Due to the variations in solar irradiation and temperature, the PV current never stabilizes, though the control stabilizes and achieves MPPT. Since the PV current decreases and the function of the WECS control system is to maintain power balance, the wind turbine current is shown to be increasing as time evolves. The load current shows a transient response in where a current much higher than the rated for the appliance, affects the output current of the battery. Also, the load transient affects the output of the DC/DC converter, inducing this same transient in the output PV current.

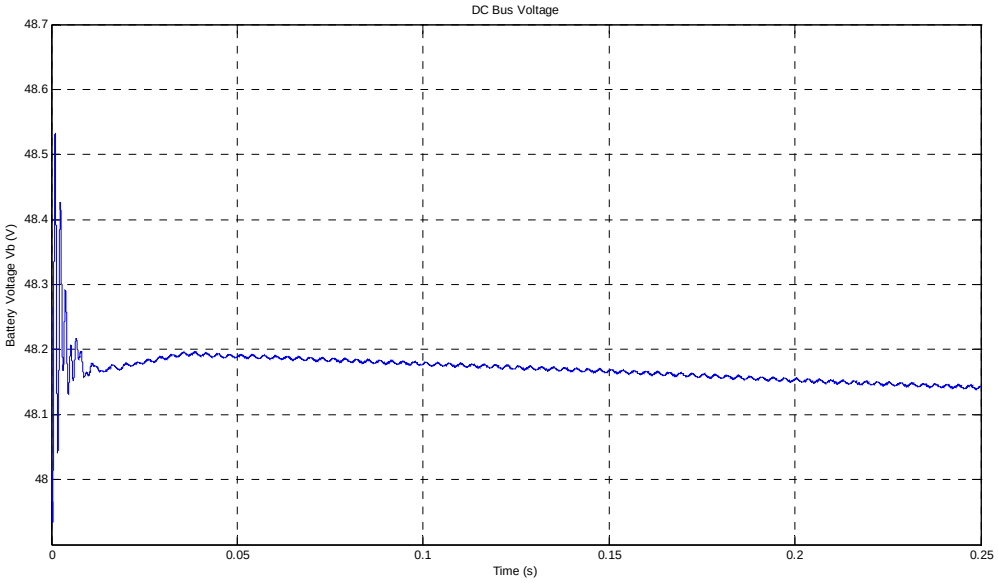

Figure 43. Battery Voltage

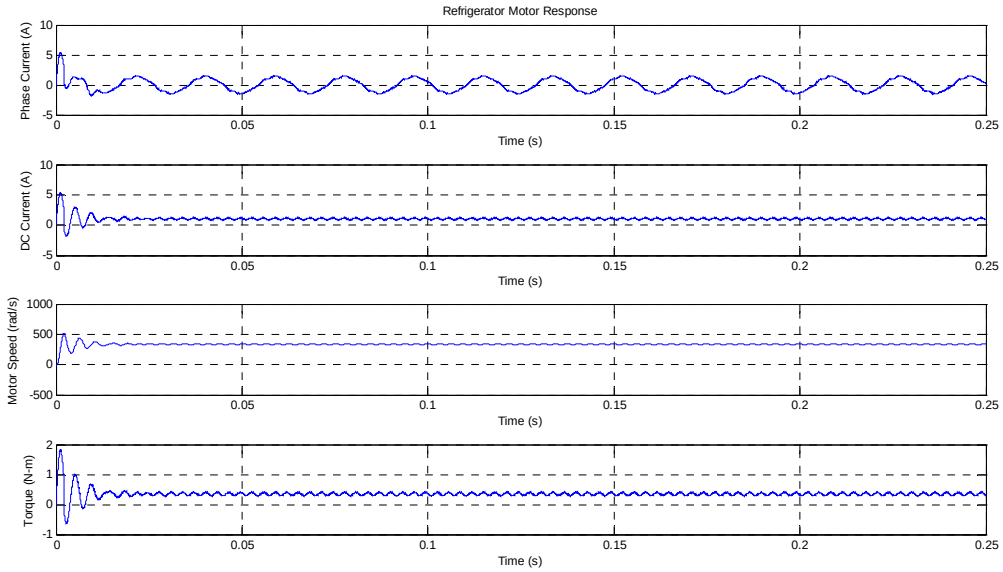

Figure 44. Refrigerator Motor Response.

As can be seen from the figure 44, the BLDC motor demands an inrush current, which varies from 2-12 times the nominal current. This is a typical characteristic of a three phase

motor. This transient can be seen in figure 42, and is the main reason for the transient at the battery current. Demanding higher amounts of currents for short periods of time damages the electrochemical cell inside the battery (figure 43), decreasing battery efficiency and life cycle, since batteries for renewable applications are designed to provide low currents over long periods of time. Furthermore, the transient in the PV system (current) extends to the battery bank (since the battery voltage depends on the bus currents).

The DC Ripple in the load current, which is also reflected on the DC current, is produced by the BLDC motor, due to the linear relationship between torque and current. The sinusoidal PWM of the BLDC motor produces a small ripple in the torque, which extends to the DC current. Since the bus voltage depends on the bus currents (figure 43), this ripple propagates through the system. Due to the fact that wiring resistances are being taken into account, the actual voltage that feeds the motor contains more ripple, and is less in magnitude. The ripple on the battery voltage is measured to be $6mV_{p-p}$ (less than 1%) which does not affect nearby loads.

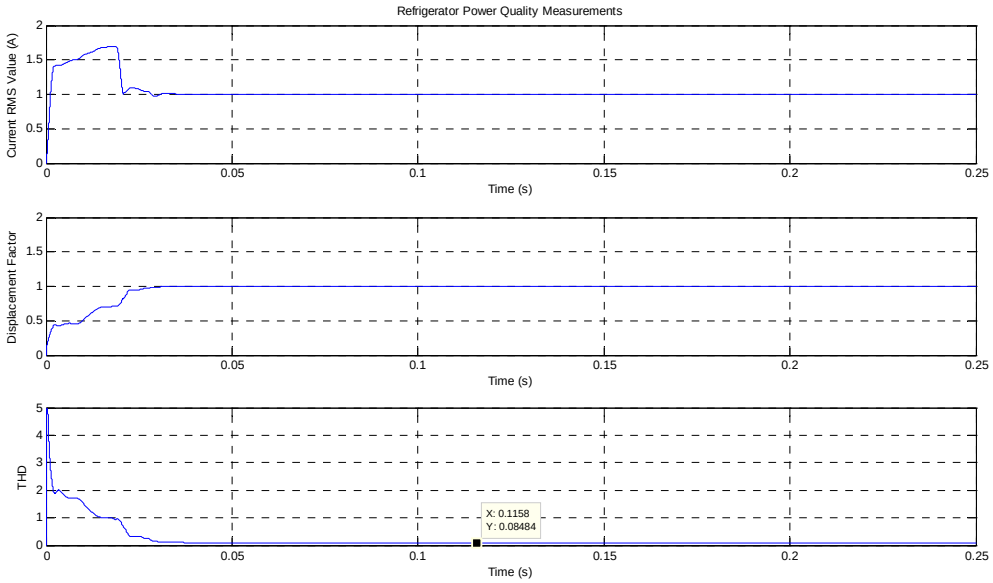

Figure 45. Power Quality Measurements for Refrigerator.

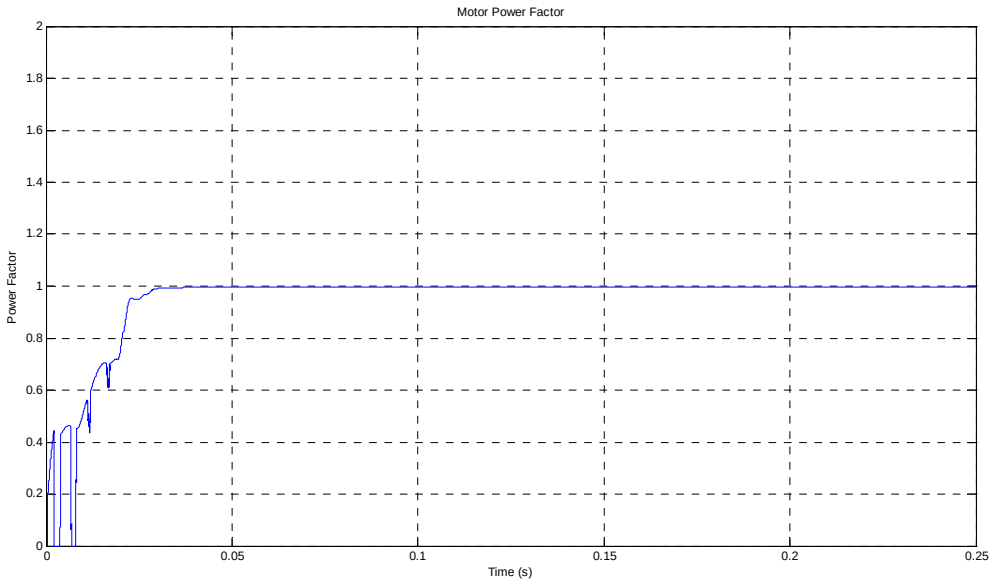

Figure 46. Refrigerator Power Factor.

Figure 45 presents the measurements on the refrigerator, in order to study issues that may arise on loads due to power quality problems in the DC bus. The Current RMS value is computed to be able to compute the displacement factor. Distortion is present in the phase

current of the motor (8.48%) due to the fact that the load torque is low; it will be later demonstrated that as the torque increases, the current waveform distortion decreases significantly. This distortion produces additional rotor heating. Using the MATLAB powergui block, a harmonic analysis of both the current and voltage waveform of the refrigerator has been performed in order to compare the percent of THD with the one calculated by the THD block of Simulink. Figures are shown in Appendix E.

Figure 46 shows the power factor (PF) of the motor, which depends on the load torque; in the cases that the torque is low, PF is unity or close to unity. PF and TPF were computed in order to demonstrate that they are equal when the distortion factor is unity.

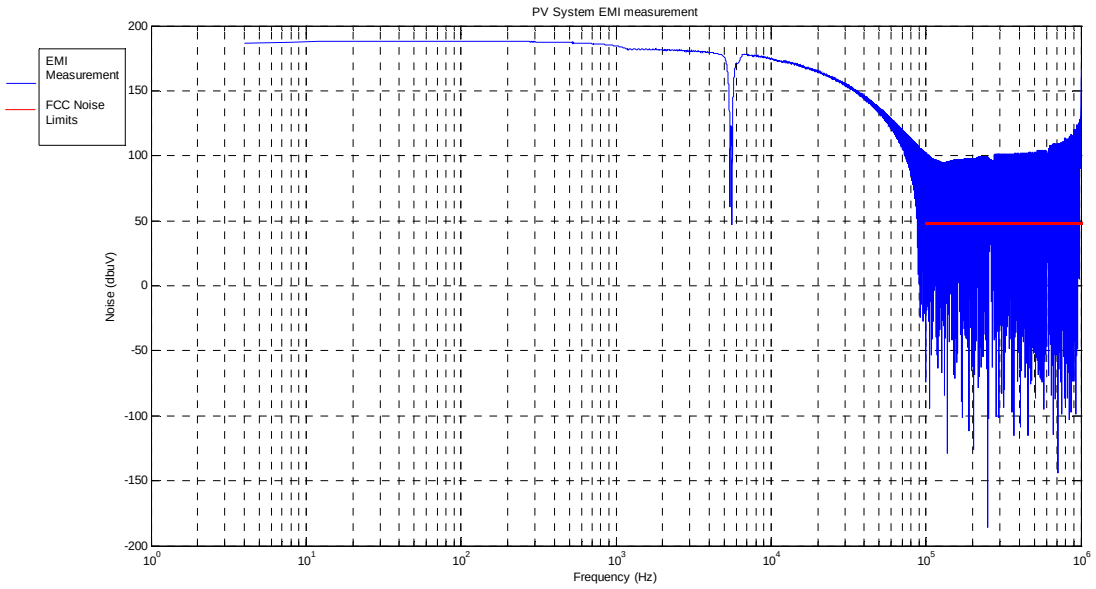

Figure 47. PV System EMI Measurements

Figure 47 above shows the EMI measurement for the PV system. Due to the nature of the DC converter, and the switching frequency involved, EMI is measured between 40-100 KHz. After 0.1 MHz, which is the lower limit at which noise is studied, EMI does not comply with

the FCC limits (shown in figure 47 as the dotted red line). However, in figure 48, the EMI measurements taken for the refrigerator in figure 48 shows that the BLDC motor does comply with the FCC noise emission limits, due to the low ripple in the bus current/voltage.

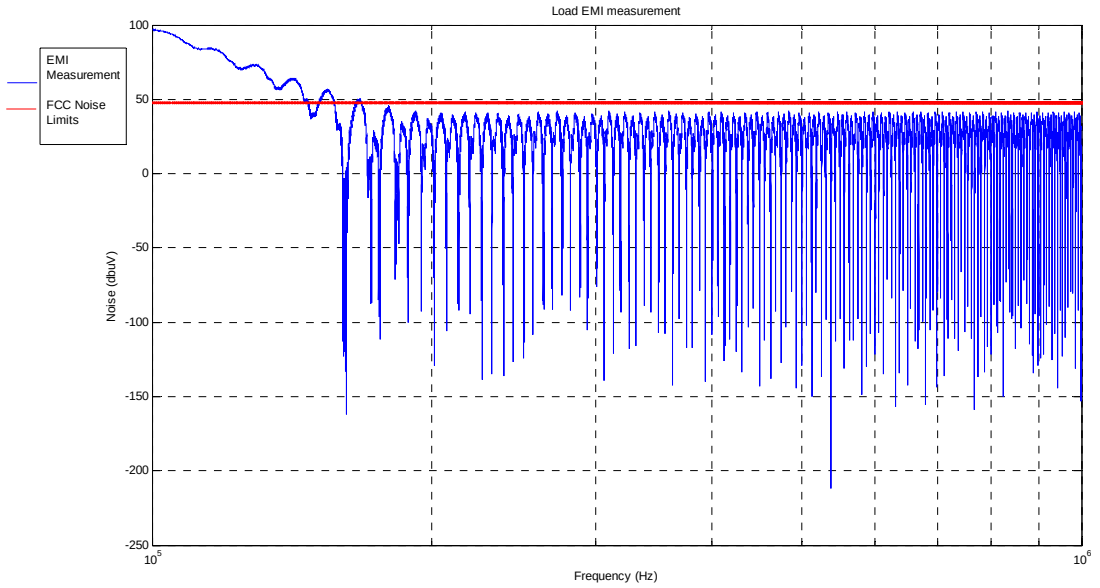

Figure 48. Refrigerator EMI Measurement.

4.2.1.2 Steady State Simulations

Steady State simulations were conducted in order to validate the performance of the SMC. Results are shown below:

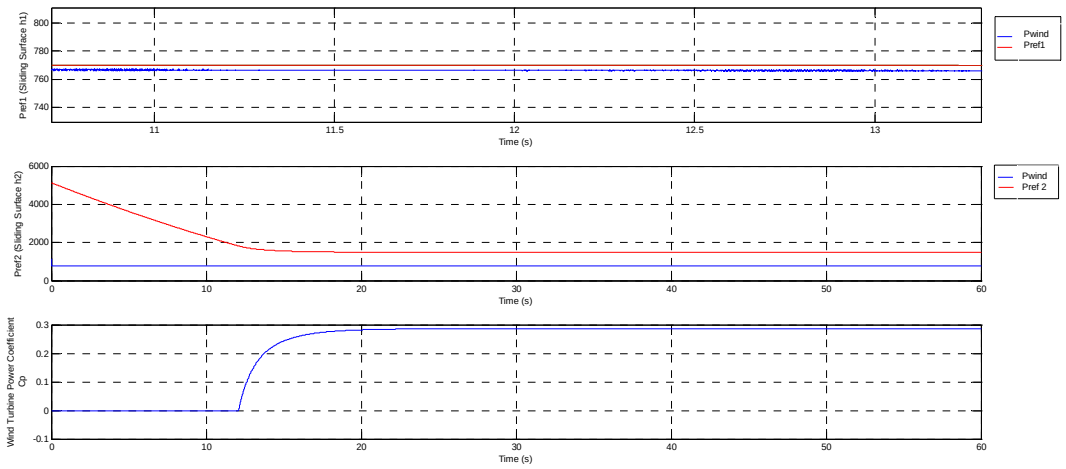

Figure 49. Reference Powers (Sliding Surfaces)

Recalling the information from the SMC for the wind turbine, the system would operate in one of two regions, depending on the wind velocity and the power generated by the WECS. $Pref_1$ corresponds to the sliding surface h_1, which means that the system is operating in power regulation mode. $Pref_2$ corresponds to the sliding surface h_2, in which the wind velocity does not suffices to supply the power demand, and the system extracts the maximum power for the turbine. The shaft velocity, ω_m, is the variable that determines the mode of operation of the WECS. Figure 49 shows that the system follows the power reference $Pref_1$, corresponding to the sliding surface h_1, since the wind velocity is high enough to supply the power demanded by the loads. The system never gets to operate on the

sliding surface h_2, since the system never follows the reference power $Pref_2$. After 10s, when $Pref_2$ stabilizes, the system starts regulating the power from the wind turbine. The wind turbine power coefficient will depend on the load power demand.

4.2.2 Case II

4.2.2.1 Transient Simulations

Simulation is conducted in order to study power quality issues at the DC bus and on loads, when people actually arrive to the residence and start using appliances. The time window for simulation is from 6:00pm-10:00pm; solar irradiation values are considered to be very close to zero, while the corresponding wind velocity values for this time window can be found in Appendix C. During the first part of the simulation, the only load present in the system is the refrigerator, along with phantom loads; after 0.10s, the AC unit, ceiling fans (3) and resistive loads such as light bulbs and the stove become active.

Results:

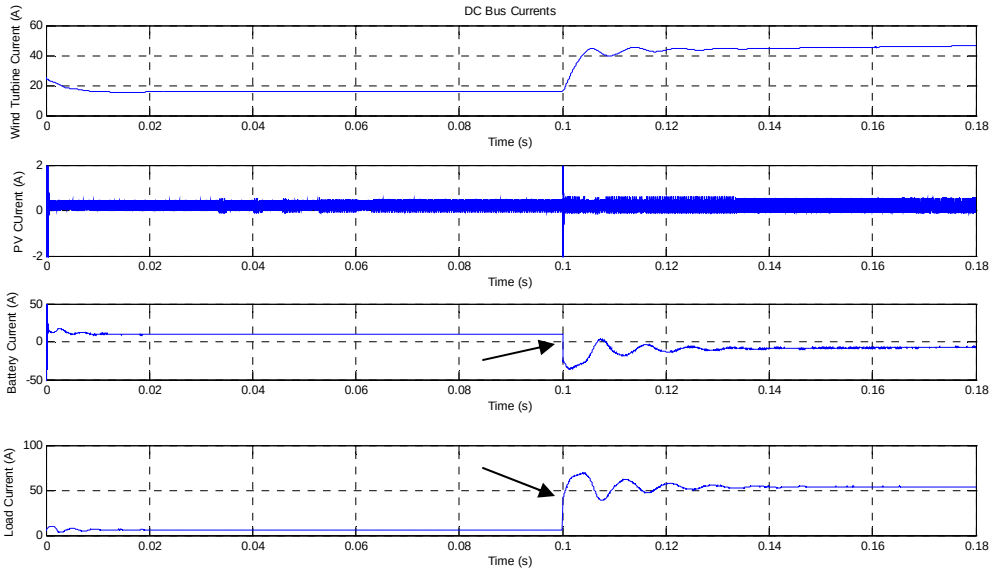

Figure 50. DC Bus Currents

Figure 50 shows the DC bus currents. Due to very low values of solar irradiation used in the simulation, the PV system control achieves MPPT; however, a considerable ripple in the PV current can be observed. At 0.10s, after the loads become active (depicted by the black arrows in the battery and load currents), the increase in current demand from the loads shows an instant increase in the turbine current as a result of the turbine control, in order to maintain all loads supplied (maintain power balance in the system). It is important to note, that, for all cases simulated, the wind turbine is not capable of supplying the load demand rapidly, neither power balance is achieved by means of the turbine current if there is not enough wind velocity. This is why steady state simulations are shown, in order to properly observe the turbine control behavior. If there is the case where the wind velocity is not enough to satisfy

the power demand from the loads, the battery must supply the current that is not supplied by the renewable sources in order to achieve power balance.

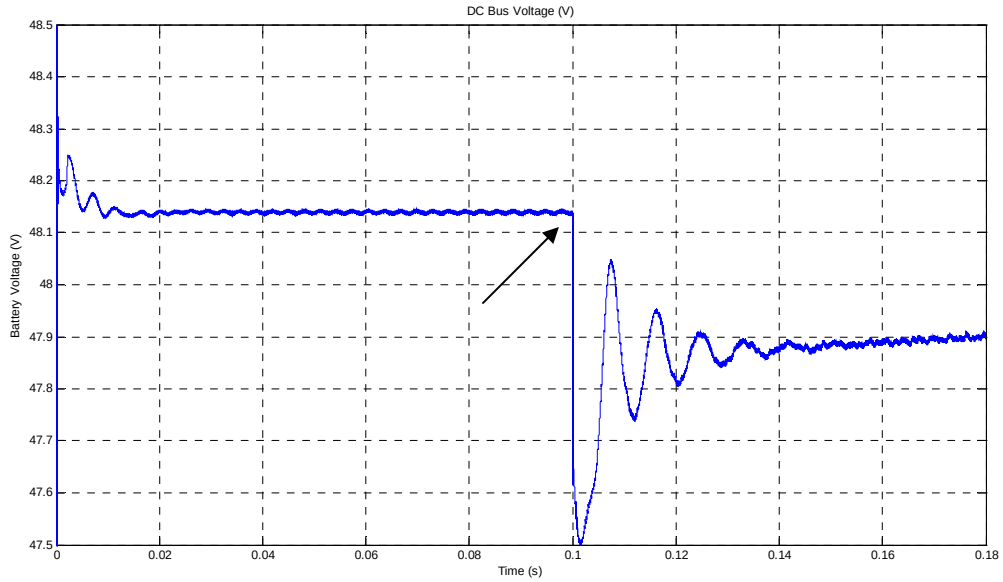

Figure 51. DC Bus Voltage

At 0.10s, the inrush current demanded by appliances becoming active (AC unit and ceiling fans, denoted by the black arrow) produces a transient in the battery voltage (figure 51), due to the high current demand at that instant. There is an instant variation of 0.8V due to the decrease in the PV system current and the increase in the wind turbine output current, and as a result, the voltage at the bus does not stabilizes. For this case, the measured voltage fluctuation is $6mV_{p\text{-}p}$ before 0.10s, and increases to $10mV_{p\text{-}p}$. This is less than 1%, which results in no flicker problems for this case.

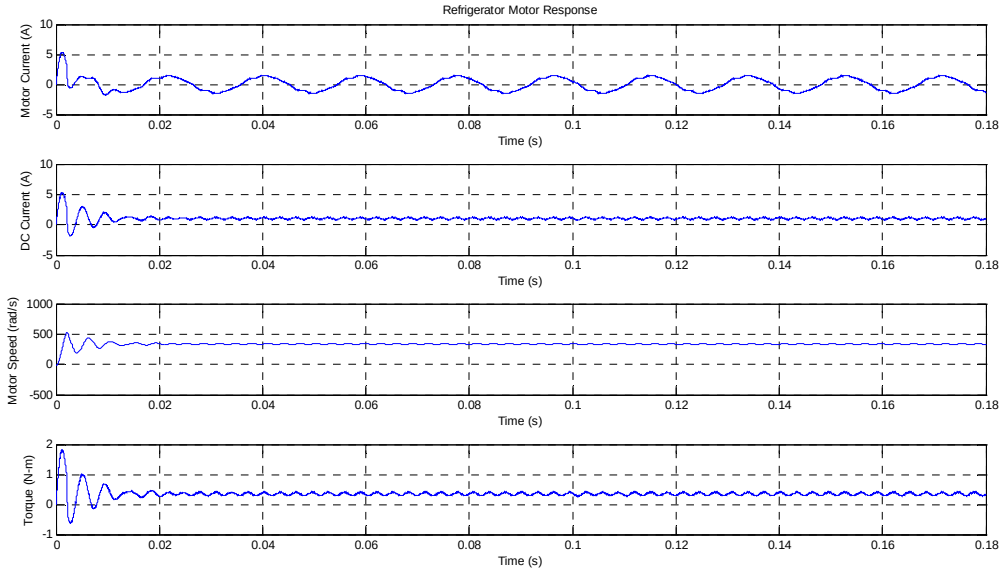

Figure 52. Refrigerator Motor Response.

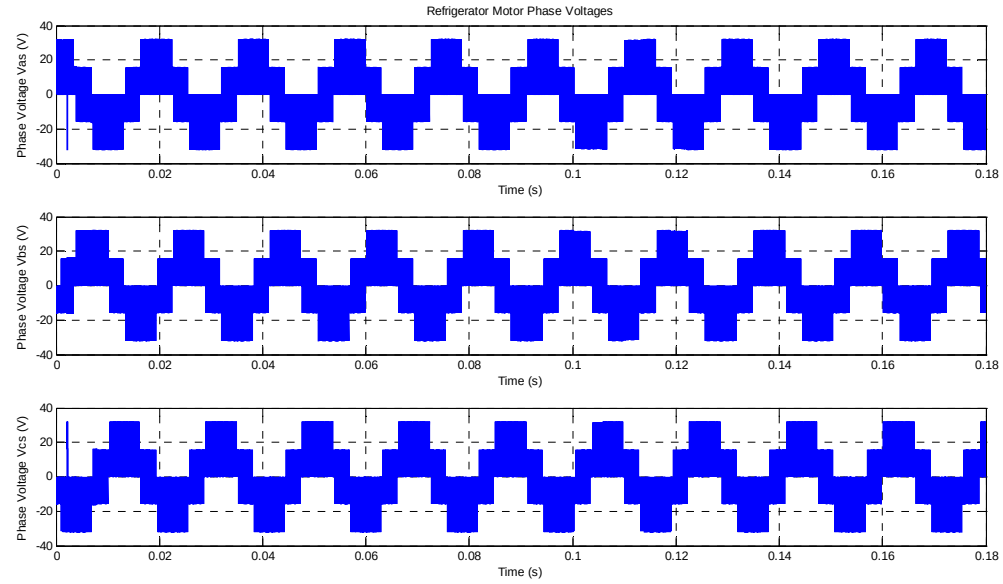

Figure 53. Refrigerator Motor Phase Voltages.

Figures 52 and 53, corresponding to the response of the refrigerator motor before and after the disturbance in current and voltage from the DC bus, shows that the refrigerator is

very robust, the perturbation in the system is minimal, and is best viewed in the motor speed response. This is due to the carrier wave frequency used for the BLDC SPWM control, which is 50 KHz. When this frequency is very low, loads with motors are sensible to variations in the input voltage/current from the DC bus.

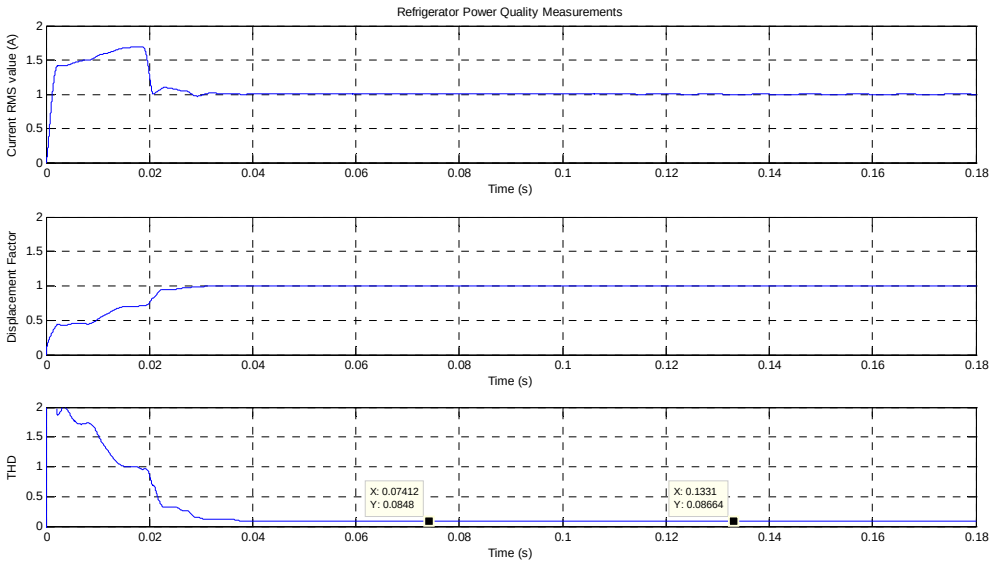

Figure 54. Power Quality Measurements for the Refrigerator Motor.

Figure 54 presents the power quality measurements for the refrigerator motor before and after the disturbance in the DC bus. The perturbation in the RMS value of the current is minimal; the DF is not affected at all since, it explicitly depends on the RMS value of the current, it implicitly depends on the control of the motor; and the perturbation (voltage sag) of the motor, which is barely seen in figure 53, is almost minimal. However, an increase in current (and voltage) ripple in the DC bus due to motor loads becoming active after 0.10s presents an increase in THD of 0.18 %.

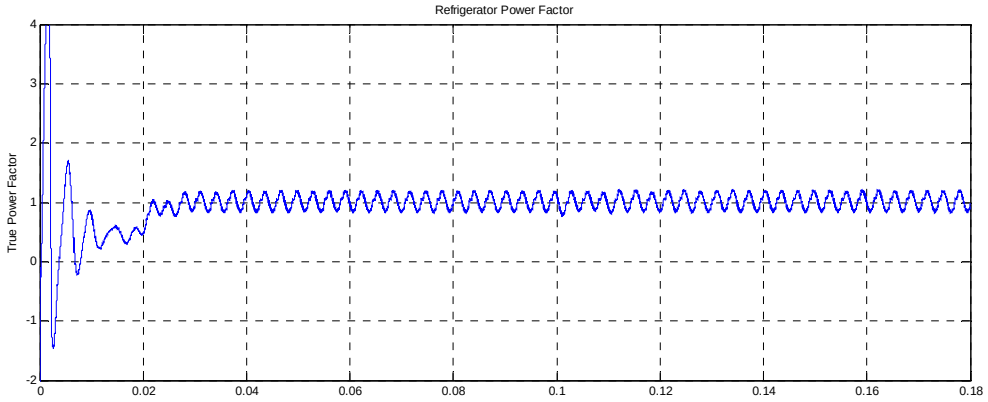

Figure 55. Refrigerator Motor Power Factor, Case II.

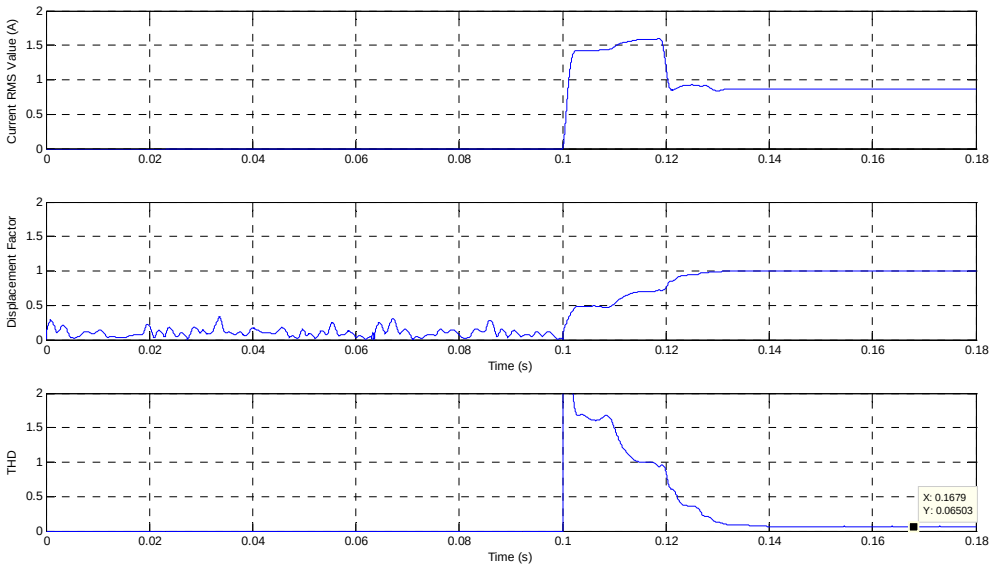

Figure 56. Power Quality Measurements at the Ceiling Fans.

Figure 55 shows the unity PF for the refrigerator motor. Again, figures for both the TPF and DF are shown to prove that the DF is unity.

Figure 56 presents the PQ measurements for the ceiling fans. Before 0.10s, the ceiling fans are inactive, which means that values for THD, DF and Current RMS are zero or close to zero. The 6.50% Current THD is lower than the refrigerator value, but is bigger if it were to be compared to the THD value when connecting this appliance alone.

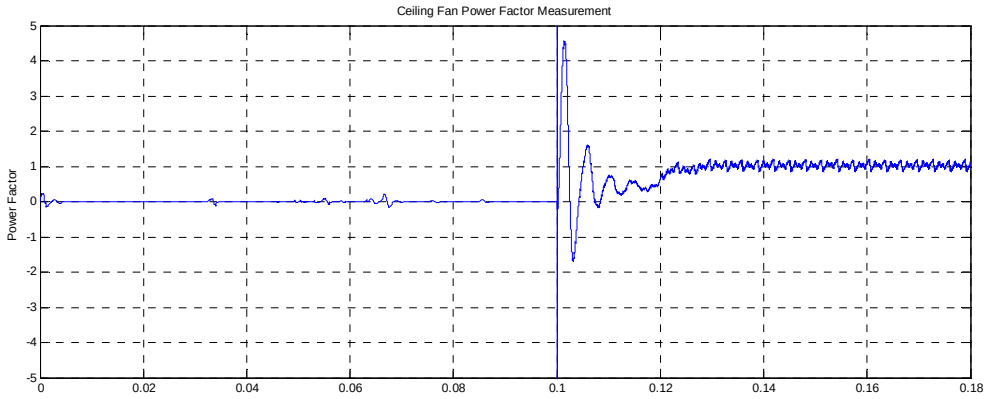

Figure 57. Ceiling Fan Power Factor.

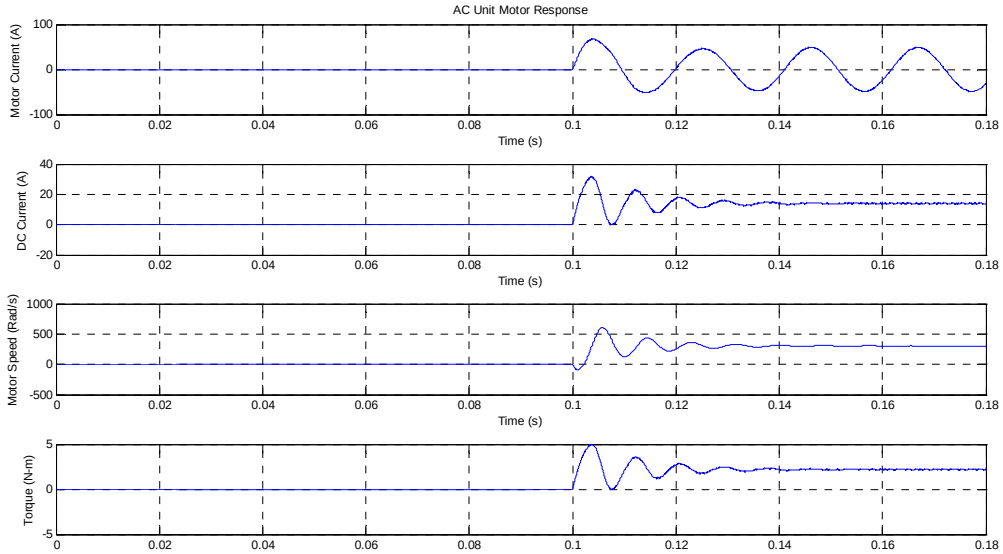

Figure 58. Air Conditioning Unit Motor Response.

Figure 58 above presents the motor response for the AC unit. Due to the fact that the load torque is higher for this appliance, the phase current presents less distortion (decrease in THD) and less ripple in the DC current. A higher load torque means that the motor frequency will be lower, compared to other motors with lighter loads. The decrease in motor frequency can be seen below in figure 59, and the THD measurement can be seen in figure 60. Figure 59 proves the statement made that when load torque is higher, the THD% is lower.

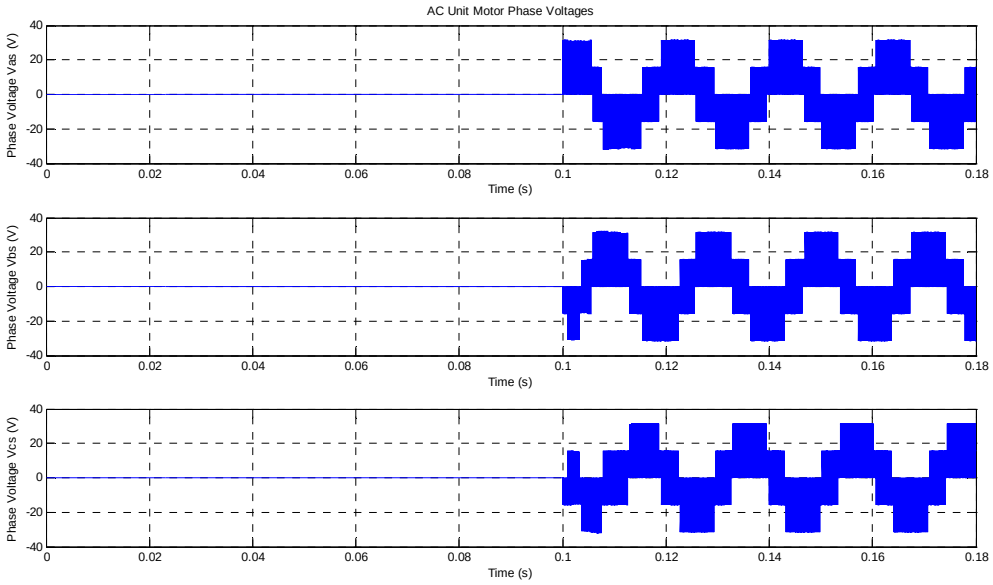

Figure 59. Air Conditioning Unit Motor Phase Voltages.

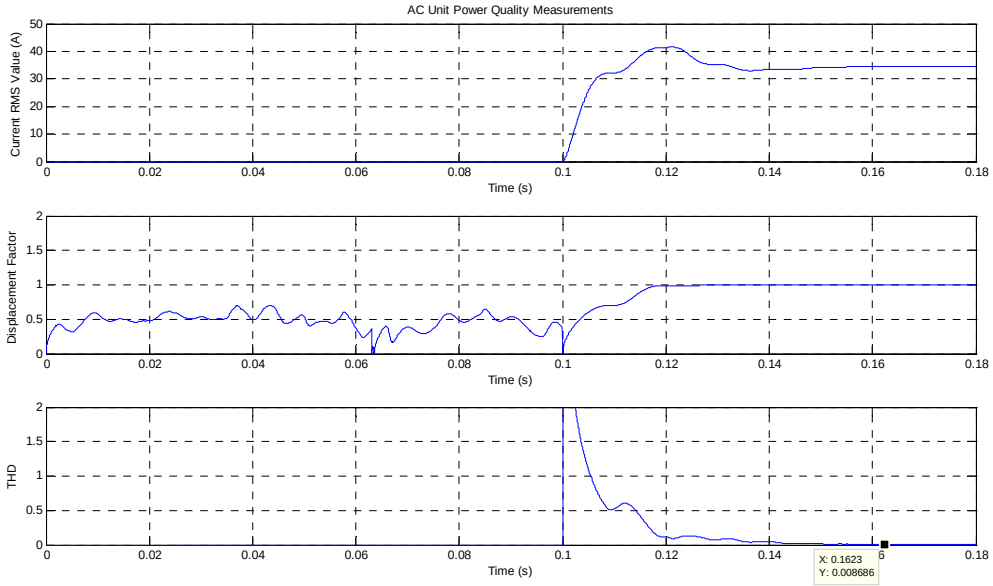

Figure 60. Power Quality Measurements for the AC unit Motor.

The AC unit power factor has been calculated in simulations; it has a value of 0.8. This is due that the power factor of brushless DC motors is not unity when the motor is nearly or fully loaded (value is close to the nominal torque load value).

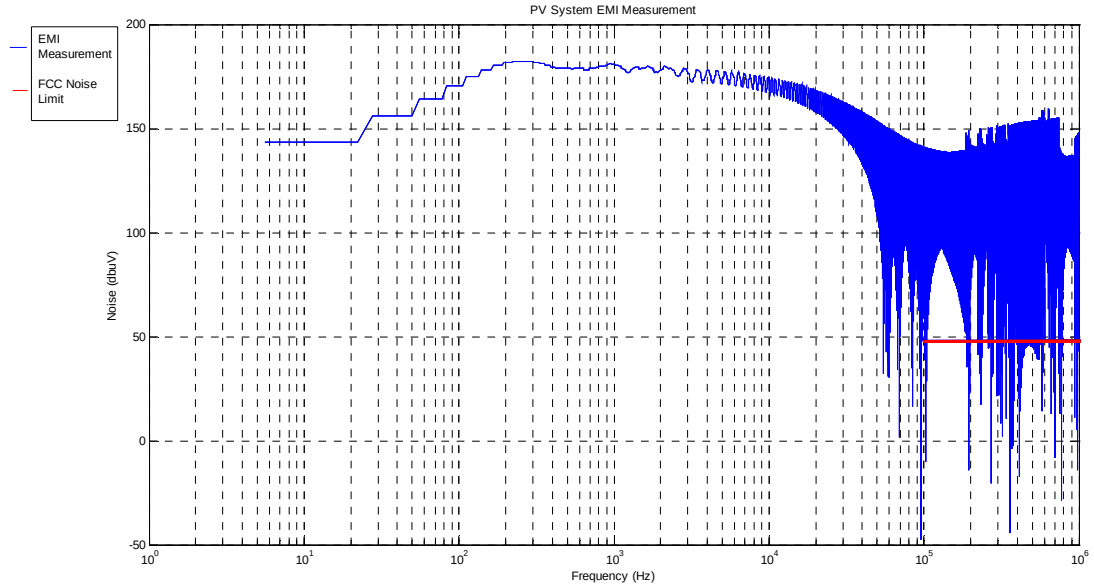

Figure 61. PV System EMI Measurement.

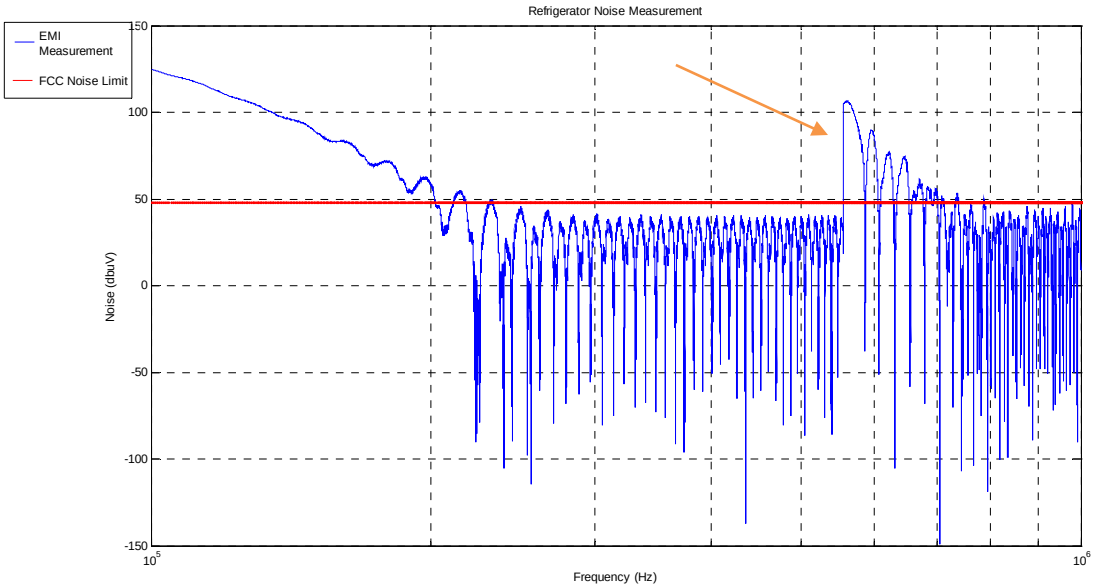

Figure 62. Refrigerator EMI Measurement.

PV System and Refrigerator EMI measurements are presented in figures 62 and 63. PV noise increases significantly compared to the EMI PV measurement from case I since after

6pm the solar irradiation value is considered to be 0; the effort of the MPPT control to drive the error signal to zero under no conditions of solar irradiation produces the noise observed in the operating point (namely current and voltage) of the PV system, increasing noise. Furthermore, the use of the dc/dc converter also contributes to the noise observed. A peak is present between 0.5 and 0.7 MHz in figure 63 due to the fact that the refrigerator is the only load that is always active in the simulation. As a result, load activity (loads becoming active or inactive, depicted by the orange arrow) will contribute to peaks in the EMI of appliances active at that moment. Noise limits are met due to the low ripple in the bus voltage and currents.

4.2.2.2 Steady State Simulations

Steady state simulations are presented in order to study the wind turbine controller behavior. The same solar irradiation, temperature and wind velocity parameters used in the transient analysis are applied in the steady state case. Results are shown below:

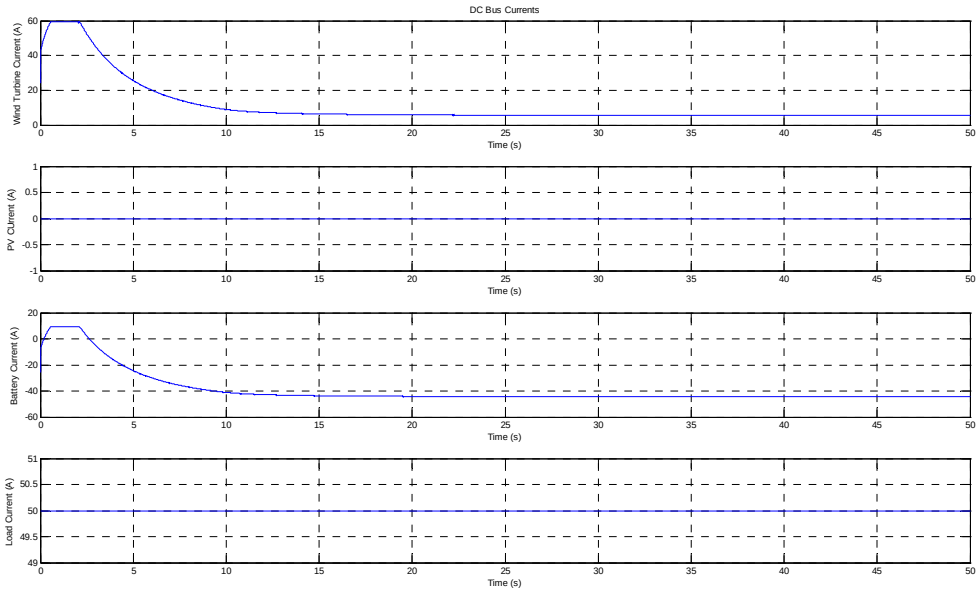

Figure 63. DC Bus Currents for Case II, Steady State.

Figure 64 shows the DC bus currents. Contrary to the results in Case I, it is clearly shown here that, under load variations, the wind controller's first response is to maintain power balance at that moment. Until the wind controller recognizes if it is able to supply the power demand with the wind input, the system will show that the power is correctly balanced. In this case, the wind velocity does not suffice to supply the power demand from the loads (due that there is no contribution from the PV system due to the absence of solar irradiation). As a result, a negative value of battery current is shown, meaning that the battery must supply part, if not all, of the power demand. The constant demand of load current, in turn, decreases the battery voltage.

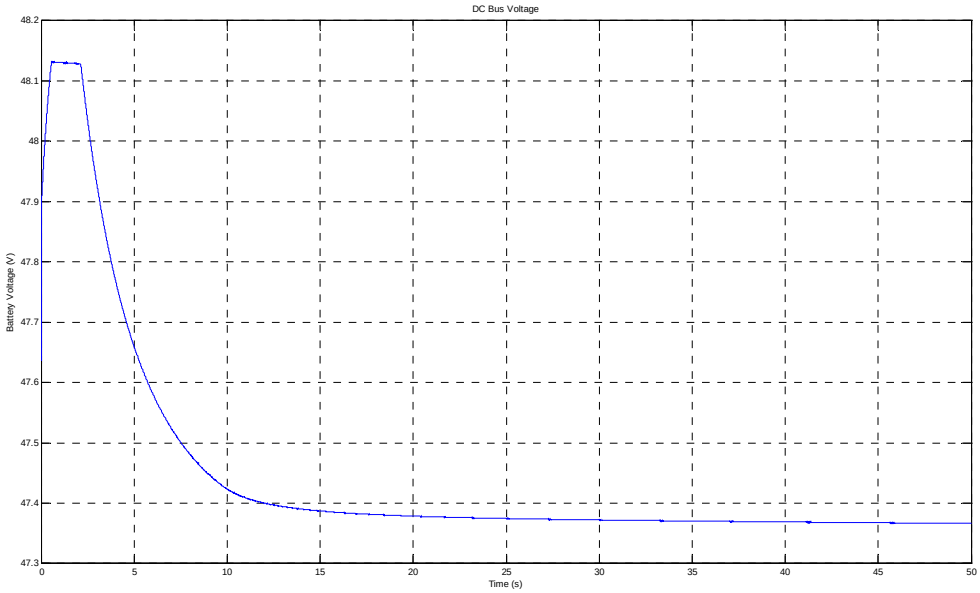

Figure 64. Battery Voltage for Case II, Steady State.

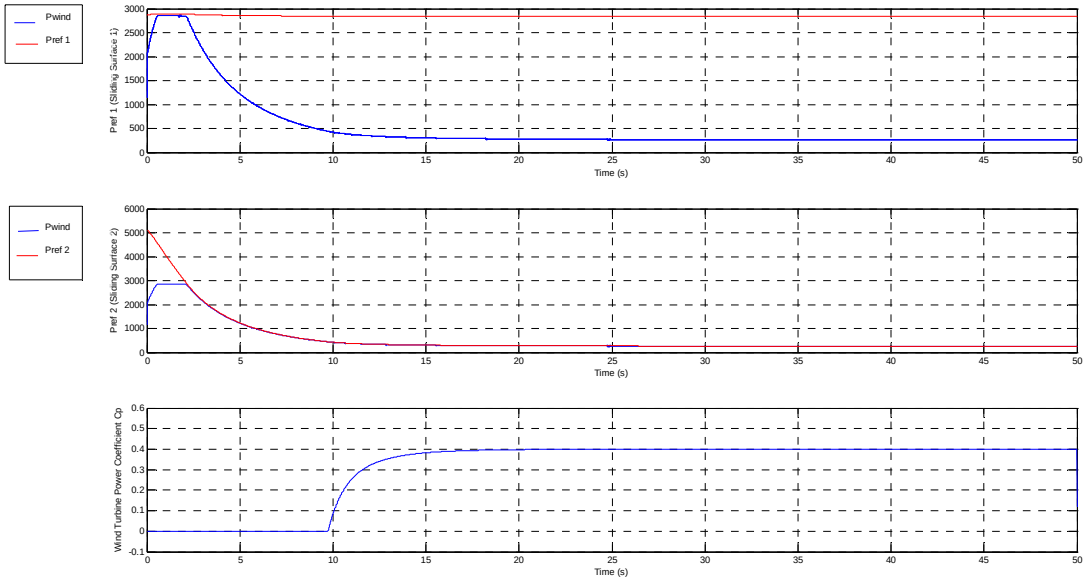

Figure 65. Reference Powers and Sliding Surfaces.

Figure 66 presents the reference powers corresponding to the system sliding surfaces. On the first seconds of simulation, the system follows the power reference P_{ref1}, corresponding to the sliding surface h_1 (power regulation mode). After around 3s, the system starts following the reference power P_{ref2}, which corresponds to the MPPT , due to the fact that

the shaft velocity ω_m is lower than the limit shaft velocity ω_{mSW}. After the power references stabilizes at 10s, the system extracts the maximum power from the wind turbine (operating in sliding surface h_2). This clearly shows the second operation mode of the controller.

4.2.3 Case III

4.2.3.1 Transient Simulations

For this scenario, the following information applies:

1. Data window used in this simulation corresponds from 8:00am to 9:00am.
2. Load profile is as follows: The cloth washer, refrigerator and laptop computer will be active during all the simulation. A step change in the load torque of the cloth washer is done to represent the change from washing cycle to the spinning cycle, at 0.08s (denoted by the orange arrow). For the first 0.05s, resistive loads (oven, lighting, stove) are active. After 0.05s, all resistive loads become inactive. At 0.12s, the TV and microwave become active. Both load changes are depicted in figure 66 by black arrows.

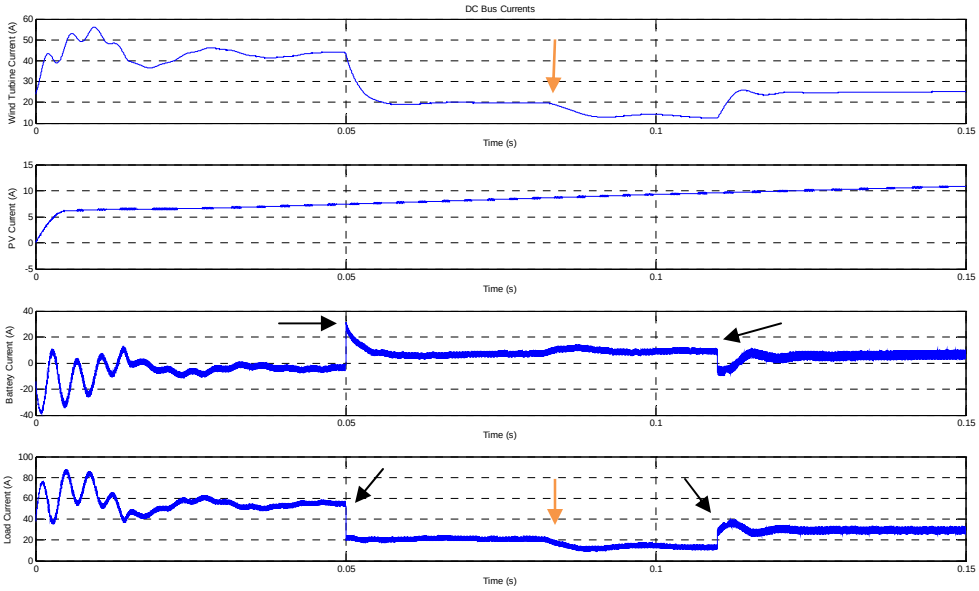

Figure 66. DC Bus Currents, Case III.

Figure 67 above shows the DC bus currents in the load profile above specified. The transient in the load voltage is due to the inrush current of the cloth washer. This current is reflected back at the input of the FB DC converter, which makes it propagate through the DC bus, and into the wind turbine. The PV current solar irradiation and temperature is varying, which explains the increasing current of the PV system. Large ripple can be observed both in the bus currents, and in the bus voltage, due to the fact that the synchronous buck converter switch (used in the laptop and LCD TV model) is connected to the input of the battery voltage; this will prove to be the main cause of the measured EMI at the loads. The ripple further increases at 0.12s, when the LCD TV is turned on. There is a current spike at the battery current at 0.05s, corresponding to the turn off of the resistive loads; the higher the current the active appliance demands, at the moment of turning it off, the higher the voltage /current peak. This is seen in the battery current figure, where there is a sudden increase in

current at 0.05s. The decrease in wind turbine current at 0.08s is due to the cycle change of the washer (from washing to spinning). It is important to note that, during the washer start up, the battery is not able to deliver the rapidly varying current from the battery. Constant and repeated exposure of the battery to this type of load with high inrush current, at a long term, will damage the battery, reducing its life cycle. Transients in the current also create the transients seen in the battery voltage, figure 68. The ripple measurement is about 200-250 mV_{p-p}, which produces considerable ripple and noise.

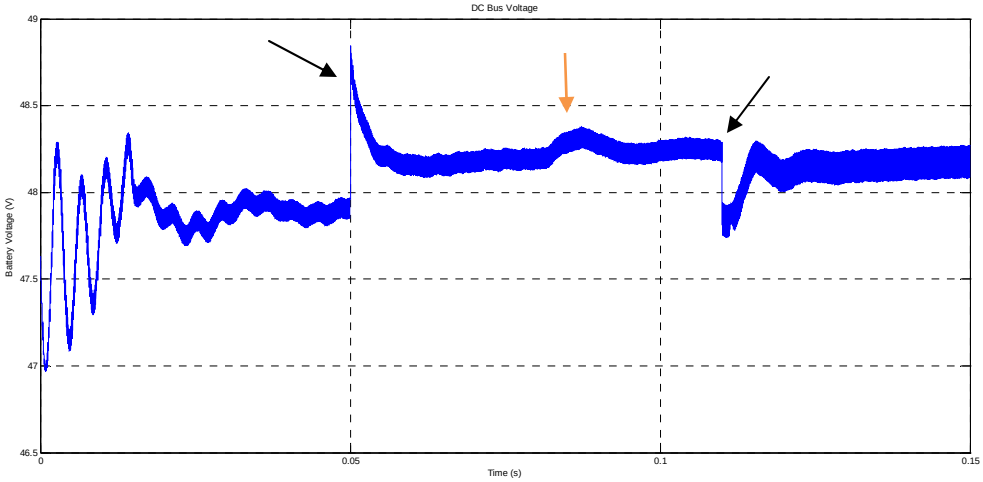

Figure 67. DC Bus Battery Voltage, Case III.

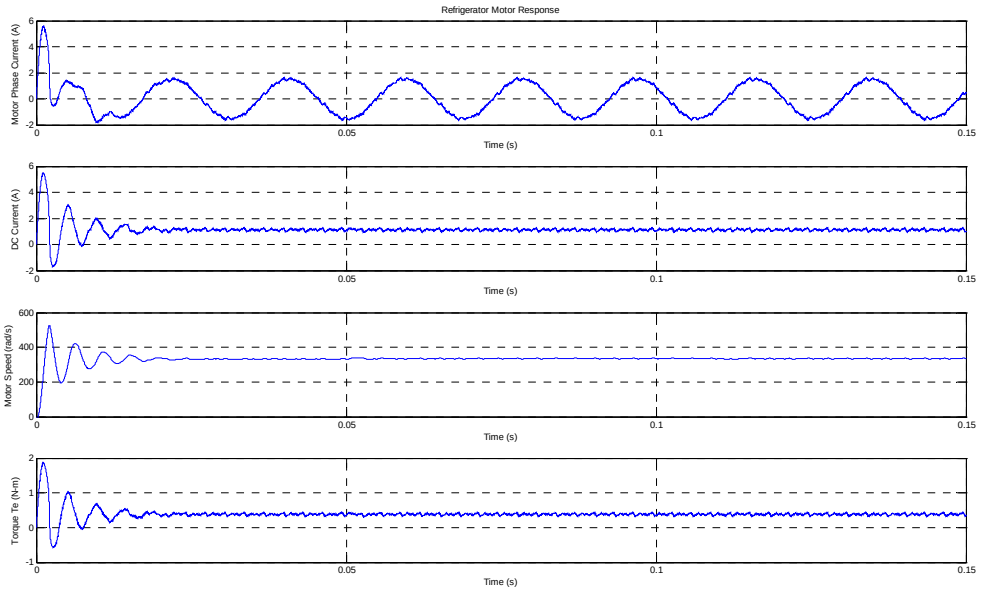

Figure 68. Refrigerator Motor Response, Case III.

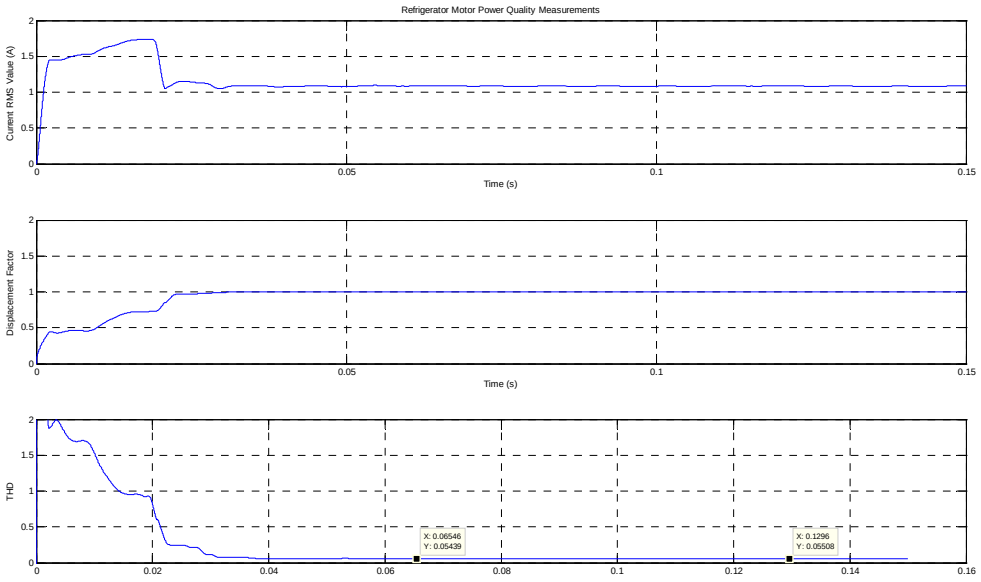

Figure 69. Refrigerator Power Quality Measurements, Case III.

Figure 69 shows the refrigerator motor response. This figure is shown once again to prove that loads incorporating BLDC motors with SPWM control are not easily perturbed, even

when the battery voltage exhibits high amount of ripple and various perturbations. Figure 70, which depicts the power quality measurements, shows an increase in THD after 0.12s. This, again, corresponds to the current ripple produced by the LCD TV synchronous converter.

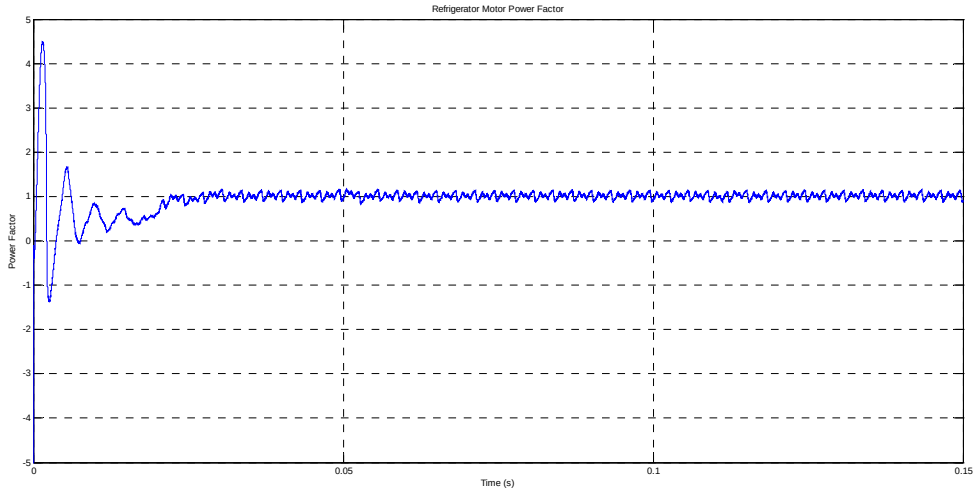

Figure 70. Refrigerator Power Factor, Case III.

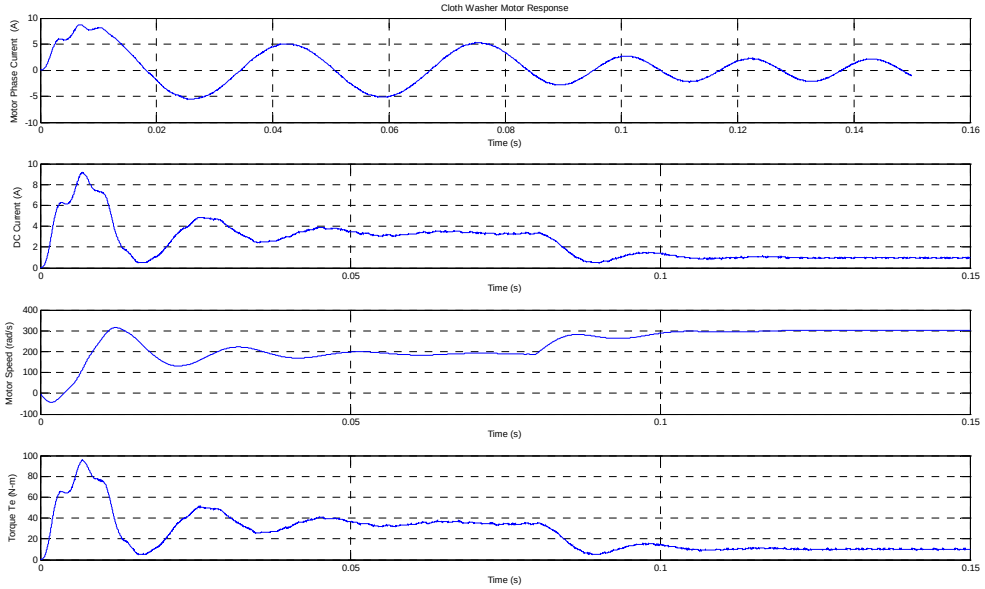

Figure 71. Cloth Washer Motor Response, Case III.

Figure 72 and 73 depicts the cloth washer motor response. The phase voltages of the motor, shown in figure 73, are affected by the current transient; this is due to the characteristics of the motors, especially the inertia. The calculation of the rotor position in the BLDC motor depends on the inertia. The rotor position is needed to calculate the inverter voltages and currents. A higher inertia means that the system will have a slower dynamic response. When the motor is highly loaded, as in the washing cycle, the BLDC motor system frequency decreases. When the washer changes from cycles, the motor frequency increases, increasing the motor speed and response as a result.

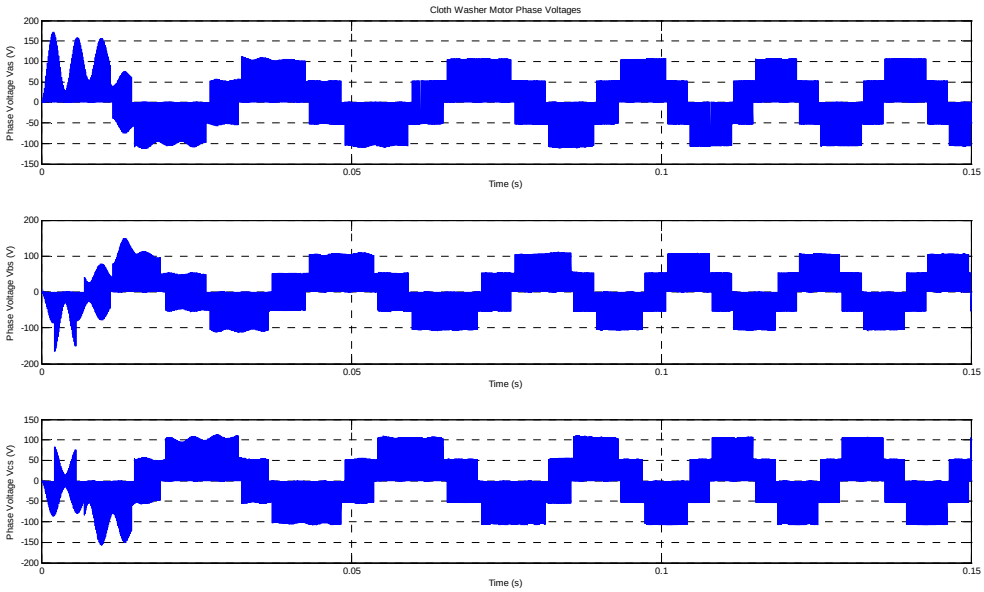

Figure 72. Cloth Washer Motor Phase Voltages.

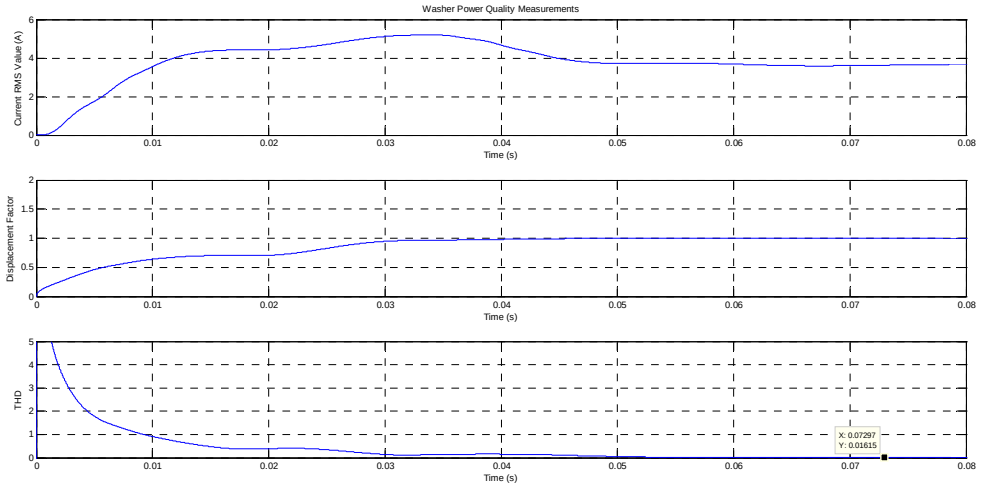

Figure 73. Washer Power Quality Measurements.

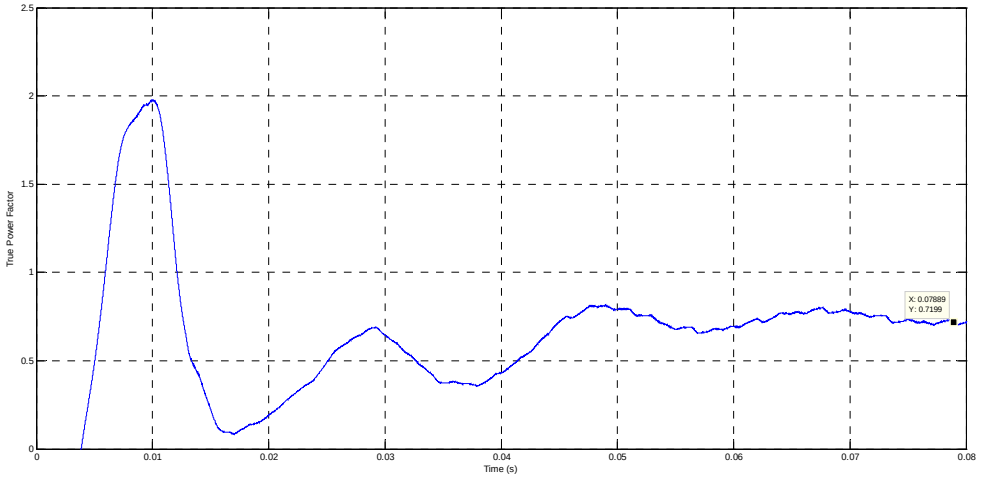

Figure 74. Cloth Washer Power Factor.

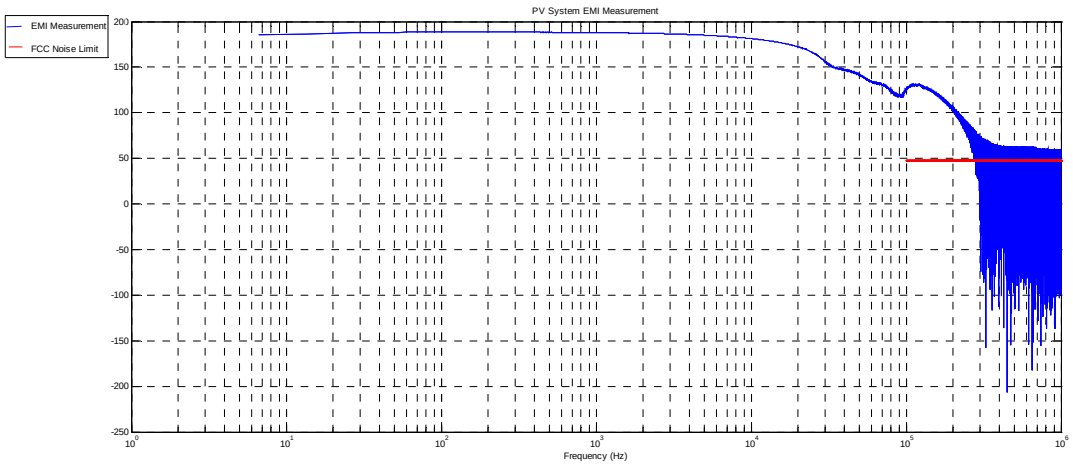

Figure 75. EMI measurement for the PV system.

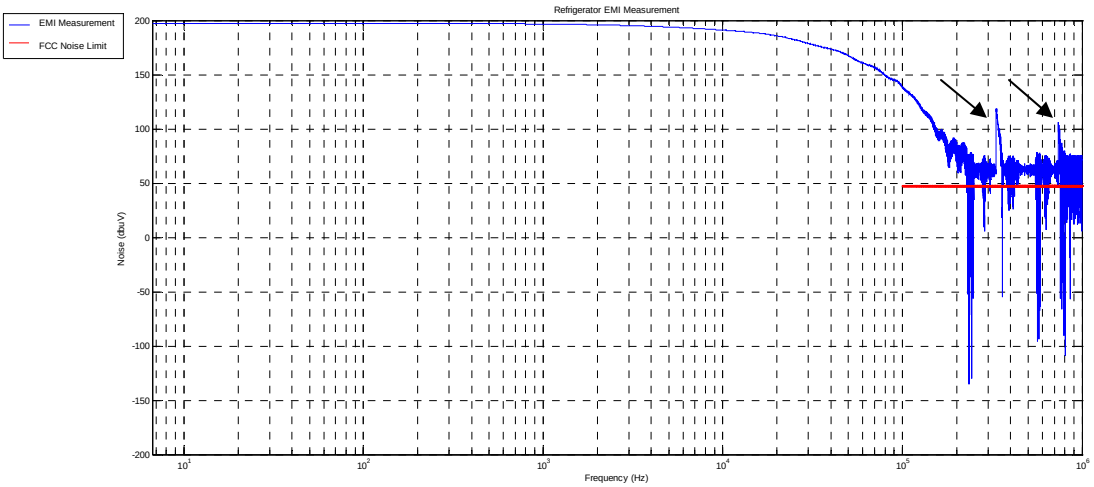

Figure 76. Refrigerator EMI measurements.

Figure 76 shows the EMI measurement for the PV system. Figure 77, which shows the EMI measurements at the refrigerator, shows noise peaks due to the laptop computer synchronous buck converter. Between 0.2-0.3 MHz, a noise peak is observed due to the removal of the resistive loads from the system; the second peak, present at 0.7-0.8Mhz, is due to the LCD TV load becoming active (all load changes depicted by the black arrows in figure 76). Another synchronous converter connected further increases noise levels. Periodic

peaks can be observed at the converter due to periodic switching of the MOSFETS of the DC/DC converter.

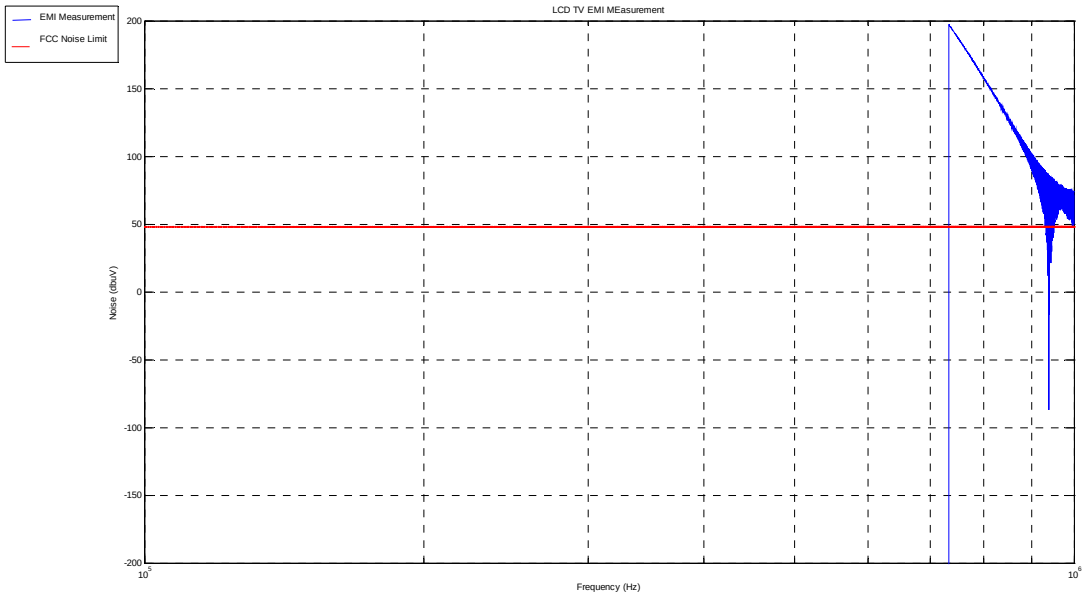

Figure 77. LCD TV EMI measurement.

Figure 78 shows the EMI measurement of the LCD TV. The peak, observed from 0.7-0.8 MHz, is due to the TV becoming active. After becoming active, noise is measured to be above the level of the FCC limit for noise, shown as the red dotted line. A peak is observed, again due periodic switching of the MOSFETs. Noise measurements on other loads show similar results, and these can be seen at appendix E.

4.2.3.2 Steady State Simulations

The results obtained for the steady state simulations are very similar to the results of Case II in steady state. As a result, the figures corresponding to the results are presented in appendix E.

4.2.4 Simulations with Net Metering

As part of the contribution of this research, simulations where the RES is interconnected with the utility grid results are conducted in order to study any possible power quality issues. Simulations presented below correspond to the same simulations done in sections 4.2.1 to 4.2.3, with the addition of the VSI inverter, and the calculation of the current used for grid injection purposes. Injection to the utility grid will be considered only on times where the load is minimal; at any other time, the system will be always supplying power to the battery bank. The inverter is interconnected to the utility grid after 0.1s, in order to allow the synchronization of the inverter and grid voltages.

4.2.4.1 Case I Results:

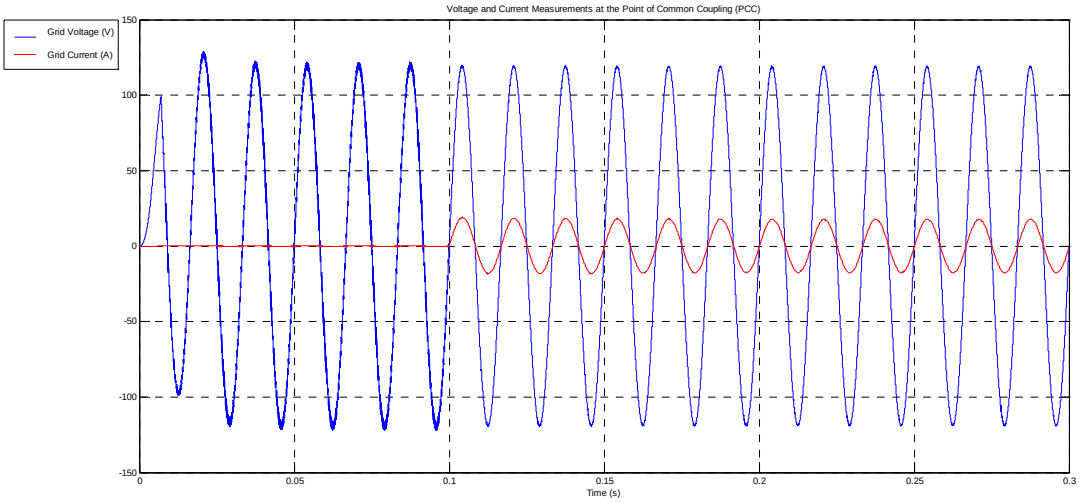

Figure 78. Current and Voltage Measurements at The PCC.

Figure 79 depicts the grid voltage and current at the PCC. As explained before, the inverter output voltage must be slightly higher in magnitude than the grid voltage in order to create power flow from the inverter to the grid. This is clearly shown above, since at the instant the inverter is connected to the utility grid, the grid current waveform is a positive sine wave. Since the measurement of the grid current is being done from the PCC into the grid, the grid current must have the same polarity than the grid voltage. Furthermore, both the grid voltage and current are completely in phase one with another, meaning an unity power factor.

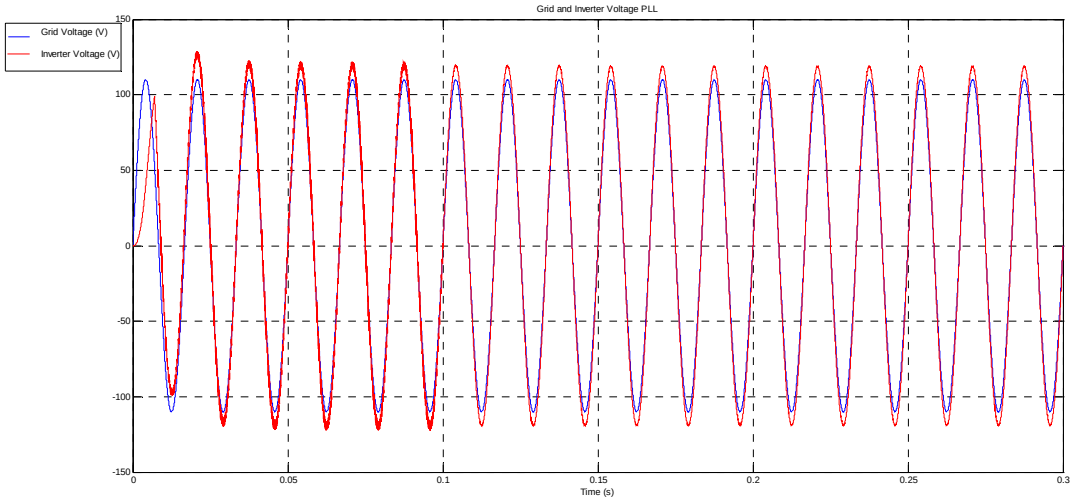

Figure 79. Grid and Inverter Voltages Synchronized.

Figure 80 presents the inverter and grid voltages. During the transient response of the inverter, a peak can be observed. This is due to synchronization process between the inverter and the utility grid. The peak produces a high control effort during a small period of time, which is likely to cause malfunctioning in some components due to this high control. A saturation block has been placed at the control signal, in order to represent simulations closely resembling real life scenarios. Results show that due to the placement of the saturation block, the synchronization does not occur in an instant.

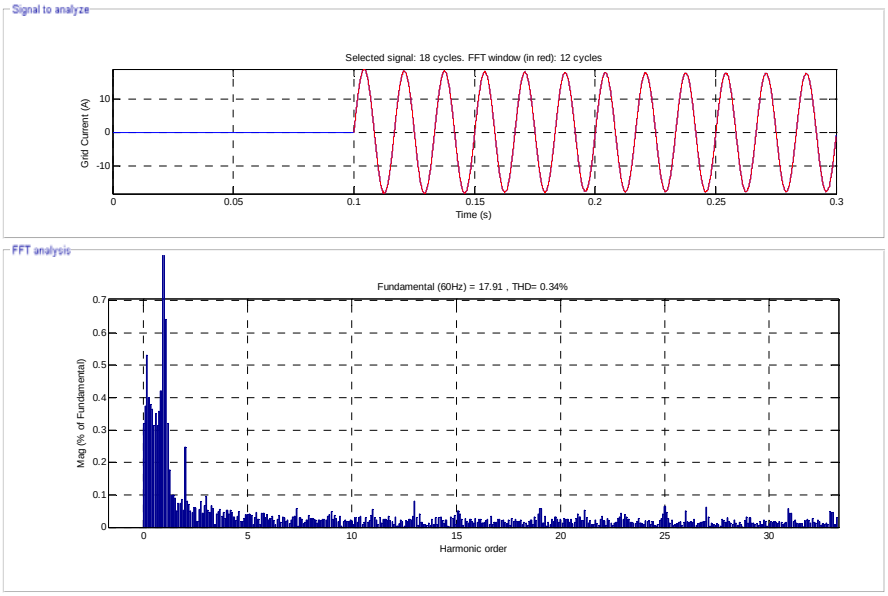

Figure 80. THD and Harmonic Analysis for the Grid Current waveform.

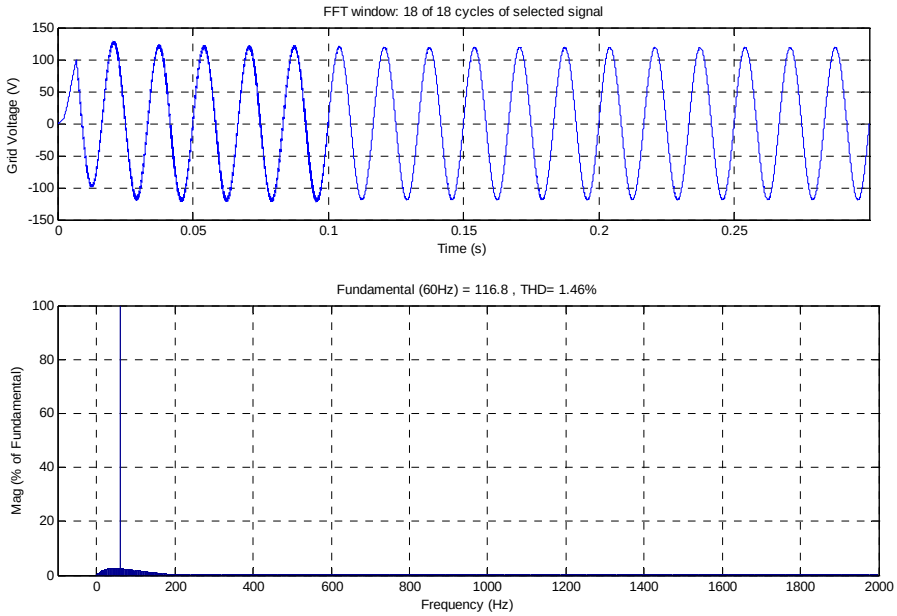

Figure 81. THD and Harmonic Analysis of the Grid Voltage at the PCC.

Figure 81 and 82 show the THD for both the voltage and current at the PCC. Both levels are below the limit of distortion for both currents and voltages.

4.2.4.2 Case II Results

Net Metering simulations for case II are not conducted, due to the fact that during the time window considered during the second simulation, which is after 6pm, the primary source that is considered to inject power into the utility grid is not producing any power. Furthermore, results from steady state simulations from case II shows the need of power from the battery bank to supply the power demand that is not able to be supplied by the WECS. As a result, no simulations will be conducted for this case, since the scope of this work is to study cases in which there exists a possibility of power excess injection into the utility grid.

4.2.5 CONCLUSIONS:

There is a tradeoff when trying to redesign current AC appliances in order to make them suitable to be powered up by DC power. For low power application appliances, an overall reduction of system components reduces the appliance overall cost. The microwave oven is the most difficult load, due to both its advantages and disadvantages: for one side, though the power consumption is lowered, the current consumption of this appliance is very high, demanding its own dedicated circuit for a DC residence; for the other side, the high voltage transformer and rectifier can be replaced by a flyback converter, which greatly reduces the number of components. In this specific appliance, the flyback converter incorporates a transformer, meaning that this appliance will still consume power in stand-by mode. EMI stages are still needed in order to comply with the FCC class B specifications.

Loads for high power applications present a problem when modified to work with a DC supply; there is a substantial increase in components. The proposed models here for both cloth washers and dryers must convert from DC to AC (single-phase), from AC back to DC (transformer/rectifier) in order to supply the BLDC motor. For these appliances, stand-by losses are not reduced. The many inverter/rectifier stages for the proposed DC model are greater than actual AC drives, which undergo 2 stages: the rectifying stage, the regulation stage (with a boost PFC), and the inverter stage (three phase). A Full Bridge DC/DC converter increases system components in a significant way, compared to the cheaper full bridge rectifiers. However, the Zero Voltage Switching (ZVS) and Zero Current Switching (ZVS) control techniques can be employed in MOSFETS to reduce switching and conduction losses. Furthermore, BLDC motors have high manufacturing costs, due to the permanent magnets employed in the rotor. As a result, the DC washer and dryer might prove to be better in terms of efficiency and lower power consumption, but the manufacturing costs will be higher than for an actual AC washer/dryer. It is more cost-effective to manufacture an AC drive than the proposed DC drive. As a result, it might be unpractical to develop the proposed high power DC appliances.

A solution that might prove the feasibility of DC appliances for high-power applications, in economic terms, is the addition of a second bus into the residence. This bar can be used to power appliances such as the cloth washer, cloth dryer and the stove. This simplifies the appliance internal circuitry, and the regulator stage can be either placed inside the appliance, or at the DC bus. In either way, costs will be reduced. This work is being done in CPES.

The main power quality issues in the DC bus are ripple in the DC voltage along with EMI. EMI issues measured here correspond to DC/DC converters; as a result, noise measurements present noise associated with DC/DC converters. This noise can be eliminated by placing input filters between the source voltage and the DC converter. Again, by placing input EMI filters, the system's transfer function is affected. As a result, a new stability analysis must be performed in order to redesign controllers.

In terms of Power Quality and system stability, though BLDC motors induce DC ripple in the bus, and it is propagated throughout the system, causing increases in harmonics and THD%, BLDC motors proves to be very robust. They are not affected at all by loads becoming active of inactive, due to the SPWM control and the carrier wave used. Furthermore, their efficiency is very high, since the rotor is composed of permanent magnets; the increase in harmonics only affects the power factor, and might induce some overheat in the motor.

When interconnecting the system with the utility grid, there is no significant issue, as results show that limits on THD are met for both current and voltage waveforms. The LCL filter, connected between the inverter output and the utility grid, absorbs harmonic components in the output voltages and currents that are not 60Hz components. Though harmonic limits are met, this will prove to be a problem when multiple residences with RES are interconnected by multiple inverters to the same PCC, since voltage THD will increase to unacceptable levels, even if all the connected inverters at the same point comply with the respective limits.

4.3 Economic Analysis

An economic analysis has been done in order to study the feasibility of a DC home in terms of the present value and the rate of return for two scenarios: The stand-alone case and the case of interconnection with the utility grid. Costs for each component considered for the system are displayed in table 13.

System Components	***Cost ($)***
Kyocera KC205GX-LP PV Module / 205W	$ 910.00
Whisper 500 Wind Turbine/ 3KW 48V	$ 6,298.00
Whisper 500 Wind Turbine Tower	$ 1,039.00
Deka 8A8D LTP AGM Batteries /12V, 245 Ah	$ 463.00
Xantrex AC Conduit Box (ACCB)	$ 315.00
Xantrex DC Conduit Box (DCCB)	$ 105.00
Xantrex XW 6048 Inverter / 6KW 120/240V Split-Phase Output	$ 3,059.00
Xantrex DC250 Disconnect	$ 299.00
Junction Box	$ 220.00
Outback MX60 MPPT Charge Controller / 48V 60A	$ 499.00
Trace PV Ground Fault Protection / 1 pole 500A	$ 355.00
CD60DC DC Breaker / 60A	$ 31.00

Table 13. System Components and Costs.

The following considerations have been made taking into account:

1. The economic analysis period considered is 20 years.
2. An annual maintenance for the whole system is considered as 1% of the total investment (after applying the 10% for installation costs).
3. The total monthly power demand, which will be considered as a benefit in both stand alone and net metering scenarios, is calculated for the various cases, and this quantity is multiplied by $0.24\,\frac{cents}{KWh}$, which is the average price at which the Electric Power

Authority sells power to their customers as of June 2008. This quantity is multiplied by 12 months to convert this benefit into a yearly amount.

4. The excess power injection is calculated to be around 30% of the yearly power demand. The quantity of power injected to the utility grid will always remain as credit, due to the stand alone approach in this research. The electric power authority establishes that, if at the end of the year, the consumer has credits, 75% of the total accumulated power will be purchased by the electric power company at a rate of $0.10\,\frac{cents}{KWh}$, while the remaining 25 percent will be used to lower electricity costs to public entities. As a result, only the 75% of the yearly credits of excess power will be considered as a benefit in the analysis.
5. For both the stand alone and net metering scenarios, a benefit considered is the reduction of Carbon Dioxide (CO_2) emissions, due to the stand alone approach taken in this research. This analysis is a simple one, since it does not considers the CO2 annual production involved in the manufacturing of PV systems. Presuming a monthly AC residence power consumption of 450 KWh/month, this quantity is converted to tons of CO_2 emissions per year by multiplying the power consumption by 1.36 $\frac{Lbs-CO2}{KWh}$, by 1.09 and by 12. The 1.36 factor converts the monthly consumption into pounds of CO_2; the 1.09 factor takes into account transmission and distribution losses, and the 12 converts the monthly amount into a yearly amount [68]. Finally, the pounds of CO_2 are divided by 2204 in order to convert them into tons. By following the steps above, the calculated production of CO_2 by an AC

residence is 4 tons/year. The estimated price for a ton of CO_2 varies from $50 to $100, according to Stern's review [69], which places a Social Cost for Energy due to the future consequences of emissions of CO_2 today. The number of tons is multiplied by the Social Cost of Energy, and considered as a benefit. The CO_2 analysis does not considers the CO_2 emissions associated with renewable equipment production, which makes the analysis done here a short one.

6. When considering excess power injection into the utility grid, a certain amount of tons of CO_2 stops being produced by the utility grid; the equivalent CO_2 reduction by power injection is calculated, and considered as benefits.
7. Equipments are considered depending their life cycle in years. Inverters are to be replaced every 10 years; batteries are to be replaced every 5 years. PV modules and wind turbines are usually manufactured to last from 20 to 25 years, and as a result a salvage value is not considered. Battery recycling is considered to give a bonus of $\frac{\$10}{Battery}$ when purchasing new batteries. Inverters are considered to give a bonus of 5% of their initial investment.
8. When purchasing renewable energy systems, up to $3000 can be deducted from the tax reports from purchases of wind systems, as long as 50% or more of the components are developed in Puerto Rico. $500 from a PV system purchase is another tax exemption that can be obtained, and is also considered here in this analysis.

The economic analysis done includes a sensibility analysis, showing different results after varying the net price of electricity costs to 50, 30 and 15 cents/KWh. Results for the economic analysis are presented below:

Case Evaluated (24 cents/KWh)	*Total System Cost*	*Present Value*	*Payback period (years)*
Case I Stand Alone	***$50,718.61***	***$(55,923.06)***	***(33.71)***
Case II Stand Alone	***$50,718.61***	***$(57,080.50)***	***(35.87)***
AC Residence Stand Alone	***$66,390.50***	***$(79,400.55)***	***(39.02)***
Case I Net Metering	***$54,619.21***	***$(59,097.61)***	***(32.09)***
Case II Net Metering	***$54,619.21***	***$(57,258.84)***	***(31.39)***
AC Residence Net Metering	***$74,190.70***	***$(59,418.83)***	***(36.11)***

Table 14. Economic Analysis Results for Mayaguez, PR.

Scenario	*Payback Period (yrs) 15 cents/KWh*	*Payback Period (yrs) 30 cents/KWh*	*Payback Period (yrs) 50 cents/KWh*
Case I Stand Alone	***46.52***	***28.49***	***18.78***
Case II Stand Alone	***49.06***	***30.42***	***20.19***
AC Residence Stand Alone	***54.71***	***32.76***	***21.34***
Case I Net Metering	***42.41***	***27.61***	***18.85***
Case II Net Metering	***40.17***	***27.40***	***19.24***
AC Residence Net Metering	***47.35***	***31.17***	***21.41***

Table 15. Sensitivity Results for the Economic Analysis.

Table 14 show the results for the economic analysis conducted for case I and II. The results are compared with a typical AC hybrid residence. Even by mitigating phantom loads (3.14 KWh per week) shows no reduction in system components, which explains the equal system costs for cases I and II, as evaluated in stand alone. For either scenario (stand alone or net metering), the payback periods obtained are high. This is why the payback period was

studied with different rates for electricity cost; this analysis reveals that the system will achieve a payback period of 18 years if we consider the electricity costs to be 50 cents/KWh, which is a price not too far from reality, since those costs are starting to increase without any boundaries.

For AC residences with net metering, batteries are often eliminated due to the fact that the utility grid is allowed to supply loads whenever renewable systems do not supply power. Since the scope of this thesis is to analyze a standalone system, the AC residence net metering option still considers batteries, in order to make a reasonable comparison to the system proposed, since the obvious choice for AC net metering is to remove batteries, which would instantly make this the best option, in terms of economic analysis.

Results in table 15 shows that by presuming a fixed electricity cost of 50 cents/KWh, the payback period for the investments reduces to 18 years(stand alone), which again makes this investment very attractive.

The option of analyzing the RES with a single autonomy day has been considered also in this economic analysis, in order to further demonstrate the feasibility of the proposed DC residence. Table 16 and 17 present the results below:

Scenario (1 Day of autonomy, 24 cents/KWh)	*Total System Costs*	*Present Value*	*Payback Period (yrs)*
Case I Stand Alone	*$42,569.81*	*$(36,553.92)*	*28.30*
Case II Stand Alone	*$42,569.81*	*$(37,556.67)*	*30.11*
AC Residence Stand Alone	*$54,167.30*	*$(50,114.81)*	*31.84*
Case I Net Metering	*$46,470.41*	*$(39,608.11)*	*27.31*
Case II Net Metering	*$46,470.41*	*$(39,929.33)*	*26.71*
AC Residence Net Metering	*$61,968.50*	*$(55,212.71)*	*30.16*

Table 16. Economic Analysis results for a single day of autonomy.

Scenario (1 Day Autonomy)	*Payback Period (yrs) 15 cents/KWh*	*Payback Period (yrs) 30 cents/KWh*	*Payback Period (yrs) 50 cents/KWh*
Case I Stand Alone	*39.05*	*23.91*	*15.76*
Case II Stand Alone	*41.18*	*25.53*	*16.94*
AC Residence Stand Alone	*44.64*	*26.73*	*17.41*
Case I Net Metering	*36.09*	*23.49*	*16.03*
Case II Net Metering	*34.18*	*23.31*	*16.37*
AC Residence Net Metering	*39.55*	*26.04*	*17.89*

Table 17. Sensibility Analysis for a single day of autonomy.

Results from table 16 and table 17 further prove the feasibility of the DC residence at higher electricity rates, considering only 1 day of autonomy. Table 16 shows a reduced net present value, due to the fact that the number of batteries required have decreased significantly, meaning that the costs associated with replacing batteries are much lower, as compared to the results in table 14. The payback period for a standalone residence is calculated to be 15 years, which further increases the viability of the dc residence. It is possible to obtain a payback period of 10 years or less by completely removing the battery bank and any associated equipment, but removing the battery bank means that the user will

use power from the utility grid at some point to supply the load demand; this case has not been evaluated in the economic analysis as it goes out of the boundary of the presumptions of this research.

The main drawback of the RES system with 1 day of autonomy, as presented in table 16-17, is the unreliability of the system at prolonged periods of null power production from the renewable sources. Since there is a tradeoff, the user must decide between system reliability and reduced payback period.

Increases in PV module efficiency, the development of new energy storage technologies, and an increase in production of RES equipment, among other factors, could positively influence the results of the economic analysis presented here. The increase in PV module efficiency will reduce the number of modules needed to supply a fixed load power demand, further reducing total system costs; the development of more efficient and more cost-effective ways of energy storage might affect the distributed power architecture(DPA), decreasing the total system costs due to reduced components; finally, the increase in demand of renewable energies will result in decreased manufacturing costs, further reducing the cost to acquire RES components.

5 Conclusions and Future Work

5.1 Conclusions

Power quality issues and a Feasibility analysis has been presented for a residence operating independently from the utility grid, supplied by only renewable sources, and to supply only DC loads. There is a tradeoff when trying to redesign current AC appliances in order to make them suitable to be powered up by DC power. For low power application appliances, an overall reduction of system components reduces the appliance overall cost.

Loads for high power applications present a problem when modified to work with a DC supply; there is a substantial increase in components. The proposed models here for both cloth washers and dryers must convert from DC to AC (single-phase), from AC back to DC (transformer/rectifier) in order to supply the BLDC motor. For these appliances, stand-by losses are not reduced. The many inverter/rectifier stages for the proposed DC model are greater than actual AC drives, which undergo 2 stages: the rectifying stage, the regulation stage (with a boost PFC), and the inverter stage (three phase). A Full Bridge DC/DC converter increases system components in a significant way, compared to the cheaper full bridge rectifiers. However, the Zero Voltage Switching (ZVS) and Zero Current Switching (ZVS) control techniques can be employed in MOSFETS to reduce switching and conduction losses. Furthermore, BLDC motors have high manufacturing costs, due to the permanent magnets employed in the rotor. As a result, the DC washer and dryer might prove to be better

in terms of efficiency and lower power consumption, but the manufacturing costs will be higher than for an actual AC washer/dryer. It is more cost-effective to manufacture an AC drive than the proposed DC drive. As a result, it might be unpractical to develop the proposed high power DC appliances. The microwave oven is another difficult load for various reasons: for one side, the power consumption is lowered significantly; for the other side, current consumption of this appliance is very high, demanding its own dedicated circuit for a DC residence; furthermore, the transformer/rectifier stage cannot be eliminated, since the DC/DC converter evaluated introduces this stage. For the appliances above mentioned, EMI stages are still needed in order to comply with the FCC class B specifications.

A solution that might prove the feasibility of DC appliances for high-power applications, in economic terms, is the addition of a second bus into the residence. This bar can be used to power appliances such as the cloth washer, cloth dryer and the stove. This simplifies the appliance internal circuitry, and the regulator stage can be either placed inside the appliance, or at the DC bus. In either way, costs will be reduced. This work is being done in CPES.

The main power quality issues in the DC bus are ripple in the DC voltage along with EMI. EMI issues measured here correspond to DC/DC converters; as a result, noise measurements present noise associated with DC/DC converters. This noise can be eliminated by placing input filters between the source voltage and the DC converter. Again, by placing input EMI filters, the system's transfer function is affected. As a result, a new stability analysis must be performed in order to redesign controllers.

In terms of Power Quality and system stability, though BLDC motors induce DC ripple in the bus, and it is propagated throughout the system, causing increases in harmonics and

THD%, BLDC motors proves to be very robust. They are not affected at all by loads becoming active of inactive, due to the SPWM control and the carrier wave used. Furthermore, their efficiency is very high, since the rotor is composed of permanent magnets; the increase in harmonics only affects the power factor, and might induce some overheat in the motor.

When interconnecting the system with the utility grid, there is no significant issue, as results show that limits on THD are met for both grid current and voltage waveforms. The LCL filter, connected between the inverter output and the utility grid, absorbs harmonic components in the output voltages and currents that are not 60Hz components. Though harmonic limits are met, this will prove to be a problem when multiple residences with RES are interconnected by multiple inverters to the same PCC, since voltage THD will increase to unacceptable levels, even if all the connected inverters at the same point comply with the respective limits.

From the sizing analysis, it can be seen that when appliances are redesigned to operate with DC power, in some cases their power consumption is lowered considerably, which is the main reason for the difference between an AC residence and a DC residence. The microwave ovens power consumption is cut to half, while the cloth dryer's consumption is greatly reduced. This makes the DC residence the most feasible option, in terms of the total system costs and payback period.

5.2 Contributions

The proposed DC residence has many advantages. The most important advantage is the completely independence from the utility grid, meaning that the residence stops contributing CO_2 emissions, while at the same time stops consuming fossil fuels, which are two of the main environmental issues as of today. This brings consumers of RES to be able to handle all the power production into their own hands, bringing them the feeling of liberty and independence from the utility grid. Due to the shortage of fossil fuels, and the need to harness the power available from renewable energies, in a near future, the possibility of supplying our homes with DC power generated from RES is becoming more feasible, as we look forward into the future. The DC appliance design done here brings that future today, by proposing models that makes possible the shift from supplying DC residences with AC sources to DC sources by reducing each appliance's power consumption, increasing overall system efficiency, (as reflected in tables 7 and 10), and reducing system components and total costs when acquiring RES. Table 10 reflects the feasibility of a DC system by reducing RES components and costs up to half as compared to an AC residence; again, this is due to the reduction in appliance consumption. The difference in components is significant; to supply the same load demand, there is a difference of 11 solar panels and 12 batteries. Though only the most critical appliances have been considered and designed here, other appliances need to be redesigned.

Another important contribution from this work is the study of power quality issues for a DC residence. Research work and papers address the benefits and feasibility of DC systems,

but none study the actual electrical issues associated with a DC residence, with DC loads, or with both combined. Power quality and stability issues must be studied and compared to issues that affect current AC residences in order to properly conclude about the feasibility of a DC residence. No work addresses such studies, which makes the electrical models developed for DC appliances a crucial component in this analysis.

Results from simulations in cases I-III show loads are not easily perturbed by variations in the supply voltage. Though ripple and noise increases as the load activity becomes more intense, loads that are sensible towards variations (namely flicker), such as lighting, can be replaced in a near future by LEDs. This, along with the fact that perturbations in the residence that are caused by the utility grid are completely eliminated due to the independence of the residence, further proves the superior stability of the DC residence, as compared to a current AC residence.

Finally, the development of a simulation integrating the most feasible RES in Puerto Rico (a hybrid power system test bed) for CPES is one of the contributions in this work; this model can be used for further studies, subjected to variations in climate conditions (solar irradiation, wind velocity and temperature).

5.3 Future Work

One of the main challenges of this work was to handle the multiple time-scales involved with the different models: from microseconds in the case of power electronics loads, to hours in the case of renewable energy resources (patterns of solar irradiation and wind velocity). In a future work, this difficulty could be managed by employing different models for the different time-scales, i.e., more detailed models for shorter periods, aggregate or simpler models for longer simulation periods. It is also important to test other DC system topologies to study the benefits in terms of cost, operating modes and overall system performance.

When considering the reduction of CO_2 emissions in the economic analysis, PV systems have an associated environmental impact, especially during manufacturing. These environmental costs were not included in the analysis, but might be included in the future with life-cycle analysis.

Further future work regarding DC residential systems are enumerated as follows:

1. The implementation of detailed battery models to account for non-ideal conditions in energy storage.
2. The consideration of non-ideal converters and transformers in some appliances, and the consideration of control techniques such as ZVS and ZCS to study further improvements in appliance efficiencies.
3. The integration of a fully bidirectional dc/ac inverter to study the interaction of the utility grid with the DC residence and also to study possible power quality/stability problems at the PCC.

4. New economic studies taking into account the removal of the energy storage elements, as a result of the implementation of the bidirectional DC/AC inverter, to further prove the economic feasibility of a DC residence, as compared to an AC residence.
5. A study that integrates fuel cells as an additional RES, due to the fact that an electrical model for fuel cells has already been developed.
6. The integration of multiple DC residences with RES to study the penetration of converters/inverters into the PCC.
7. Stability studies in the DC system, including EMI filters on DC/DC converter loads requiring them.

REFERENCES

[1]. Nilsson, D.; Sannino, A.: "Efficiency analysis of low- and medium- voltage DC distribution systems" in *IEEE Power Engineering Society General Meeting, 2004.* Vol.2 , Pages 2315 – 2321, 6-10 June 2004.

[2]. Hamilton, H.; Schulz, N.N.: **"**DC Protection on the Electric Ship" in *IEEE Electric Ship Technologies Symposium, 2007. ESTS '07.* Pages 294 – 300, 21-23 May 2007.

[3]. Nilsson,D: "DC Distribution Systems" Licenciate of Engineering Thesis[Online]. http://webfiles.portal.chalmers.se/et/Lic/NilssonDanielLic.pdf.

[4]. Puerto Rican Alliance for the education in renewable systems (ACEER) [online]. Laws of Pueto Rico, 15th legislature, 5th ordinary session No. 114. Senate Bill 1212 Conference 2007 2007. PR ALS 114; 2007 PR LAWS 114; 2007 PR ACT 114; 2007 PR S.B. 1212 http://aceer.uprm.edu/leyes/2007LPR114.pdf . Available as of July 7, 2008.

[5]. Friedeman, M.M., Boelman, E., Timmeren, A.van and Schoonman, J.: "Concept for a DC Low Voltage House" in *Sustainable Building 2002 Conference*, Oslo, Norway, no. 513, September 23-25 2002. [Online] http://www.bk.tudelft.nl/bt//installaties//onderzoek//paper_sb02_217.pdf Available as of April 15, 2008.

[6]. Erickson, Robert W.: "DC-DC Power Converters" [online]. http://ece-www.colorado.edu/~rwe/papers/Encyc.pdf . Available as of July 7, 2008.

[7]. Ortiz-Rivera, E.I.; Peng, F.Z. "Analytical Model for a Photovoltaic Module using the Electrical Characteristics provided by the Manufacturer Data Sheet" on *2005 IEEE 36th Conference* on *Power Electronics Specialists*, Pages 2087 – 2091, 11-14 September 2005.

[8]. Esram, T.; Chapman, P.L. **"**Comparison of Photovoltaic Array Maximum Power Point Tracking Techniques" in *IEEE Transaction on Energy Conversion,* Volume 22, Issue 2, Pages 439 – 449, June 2007.

[9]. Knight, A.M.; Peters, G.E. **"**Simple wind energy controller for an expanded operating range" In *IEEE Transactions on Energy Conversion,* Volume 20, Issue 2, Pages 459 – 466, June 2005.

[10]. Ahmed, N.A.; Miyatake, M. **"**A Stand-Alone Hybrid Generation System Combining Solar Photovoltaic and Wind Turbine with Simple Maximum Power Point Tracking Control" in *Power Electronics and Motion Control Conference*, 2006. Volume 1, Pages 1 – 7, Aug. 2006.

[11]. Horiuchi, N.; Kawahito, T.: **"**Torque and power limitations of variable speed wind turbines using pitch control and generator power control" in *IEEE Power Engineering Society Summer Meeting, 2001.* Volume 1, Pages 638 – 643, 15-19 July 2001.

[12]. Young, K.D.; Utkin, V.I.; Ozguner, U.: **"**A control engineer's guide to sliding mode control" in *IEEE Transactions on Control Systems Technology.* Volume 7, Issue 3, Pages 328-342, May 1999.

[13]. Khalil, H.: "Nonlinear Systems", third edition, Prentice Hall, 2002.

[14]. Valenciaga, F.; Puleston, P.F.; Battaiotto, P.E.; Mantz, R.J.: **"**Passivity/sliding mode control of a stand-alone hybrid generation system" in *IEE Proceedings on Control Theory and Applications.* Volume 147, Issue 6, Pages 680 – 686, Nov. 2000.

[15]. F. Valenciaga and P. F. Puleston, "Supervisor Control for a stand alone hybrid generation system using wind and photovoltaic energy," In *IEEE Transactions on Energy Conversion*, Volume 20, number 2, Pages 398-405, June 2005.

[16]. IEEE Recommended Practices and Requirements for Harmonic Control in Electrical Power Systems**.** *IEEE Std 519-1992*.

[17]. IEEE Standard for interconnecting distributed resources with the Electric Power System. *IEEE Std 1547*.

[18]. Sustainable Energy Program Report "The Use of Direct Current Output from PV Systems in Buildings" [Online]. http://www.berr.gov.uk/files/file17277.pdf
Available as of July 7, 2008.

[19]. O'Donovan, P.: **"**Goodbye, CRT" in *IEEE Spectrum.* Volume 43, Issue 11, Pages 38 – 43, Nov. 2006.

[20]. Donahue, J.A.; Jovanovic, M.M.: **"**The LCC inverter as a cold cathode fluorescent lamp driver" in the *Ninth Annual Proceedings Conference and Exposition in Applied Power Electronics. APEC 1994.* Vol. 1, Pages 427 - 433 13-17 Feb. 1994.

[21]. Akpinar, E.; Yilmazlar, I.: **"**Transformerless Single Phase Inverter Design for LCD Television" *in IEEE Transactions on Consumer Electronics.* Volume 53, Issue 2, Pages 697 – 703, May 2007.

[22]. Liang, S.-A.: **"**Design Optimization for LCD TV Power Supply with Resonant Technique" in *IEEE Power Electronics Specialists Conference, 2007. PESC 2007.* Pages 702 – 707, 17-21 June 2007.

[23]. Jia Wei; Lee, F.C.: **"**Two-stage voltage regulator for laptop computer CPUs and the corresponding advanced control schemes to improve light-load performance" in *IEEE Nineteenth Annual Conference and Exposition in Applied Power Electronics. APEC 2004.* Volume 2, Pages 1294 – 1300, 2004.

[24]. Harfman-Todorovic, M.; Palma, L.; Enjeti, P.: **"**A Hybrid DC-DC Converter for Fuel Cells Powered Laptop Computers" in *IEEE 37th Power Electronics Specialists Conference.PESC '06.* Pages 1 – 5, 18-22 June 2006.

[25]. Abe, K.; Nishijima, K.; Harada, K.; Nakano, T.; Nabeshima, T.; Sato, T.: "A Novel Multi-Phase Buck Converter for Lap-top PC" in *Power Conversion Conference Nagoya, 2007.* Pages 885 – 891, 2-5 April 2007.

Article "Magnetron used in Microwaves: Structure and Operation" [Online]. http://www.gallawa.com/microtech/magnetron.html. Available as of July 7, 2008.

[26]. Company "Raker Appliance Repair Professionals" Microwave Oven [Online]. http://www.appliance-repair.org/SAMPLES/Manual Samples/lesson15_part_01.pdf Available as of July 7, 2008.

[27]. DaFeng Weng; Yuvarajan, S.: **"**Constant-switching-frequency AC-DC converter using second-harmonic-injected PWM" in *IEEE Transactions on Power Electronics.* Volume 11, Issue 1, Pages 115 – 121, Jan. 1996.

[28]. Application Notes "Brushless DC (BLDC) Motor Fundamentals" AN885 [Online]. http://ww1.microchip.com/downloads/en/AppNotes/00885a.pdf Available as of July 7, 2008.

[29]. Elnady, A.; Yan-Fei Liu: **"**A Simple and Effective Speed Control Strategy for the Brushless DC Motor" in the *Canadian Conference on Electrical and Computer Engineering, 2007. CCECE 2007.* Pages 119 – 122, 22-26 April 2007.

[30]. Akons, I.; Alexandrovitz, A.: **"**Dynamic investigation and simulation of brushless DC motor" in *Nineteenth Convention of Electrical and Electronics Engineers in Israel, 1996.* Pages 76-82, 5-6 Nov. 1996.

[31]. Cho, K.Y.; Yang, S.B.; Hong, C.H.: **"**Sensorless control of a PM synchronous motor for direct drive washer without rotor position sensors" in *IEEE Proceedings in Electric Power Applications.* Volume 151, Issue 1, Pages 61 – 69, 9 Jan. 2004.

[32]. Dr. Agustin Irizarry Rivera, UPRM professor. [online]. http://ece.uprm.edu/~agustin Available as of July 7, 2008.

[33]. Enslin, J.H.R.; "Interconnection of distributed power to the distribution network" In *Power Systems Conference and Exposition*, 2004. IEEE PES 10-13, Volume 2, Pages 726 – 731, October 2004.

[34]. Chen, Z. "Issues of Connecting Wind Farms into Power Systems" in *Transmission and Distribution Conference and Exhibition: Asia and Pacifi*c, 2005 IEEE/PES, Pages 1 – 6.

[35]. Sharma, V.K.; Khan, M.A.; Singh, B.; Murthy, S.S.: **"**Comparison of power quality aspects of switched reluctance and permanent magnet brushless DC motor" in *TENCON 2000 Proceedings*. Volume 3, Pages 300 – 303, 24-27 Sept. 2000.

[36]. Tihanyy, L.: "Electromagnetic Compatibility in Power Electronics" *IEEE Press 1995*.

[37]. Iftikhar, M.U.; Sadarnac, D.; Karimi, C.: **"**Conducted EMI Suppression and Stability Issues in Switch-mode DC-DC Converters" in *IEEE Multitopic Conference, 2006. INMIC '06.* Pages 389 – 394, 23-24 Dec. 2006.

[38]. Makaran, J.E.; LoVetri, J.: **"**BLDC motor and drive conducted RFI simulation for automotive applications" in *IEEE Transactions on Electromagnetic Compatibility,* Volume 45, Issue 2, Pages 316 – 329, May 2003.

[39]. Notes "Flyback DC/DC converter" [Online].
http://www.ece-colorado.edu/~ecen4517/materials/flyback.pdf .
Available as of April 15, 2008.

[40]. Rashid, Muhammad H.: "Power Electronics: Circuits, Devices and Applications." Third edition.

[41]. Roshan, A.; Burgos, R.; Baisden, A.C.; Wang, F.; Boroyevich, D.: "A D-Q Frame Controller for a Full-Bridge Single Phase Inverter Used in Small Distributed Power Generation Systems" in *IEEE Twenty Second Annual Conference in Applied Power Electronics, APEC 2007.* Pages 641 – 647, Feb. 25 2007-March 1 2007.

[42]. Xantrex 6048 Grid tie inverter [online]. http://www.affordable-solar.com/Xantrex%20XW6048.120.240.60.Inverter.Charger.htm
Available as of July 7, 2008.

[43]. Kyocera KC205GX-LP Solar Panel [online].
http://www.affordable-solar.com/kyocera.kd205X.LP.205.watt.solar.panel.htm
Available as of July 7, 2008.

[44]. Borowy, B.S.; Salameh, Z.M. "Dynamic response of a stand-alone wind energy conversion system with battery energy storage to a wind gust" In *IEEE Transactions on Energy Conversion,* Volume 12, Issue 1, Pages 73-78, March 1997.

[45]. Fisher and Paykel GW11 ecosmart washer [online].
http://www.abt.com/scripts/site/site_product.php3?id=10861
Available as of July 8, 2008.

[46]. Fisher and Paykel Dryer with induction drive [online]. http://fisher-paykel.amroyal.com/fisherpaykel-de27cw1-6-2-cu-ft-aerosmart-electric-top-load-dryer-in-white.html
Available as of July 8, 2008.

[47]. Rajamani, H.S.; McMahon, R.A.: **"**Universal and high-speed, three phase induction motor drives for domestic appliances" in *IEEE AFRICON 4th, 1996.* Volume 1, 24-27, Pages 441 – 446, Sept. 1996.

[48]. Spin X Dryer [online]. http://www.kansaswindpower.net/spin_x%20dryer.htm
Available as of July 8, 2008.

[49]. Store/Company "DC Airco." DC Air Conditioning units. [Online]. http://www.dcairco.com/products.html
Available as of July 8, 2008.

[50]. Company "SunDanzer" DC Refrigerator and Freezer [Online]. http://sundanzer.com/Products.html
Available as of July 8, 2008.

[51]. Store "Farrey's" BLDC Ceiling Fan [Online]. http://www.farreys.com/ventilation/panasonic/
Available as of July 8, 2008.

[52]. Akpinar, E.; Yilmazlar, I.: **"**Transformerless Single Phase Inverter Design for LCD Television" *in IEEE Transactions on Consumer Electronics.* Volume 53, Issue 2, Pages 697 – 703, May 2007.

[53]. Jia Wei; Lee, F.C.: **"**Two-stage voltage regulator for laptop computer CPUs and the corresponding advanced control schemes to improve light-load performance" in *IEEE Nineteenth Annual Conference and Exposition in Applied Power Electronics. APEC 2004.* Volume 2, Pages 1294 – 1300, 2004.

[54]. Company "Raker Appliance Repair Professionals" Microwave Oven [Online]. http://www.appliance-repair.org/SAMPLES/Manual Samples/lesson15_part_01.pdf
Available as of July 8, 2008.

[55]. Store “Sensible Solutions for your Mobile Lifestyle.” Portable Oven. [Online]. http://www.skingcompany.com/detail.asp?product_id=rpsc900 Available as of July 8, 2008.

[56]. Hart, Daniel W. “Introduction to Power Electronics”. 1997.

[57]. Ciobotaru, M.; Teodorescu, R.; Rodriguez, P.; Timbus, A.; Blaabjerg, F.; **“**Online grid impedance estimation for single-phase grid-connected systems using PQ variations” in *IEEE Power Electronics Specialists Conference, 2007.* Pages 2306 – 2312, 17-21 June 2007.

[58]. Installation and operations manual for Grid Tied Residential Inverter Models 2500, 3500, 4600, 4800, and 5200 [online]. http://www.pvpowered.com/manuals/Installation-and-Operations-Manual_rev9_21.pdf Available as of July 8, 2008.

[59]. Visscher, K.; Heskes, P.J.M.: “A method for operational grid and load impedance measurements” in 2005 International Conference on Future Power Systems.” Pages: 4, Nov. 2005.

[60]. Store “Sensible Solutions for your Mobile Lifestyle.” Portable Oven. [Online]. http://www.skingcompany.com/detail.asp?product_id=rpsc900 Available as of July 8, 2008.

[61]. Store “Creative User Technologies Inc.” Hair Dryer. [Online]. http://www.cetsolar.com/dchairdryer.htm. Available as of July 8, 2008.

[62]. Store “Creative User Technologies Inc.” Fluorescent Light. [Online]. http://www.cetsolar.com/energylight.htm Available as of July 8, 2008.

[63]. Panasonic Viera LCD & Plasma TV’s power consumption [online]. http://www.prokare.com.tr/pdf2/panasonic_viera_2006_brochure.pdf Available as of July 8, 2008.

[64]. 550W 12V Microwave oven with 750W inverter [online]. http://www.sports-imports.stores.yahoo.net/12volmic.html
Available as of April 15, 2008.

[65]. Energy Efficiency, Phantom Loads [online]. http://www.energitjenesten.dk/files/resource_4/videnskassen/stroemtyv/phantom_loads.pdf.
Available as of July 8, 2008.

[66]. 2005 National Electric Code (NEC).

[67]. Calculation of CO_2 emissions [online]. http://www.b-e-f.org/greentags/faq_pages/calculator.shtm
Available as of July 8, 2008.

[68]. Stern's Review on the Economics of Climate Change [online]. http://www.hm-treasury.gov.uk/independent_reviews/stern_review_economics_climate_change/sternreview_index.cfm
Available as of July 8, 2008.

[69]. Luo,S.: "A Review of Distributed Power Systems" in *IEEE Aerospace and Electronic Systems Magazine* Vol.20, Issue 8, Part 2, Pages 5-16. August 2005.

[70]. US Department of Energy Strategic Plan for Distributed Energy Resources , Septemer 2000. [online].http://www.eere.energy.gov/de/pdfs/de_program_plan.pdf
Available as of July 8, 2008.

[71]. Renewable Energy Products Online Store [online[. http://www.affordable-solar.com/
Available as of July 8, 2008.

APPENDIX A: Calculation of the b parameter of a PV module.

```
clc
clear all

syms Vop Iop Voc Isc bo
b = ((Vop / Voc) - 1) / log(1 - (Iop/Isc*(1-exp(-1/bo))))

Voc = 30.7
Isc = 8.6

Vop = 24.4;
Iop = 7.96;

bo = 42;
bnew = 0;
error=10;
k=0;
while ( error > 10^-10 )

    bnew = ((Vop / Voc) - 1) / log(1 - (Iop/Isc*(1-exp(-1/bo))));
    error = abs(bnew - bo);
    bo = bnew;
    k = k+1;
end

bnew
k
```

APPENDIX B: Park's Transform

To convert any set of three phase vectors from the ABC reference frame to the dq reference frame, the following transformation, known as Park's Transform, must be applied to the desired vectors:

$$\begin{bmatrix} V_q \\ V_d \\ V_0 \end{bmatrix} = \frac{2}{3}\begin{bmatrix} \cos(\theta_r) & \cos(\theta_r - 120) & \cos(\theta_r + 120) \\ \sin(\theta_r) & \sin(\theta_r - 120) & \sin(\theta_r + 120) \\ 1/2 & 1/2 & 1/2 \end{bmatrix} * \begin{bmatrix} V_{as} \\ V_{bs} \\ V_{cs} \end{bmatrix} \tag{B-1}$$

Where

$$T = \begin{vmatrix} \cos\theta_r & \cos\theta_r - 120 & \cos\theta_r + 120 \\ \sin\theta_r & \sin\theta_r - 120 & \sin\theta_r + 120 \\ 1_2 & 1_2 & 1_2 \end{vmatrix} \tag{B-2}$$

And T is denoted as Park's Transform. Park's inverse transform, denoted by T^{-1} is:

$$T^{-1} = \begin{bmatrix} \cos(\theta_r) & \sin(\theta_r) & 1/2 \\ \cos(\theta_r - 120) & \sin(\theta_r - 120) & 1/2 \\ \cos(\theta_r + 120) & \sin(\theta_r + 120) & 1/2 \end{bmatrix} \tag{B-3}$$

For the Single-Phase Case, the transformation from the *αβ* reference frame to the *dq* reference frame is done by:

$$\begin{bmatrix} V_q \\ V_d \end{bmatrix} = \begin{bmatrix} \cos(\theta_r) & -\sin(\theta_r) \\ \sin(\theta_r) & \cos(\theta_r) \end{bmatrix} * \begin{bmatrix} V_\alpha \\ V_\beta \end{bmatrix} \tag{B-4}$$

The inverse transformation is:

$$\begin{bmatrix} V_\alpha \\ V_\beta \end{bmatrix} = \begin{bmatrix} \cos(\theta_r) & \sin(\theta_r) \\ -\sin(\theta_r) & \cos(\theta_r) \end{bmatrix} * \begin{bmatrix} V_q \\ V_d \end{bmatrix} \tag{B-5}$$

APPENDIX C : Solar Irradiation and Wind Velocity Data for Aguadilla, Puerto Rico.

In this appendix, solar irradiation and temperature data is presented for the city of Mayaguez, PR. Data available for the wind turbine was measured in Aguadilla, PR.

Hour	***Solar Irradiation (W/m^2)***
6:00 AM	2.52
7:00 AM	66.56
8:00 AM	241.96
9:00 AM	405.36
10:00 AM	542.27
11:00 AM	573.19
12:00 PM	531.86
1:00 PM	472.56
2:00 PM	368.77
3:00 PM	268.46
4:00 PM	141.33
5:00 PM	33.12
6:00 PM	1.89

Table 18. Solar Irradiation Data for Mayaguez, PR.

Hour	***Temperature (°C)***	***Hour***	***Temperature (°C)***
12:00AM	***22.87***	***12:00 PM***	29.54
1:00 AM	23.56	***1:00 PM***	29.14
2:00 AM	23.08	***2:00 PM***	29.20
3:00 AM	22.60	***3:00 PM***	28.61
4:00 AM	22.12	***4:00 PM***	28.25
5:00 AM	21.64	***5:00 PM***	27.42
6:00 AM	21.17	***6:00 PM***	26.40
7:00 AM	20.82	***7:00 PM***	25.81
8:00 AM	22.42	***8:00 PM***	25.22
9:00 AM	23.95	***9:00 PM***	24.64
10:00 AM	26.07	***10:00 PM***	24.05
11:00 AM	28.49	***11:00 PM***	23.46

Table 19. Ambient Temperature Data for the City of Mayaguez, PR.

Hour	*Average Wind Velocity (m/s)*	*Hour*	*Average Wind Velocity (m/s)*
12:00AM	***5.97***	***12:00 PM***	4.91
1:00 AM	***5.24***	***1:00 PM***	6.08
2:00 AM	***4.87***	***2:00 PM***	6.96
3:00 AM	***4.58***	***3:00 PM***	7.89
4:00 AM	***4.60***	***4:00 PM***	8.46
5:00 AM	***3.84***	***5:00 PM***	8.38
6:00 AM	3.81	***6:00 PM***	8.92
7:00 AM	3.67	***7:00 PM***	8.98
8:00 AM	3.69	***8:00 PM***	8.49
9:00 AM	3.58	***9:00 PM***	8.26
10:00 AM	3.69	***10:00 PM***	6.48
11:00 AM	3.87	***11:00 PM***	6.55

Table 20. Average Wind velocity values for Aguadilla, PR.

APPENDIX D: Sizing of a RES System.

CASE I: INCLUDES PHANTOM LOADS

STEP 1 CALCULATE YOUR AC/DC LOADS.

ORANGE DENOTES TYPICAL LOADS, YELLOW DENOTES PHANTOM LOADS.

LOAD	QUANTITY	WATTS	HRS / DAY	DAY/WK	WH/WK
AIR CONDITIONER	1	670	5	5	16750
LIGHT BULBS	20	13	5	7	9100
OVEN	1	120	0.5	2	120
STOVE	1	1425	1	7	9975
CLOTH WASHER	1	500	2	1	2000
CLOTH DRYER	1	400	2	1	800
LAPTOP	1	110	5	6	3300
VENTILATION FAN	5	25	6	7	5250
FRIDGE & FREEZER	1		850	7	5950
HAIR DRYER	1	168	0.5	4	336
TOASTER	1	60	0.5	4	120
MICROWAVE	1	750	1	1	750
MIXER	1	156	1	1	156
PUMPS	1	150	1	1	150
COFFEE MAKER	1	140	1	7	980
LCD TV	4	168	3	7	14112
TOTAL					69649
DIGITAL CLOCKS	2	2	24	7	672
RADIO CLOCK	2	2.3	24	7	772.8
TV	4	0.4	21	7	14.7
MICROWAVE OVEN & CLOCK	1	8	23	7	1288
PC	1	3.4	19	7	452.2
LASERJET PRINTER	1	1	24	7	168
TOTAL					3588.2

TOTAL WEEKLY DEMAND (WH/WK)	**76825.4**
TOTAL MONTHLY DEMAND (KWH/MO) MULTIPLIED BY 1.25 TO CONSIDER INVERTER AND BATTERY EFFICIENCIES	**384.127**
PEAK LOAD SUPPLIED BY THE PV SYSTEM (75% OF TOTAL WEEKLY DEMAND)	**72023.81**
PEAK LOAD SUPPLIED BY THE WIND SYSTEM (25% OF TOTAL WEEKLY DEMAND)	**24007.94**

- **SYSTEM VOLTAGE = 48V**
- **DIVIDE TOTAL WH/WK BY SYSTEM VOLTAGE. THIS IS TOTAL AMP HOURS PER WEEK USED BY DC LOADS. = 2000.61**
- Divide total amp hours per week by 7 days. This is total average amp hours per day. = 285.8088

PV SIZING:

A. **TOTAL AVERAGE AMPS PER DAY TO BE SUPPLIED BY THE PV SYSTEM. DIVIDE PV WEEKLY DEMAND BY SYSTEM VOLTAGE, THEN DIVIDE AGAIN BY 7 DAYS. =214.3566**

B. **MULTIPLY LINE 5 BY 1.2 TO COMPENSATE FOR BATTERY CHARGE/DISCHARGE = 257.2279**

C. **AVERAGE SUN HOURS PER DAY IN YOUR AREA. = 6**

D. **DIVIDE LINE 6 BY LINE 7. THIS IS THE TOTAL SOLAR ARRAY AMPS REQUIRED. =34.2970**

E. **CALCULATE CURRENT OUTPUT FOR THE PV MODULE. MULTIPLY WATTS BY AVERAGE SOLAR IRRADIATION, AND DIVIDE BY MODULE VOLTAGE. = 3.9249**

F. **NUMBER OF MODULES REQUIRED IN PARALLEL. DIVIDE TOTAL SOLAR ARRAY AMPERAGE BY CURRENT OUTPUT FOR THE PV MODULE. = 11**

G. NUMBER OF MODULES TO PROVIDE SYSTEM VOLTAGE = 2 PER STRING

H. PV ARRAY =22 PANELS.

WIND TURBINE SIZING:

A. PEAK LOAD TO BE SUPPLIED BY THE WIND SYSTEM (WH/WK) =24007.94

B. PEAK LOAD TO BE SUPPLIED DAILY. DIVIDE PEAK LOAD SUPPLIED BY WIND TURBINE BY 7 DAYS. = 3429.70

C. WIND TURBINE POWER RATING CHOSEN = 3 KW

D. DIVIDE DAILY PEAK LOAD BY TURBINE POWER RATING. = 1

E. NUMBER OF WIND TURBINES = 1

BATTERY SIZING:

A. NUMBER OF CLOUDY DAYS IN YOUR AREA. THIS NUMBER DETERMINES THE NUMBER OF DAYS THE SYSTEM WILL BE AUTONOMOUS. = 3

B. MULTIPLY TOTAL MPS-HOURS PER DAY BY THE AMOUNT OF CLOUDY DAYS. =1028.912

C. DIVIDE LINE 3 BY 0.6 TO MAINTAIN A 40% RESERVE AFTER A DEEP DISCHARGING PERIOD. =1714.853

D. RATING OF THE BATTERY CHOSEN: 245AH, 12V.

E. DIVIDE QUANTITY IN LINE 15 BY AH OF THE CHOSEN BATTERY TO OBTAIN THE NUMBER OF BATTERIES REQUIRED FOR THE HYBRID SYSTEM. =7

F. NUMBER OF BATTERIES IN SERIES TO PROVIDE SYSTEM VOLTAGE = 28

G. TOTAL NUMBER OF BATTERIES = 28

CASE II: DOES NOT INCLUDES PHANTOM LOADS

STEP 1 CALCULATE YOUR AC/DC LOADS.

ORANGE DENOTES TYPICAL LOADS, YELLOW DENOTES PHANTOM LOADS.

LOAD	QUANTITY	WATTS	HRS / DAY	DAY/WK	WH/WK
AIR CONDITIONER	1	670	5	5	16750
LIGHT BULBS	20	13	5	7	9100
OVEN	1	120	0.5	2	120
STOVE	1	1425	1	7	9975
CLOTH WASHER	1	500	2	1	2000
CLOTH DRYER	1	400	2	1	800
LAPTOP	1	110	5	6	3300
VENTILATION FAN	5	25	6	7	5250
FRIDGE & FREEZER	1		850	7	5950
HAIR DRYER	1	168	0.5	4	336
TOASTER	1	60	0.5	4	120
MICROWAVE	1	750	1	1	750
MIXER	1	156	1	1	156
PUMPS	1	150	1	1	150
COFFEE MAKER	1	140	1	7	980
LCD TV	4	168	3	7	14112
TOTAL					69649
DIGITAL CLOCKS	0	0	0	0	0
RADIO CLOCK	0	0	0	0	0
TV	0	0	0	0	0
MICROWAVE OVEN & CLOCK	0	0	0	0	0
PC	0	0	0	0	0
LASERJET PRINTER	0	0	0	0	0
TOTAL					0

TOTAL WEEKLY DEMAND (WH/WK)	**69649**
TOTAL MONTHLY DEMAND (KWH/MO) MULTIPLY BY 1.25 TO ACCOUNT FOR INVERTER AND BATTERY EFFICIENCIES	**348.24**
PEAK LOAD SUPPLIED BY THE PV SYSTEM (75% OF TOTAL WEEKLY DEMAND)	**65295.94**
PEAK LOAD SUPPLIED BY THE WIND SYSTEM (25% OF TOTAL WEEKLY DEMAND)	**21765.31**

- **SYSTEM VOLTAGE = 48V**
- **DIVIDE TOTAL WH/WK BY SYSTEM VOLTAGE. THIS IS TOTAL AMP HOURS PER WEEK USED BY DC LOADS. = 1813.7760**
- Divide total amp hours per week by 7 days. This is total average amp hours per day. = 259.1109

PV SIZING:

A. **TOTAL AVERAGE AMPS PER DAY TO BE SUPPLIED BY THE PV SYSTEM. DIVIDE PV WEEKLY DEMAND BY SYSTEM VOLTAGE, THEN DIVIDE AGAIN BY 7 DAYS. =194.3331**

B. **MULTIPLY LINE 5 BY 1.2 TO COMPENSATE FOR BATTERY CHARGE/DISCHARGE =233.1998**

C. **AVERAGE SUN HOURS PER DAY IN YOUR AREA. = 6**

D. **DIVIDE LINE 6 BY LINE 7. THIS IS THE TOTAL SOLAR ARRAY AMPS REQUIRED. =38.8663**

E. **CALCULATE CURRENT OUTPUT FOR THE PV MODULE. MULTIPLY WATTS BY AVERAGE SOLAR IRRADIATION, AND DIVIDE BY MODULE VOLTAGE. = 3.92**

F. **NUMBER OF MODULES REQUIRED IN PARALLEL. DIVIDE TOTAL SOLAR ARRAY AMPERAGE BY CURRENT OUTPUT FOR THE PV MODULE. = 10**

G. **NUMBER OF MODULES TO PROVIDE SYSTEM VOLTAGE = 2 PER STRING**

H. PV ARRAY = 20 PANELS.

WIND TURBINE SIZING:

F. PEAK LOAD TO BE SUPPLIED BY THE WIND SYSTEM (WH/WK) =21765.31

G. PEAK LOAD TO BE SUPPLIED DAILY. DIVIDE PEAK LOAD SUPPLIED BY WIND TURBINE BY 7 DAYS. = 3109.33

H. WIND TURBINE POWER RATING CHOSEN = 3 KW

I. DIVIDE DAILY PEAK LOAD BY TURBINE POWER RATING. = 1

J. NUMBER OF WIND TURBINES = 1

BATTERY SIZING:

H. NUMBER OF CLOUDY DAYS IN YOUR AREA. THIS NUMBER DETERMINES THE NUMBER OF DAYS THE SYSTEM WILL BE AUTONOMOUS. = 3

I. MULTIPLY TOTAL MPS-HOURS PER DAY BY THE AMOUNT OF CLOUDY DAYS. =932.7991

J. DIVIDE LINE 3 BY 0.6 TO MAINTAIN A 40% RESERVE AFTER A DEEP DISCHARGING PERIOD. =1554.665

K. RATING OF THE BATTERY CHOSEN: 245AH, 12V.

L. DIVIDE QUANTITY IN LINE 15 BY AH OF THE CHOSEN BATTERY TO OBTAIN THE NUMBER OF BATTERIES REQUIRED FOR THE HYBRID SYSTEM. =7

M. NUMBER OF BATTERIES IN SERIES TO PROVIDE SYSTEM VOLTAGE = 4

N. TOTAL NUMBER OF BATTERIES = 28

CASE III: AC RESIDENCE

STEP 1 CALCULATE YOUR AC/DC LOADS.

TOTAL MONTHLY DEMAND (KWH/MO) MULTIPLY BY 1.25 TO ACCOUNT FOR INVERTER AND BATTERY EFFICIENCIES	451.887 564,859
PEAK LOAD SUPPLIED BY THE PV SYSTEM (75% OF TOTAL WEEKLY DEMAND)	84728.85
PEAK LOAD SUPPLIED BY THE WIND SYSTEM (25% OF TOTAL WEEKLY DEMAND)	28242.95

- SYSTEM VOLTAGE = 48V
- Divide total amp hours per week by 7 days. This is total average amp hours per day. = 393.2632

PV SIZING:

A. TOTAL AVERAGE AMPS PER DAY TO BE SUPPLIED BY THE PV SYSTEM. DIVIDE PV WEEKLY DEMAND BY SYSTEM VOLTAGE, THEN DIVIDE AGAIN BY 7 DAYS. =315.2115

B. MULTIPLY LINE 5 BY 1.2 TO COMPENSATE FOR BATTERY CHARGE/DISCHARGE = 378.2538

C. AVERAGE SUN HOURS PER DAY IN YOUR AREA. = 6

D. DIVIDE LINE 6 BY LINE 7. THIS IS THE TOTAL SOLAR ARRAY AMPS REQUIRED. =63.0423

E. CALCULATE CURRENT OUTPUT FOR THE PV MODULE. MULTIPLY WATTS BY AVERAGE SOLAR IRRADIATION, AND DIVIDE BY MODULE VOLTAGE. = 3.8522

F. NUMBER OF MODULES REQUIRED IN PARALLEL. DIVIDE TOTAL SOLAR ARRAY AMPERAGE BY CURRENT OUTPUT FOR THE PV MODULE. = 17

G. NUMBER OF MODULES TO PROVIDE SYSTEM VOLTAGE = 2 PER STRING

H. PV ARRAY = 34 PANELS.

WIND TURBINE SIZING:

K. PEAK LOAD TO BE SUPPLIED BY THE WIND SYSTEM (WH/WK) =28242.75

L. PEAK LOAD TO BE SUPPLIED DAILY. DIVIDE PEAK LOAD SUPPLIED BY WIND TURBINE BY 7 DAYS. = 4034

M. WIND TURBINE POWER RATING CHOSEN = 3 KW

N. DIVIDE DAILY PEAK LOAD BY TURBINE POWER RATING. = 1

O. NUMBER OF WIND TURBINES = 1

BATTERY SIZING:

O. NUMBER OF CLOUDY DAYS IN YOUR AREA. THIS NUMBER DETERMINES THE NUMBER OF DAYS THE SYSTEM WILL BE AUTONOMOUS. = 3

P. MULTIPLY TOTAL MPS-HOURS PER DAY BY THE AMOUNT OF CLOUDY DAYS. =470.7158

Q. DIVIDE LINE 3 BY 0.6 TO MAINTAIN A 40% RESERVE AFTER A DEEP DISCHARGING PERIOD. =784.5264

R. RATING OF THE BATTERY CHOSEN: 245AH, 12V.

S. DIVIDE QUANTITY IN LINE 15 BY AH OF THE CHOSEN BATTERY TO OBTAIN THE NUMBER OF BATTERIES REQUIRED FOR THE HYBRID SYSTEM. =10

T. NUMBER OF BATTERIES IN SERIES TO PROVIDE SYSTEM VOLTAGE = 4

U. TOTAL NUMBER OF BATTERIES = 40

APPENDIX E: Additional Simulation Results

CASE I Simulations (Transient):

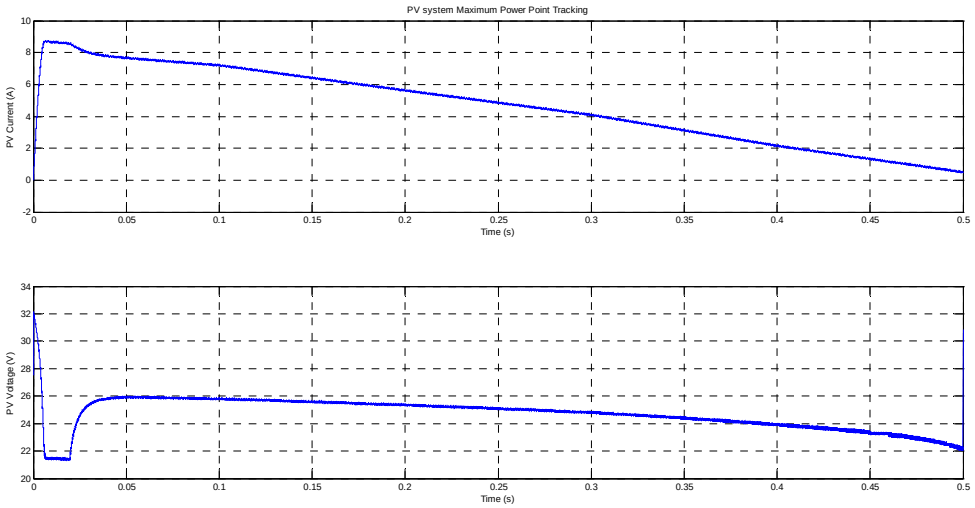

Figure 82. MPPT for PV System, Case I.

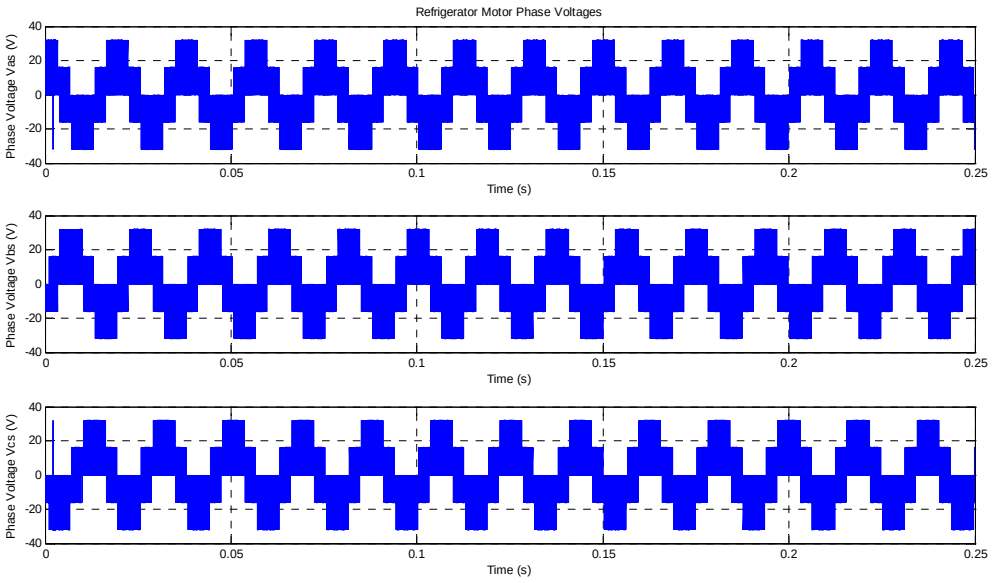

Figure 83. Refrigerator Motor Phase Voltages, Case I.

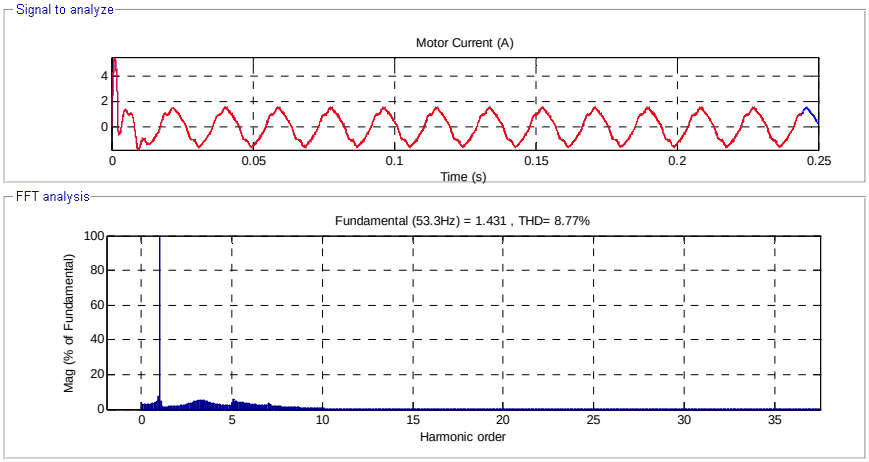

Figure 84. Harmonic Analysis for Refrigerator Motor Current, Case I.

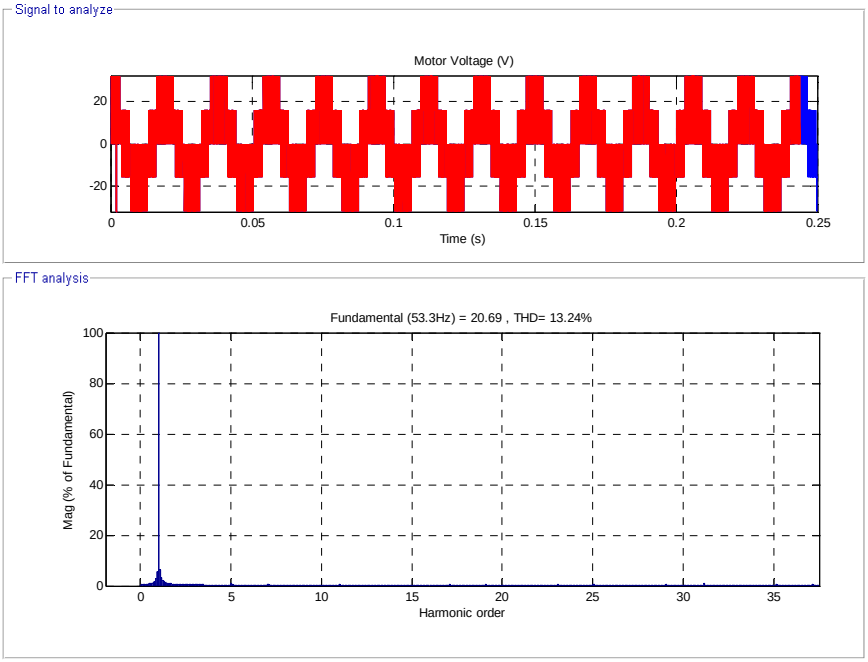

Figure 85. Harmonic Analysis for Refrigerator Motor Voltage, Case I.

CASE I Simulations (Steady State)

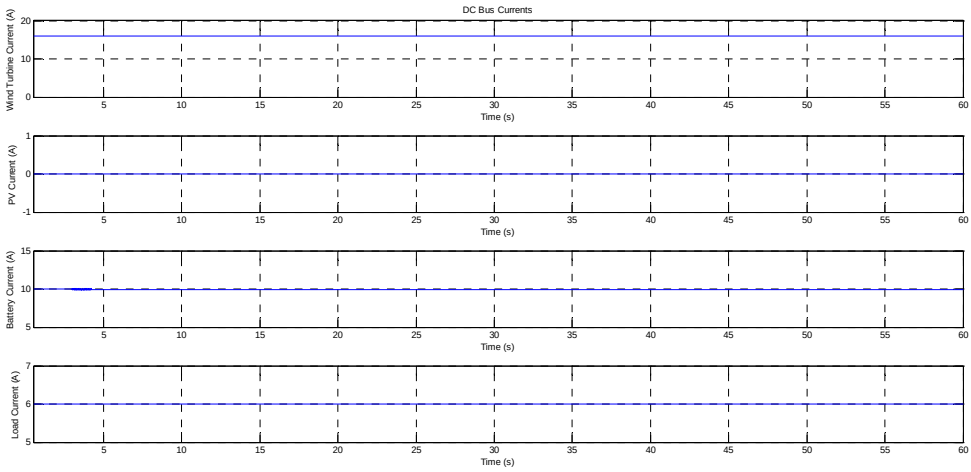

Figure 86. DC Bus Currents at Steady State.

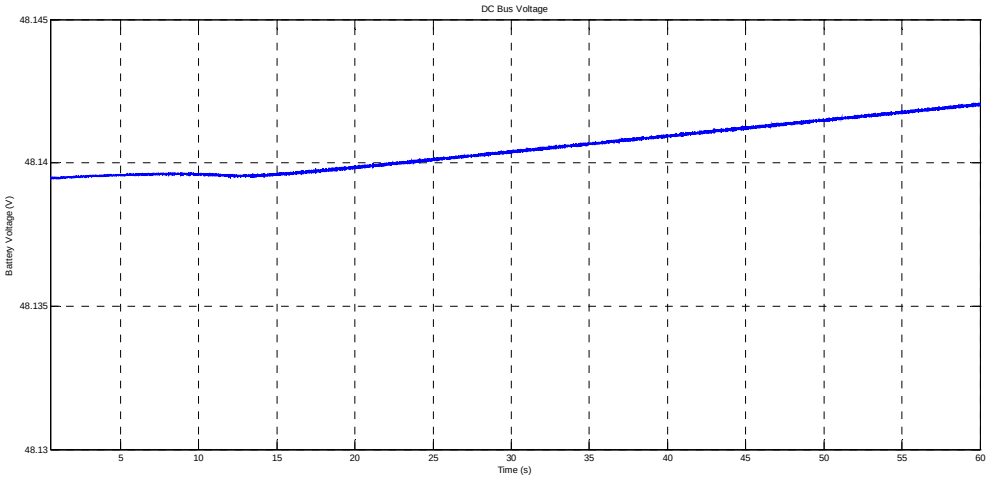

Figure 87. DC Bus Voltage at Steady State.

CASE II Simulations (Transient):

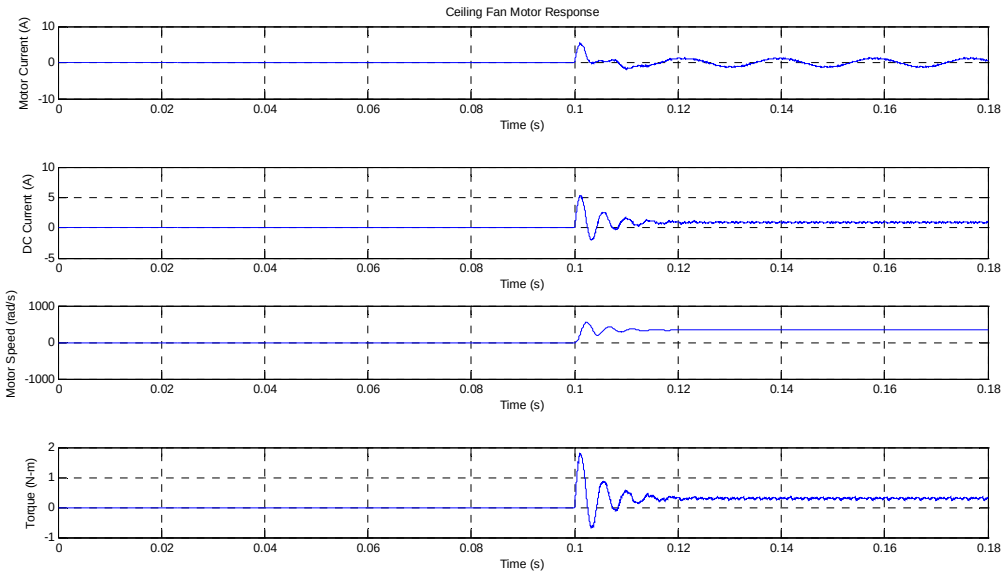

Figure 88. Ceiling Fan Motor Response, Case II.

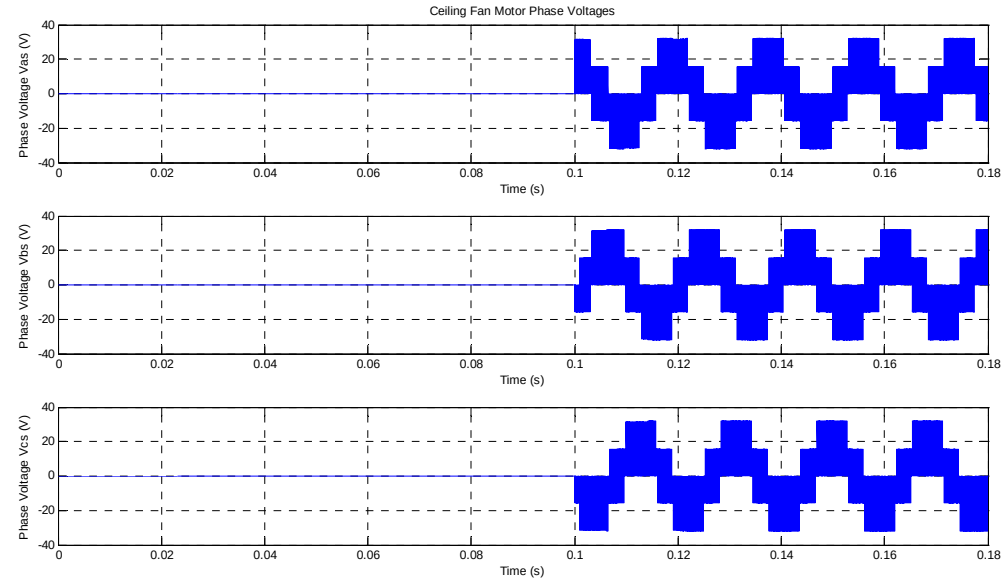

Figure 89. Ceiling Fan Motor Phase Voltages, Case II.

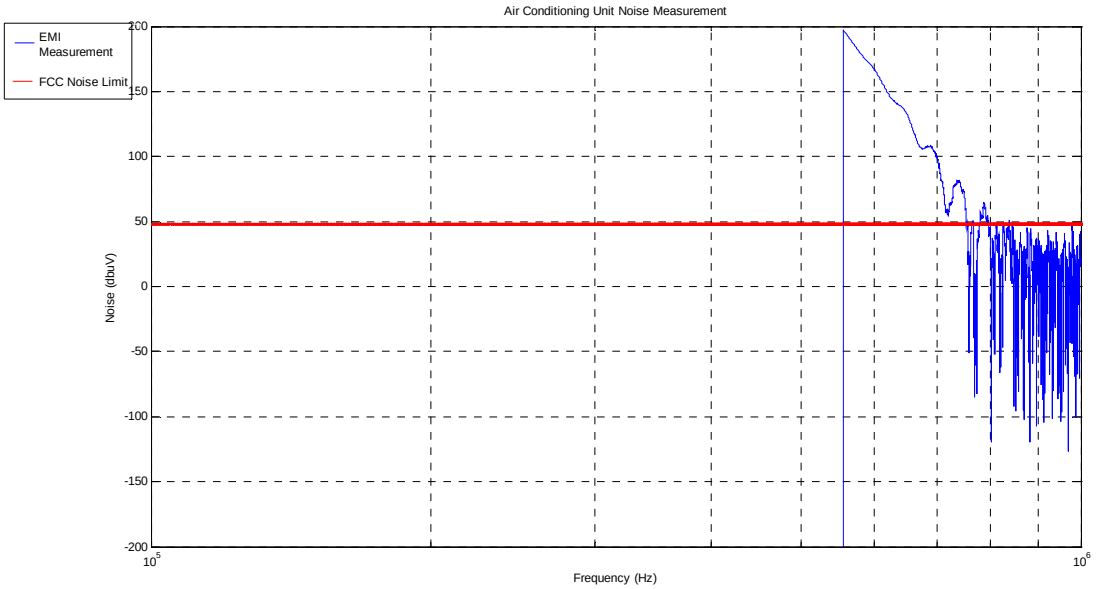

Figure 90. AC Unit EMI Measurement, Case II.

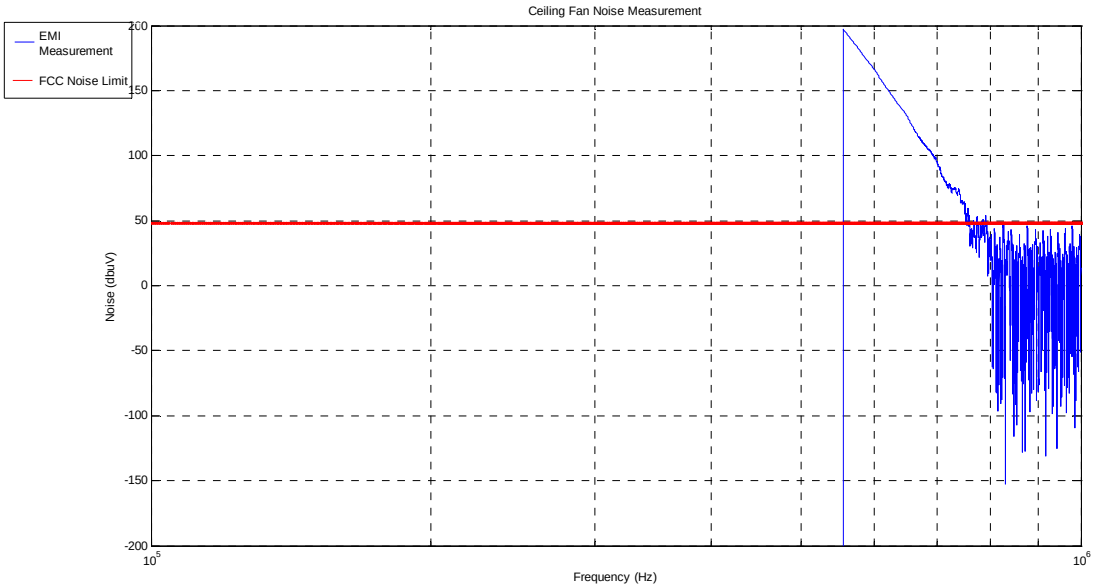

Figure 91. Ceiling Fan EMI Measurement, Case II.

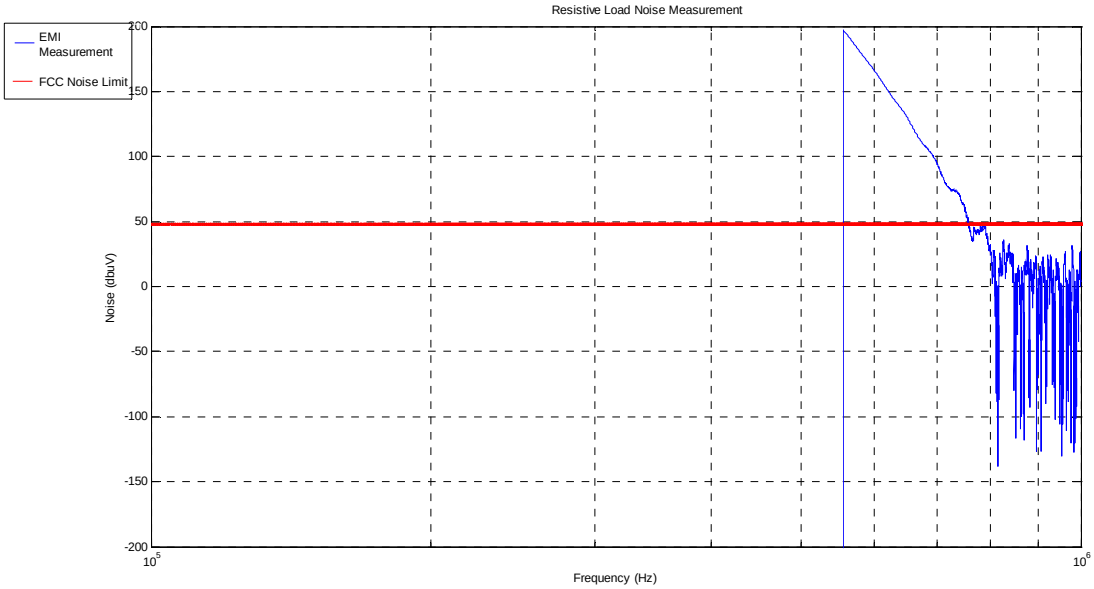

Figure 92. Resistive Loads EMI Measurement, Case II.

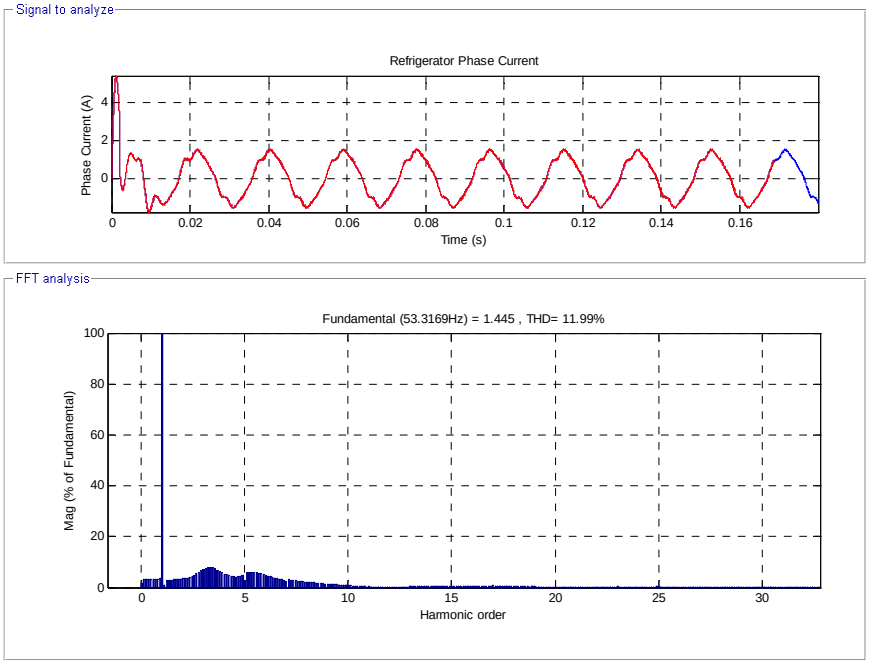

Figure 93. Harmonic Analysis for Refrigerator Motor Current, Case II.

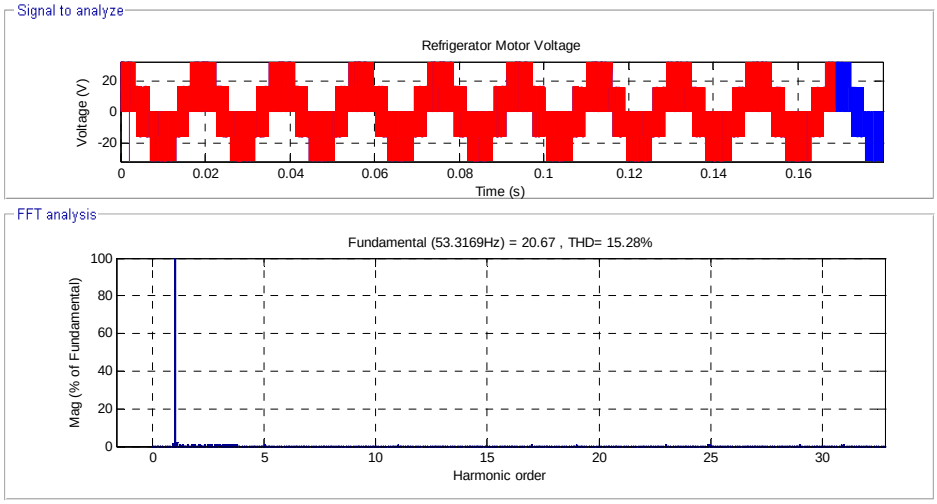

Figure 94. Harmonic Analysis for Refrigerator Motor Voltage, Case II.

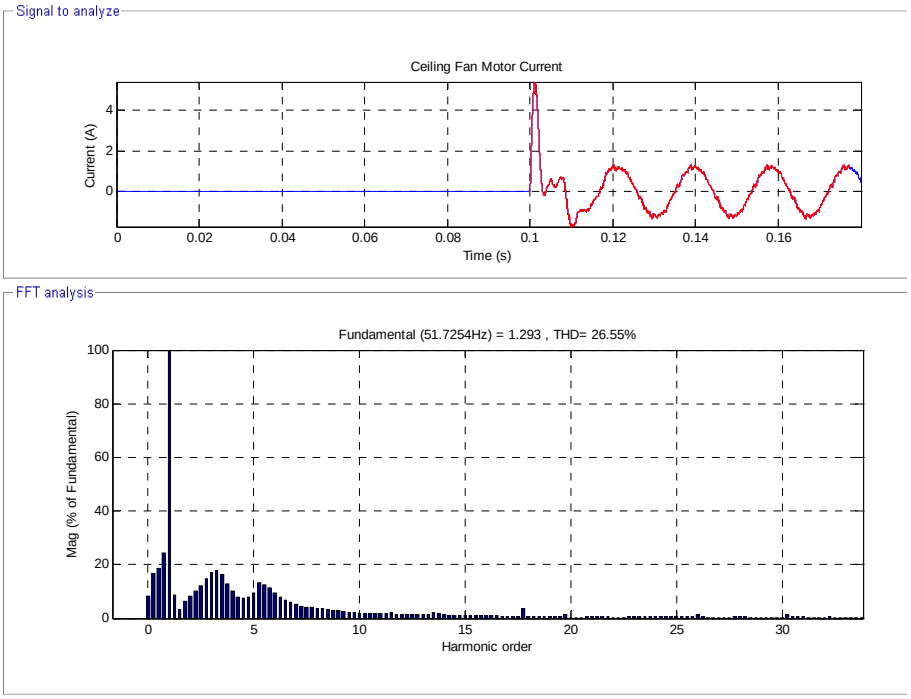

Figure 95. Harmonic Analysis for Ceiling Fan Motor Current, Case II.

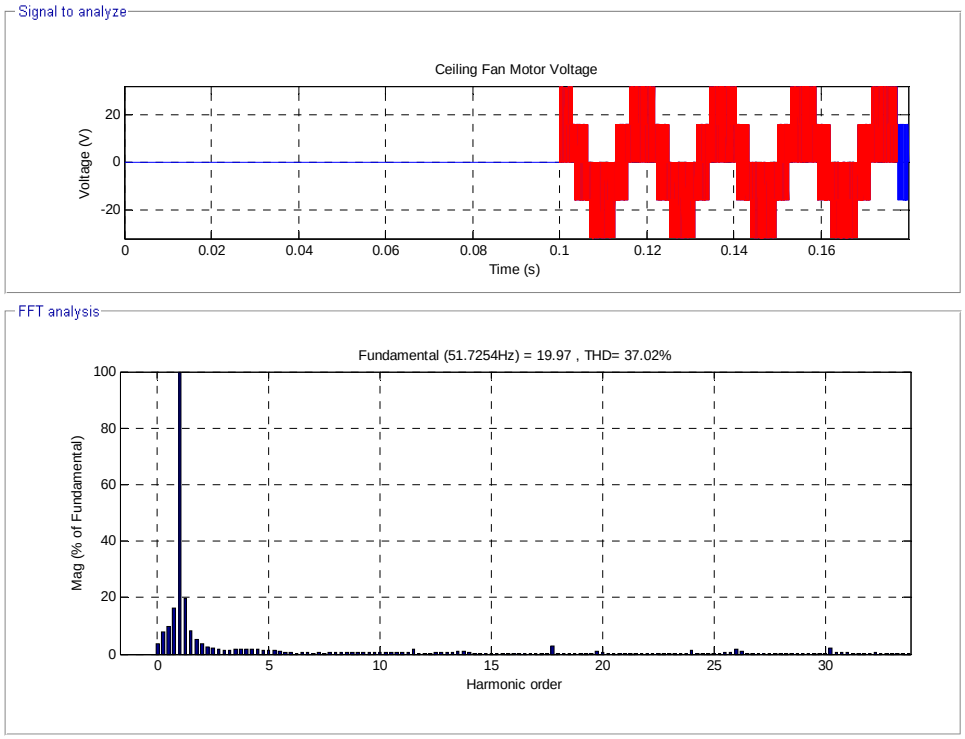

Figure 96. Harmonic Analysis for Ceiling Fan Motor Voltage, Case II.

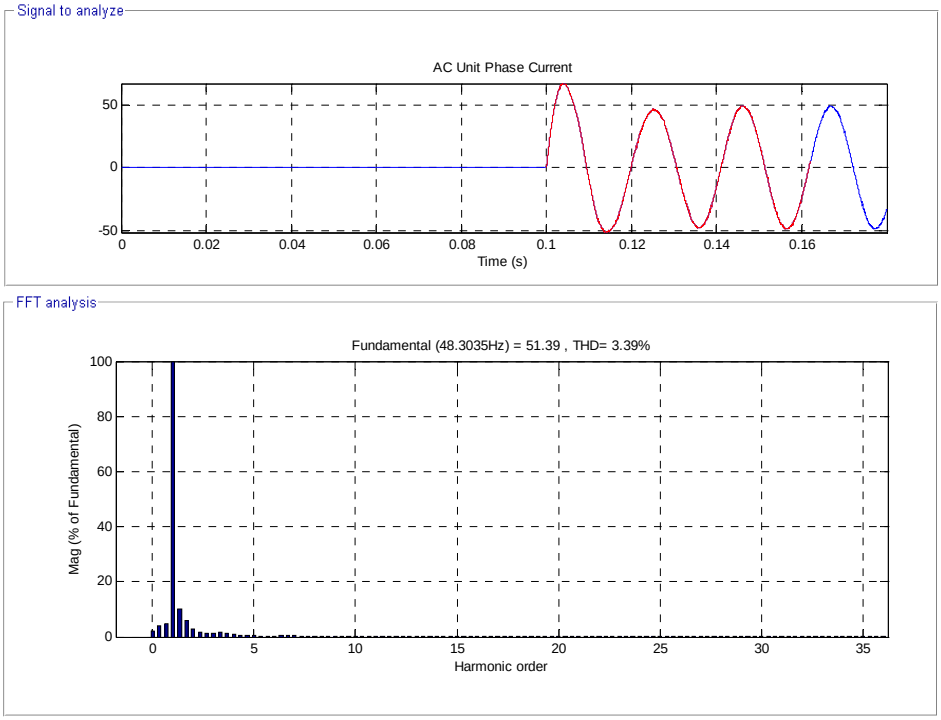

Figure 97. Harmonic Analysis for AC Unit Motor Current, Case II.

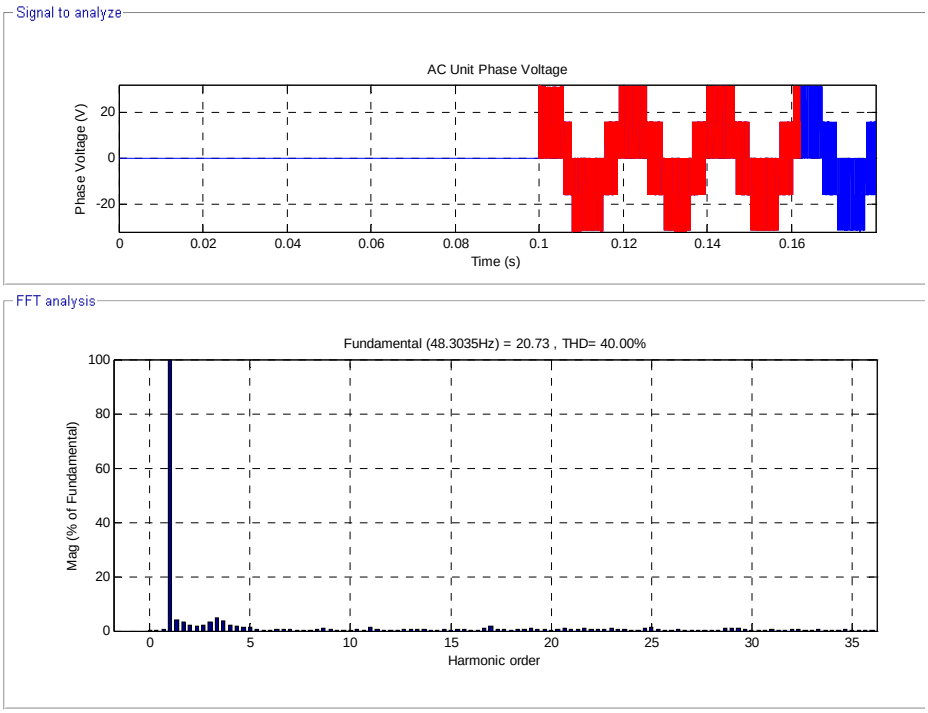

Figure 98 Harmonic Analysis for AC Unit Motor Voltage, Case II.

CASE III Simulations (Transient):

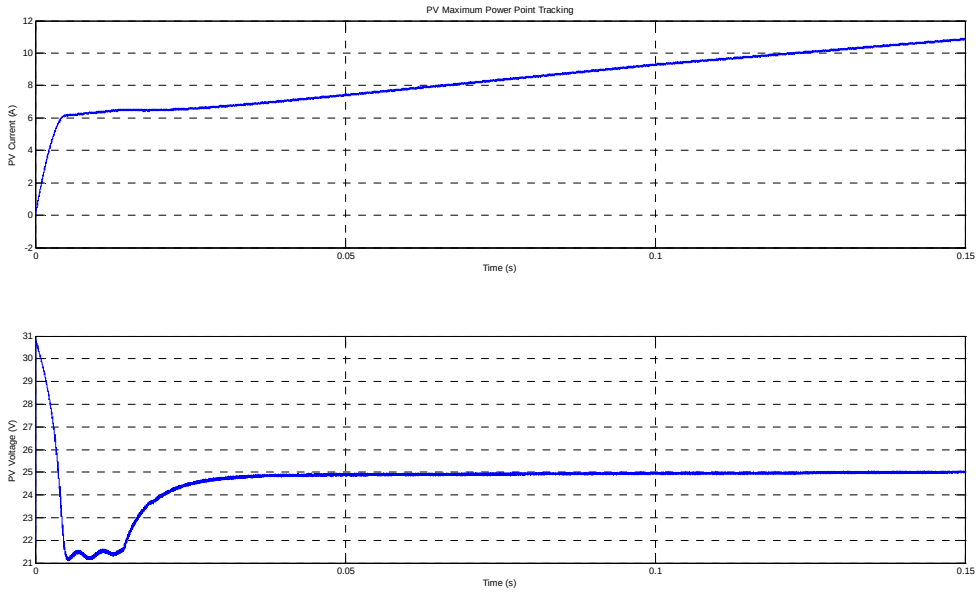

Figure 99. MPPT for Case III.

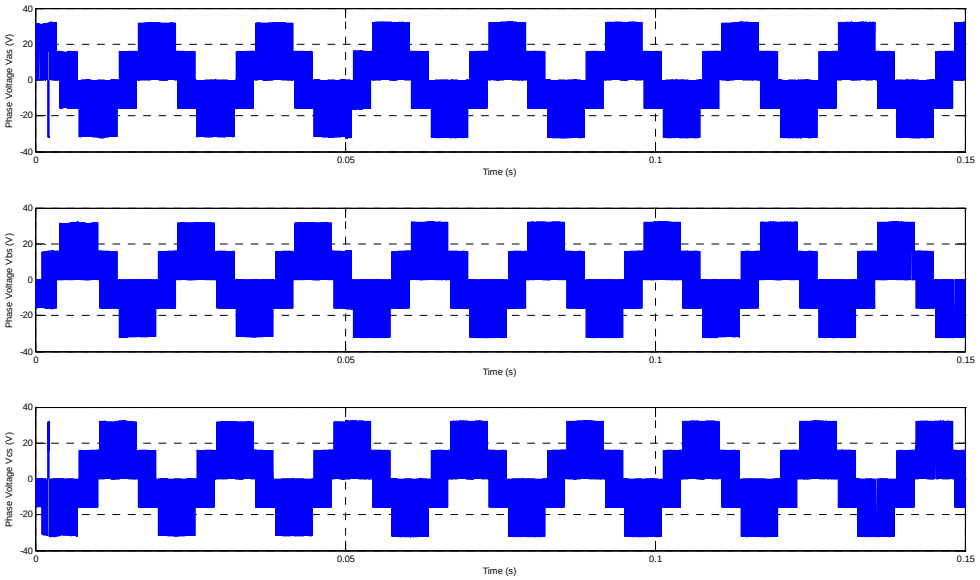

Figure 100. Refrigerator Motor Phase Voltages, Case III.

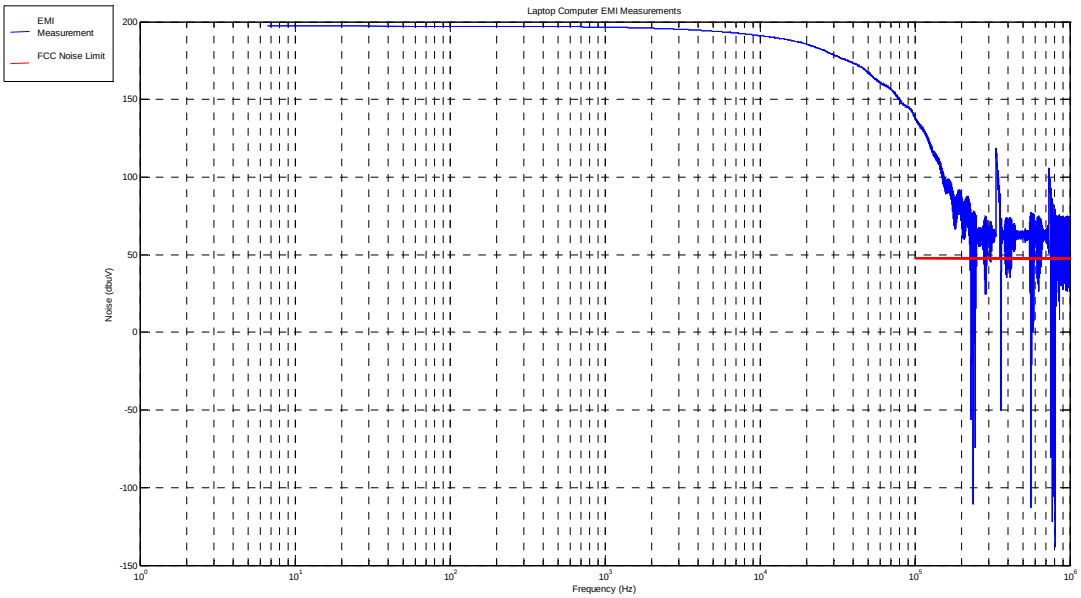

Figure 101. Laptop Computer EMI measurement.

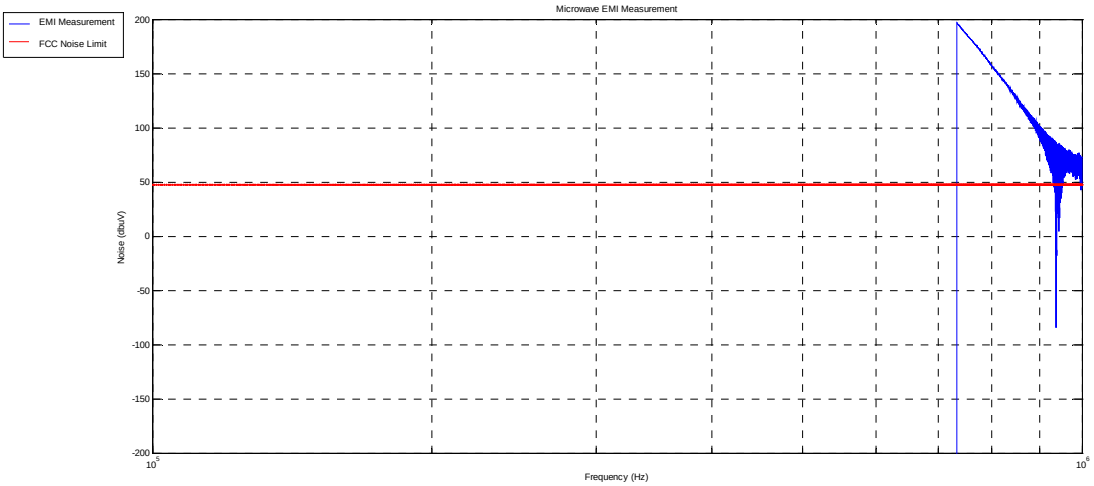

Figure 102. Microwave EMI measurement.

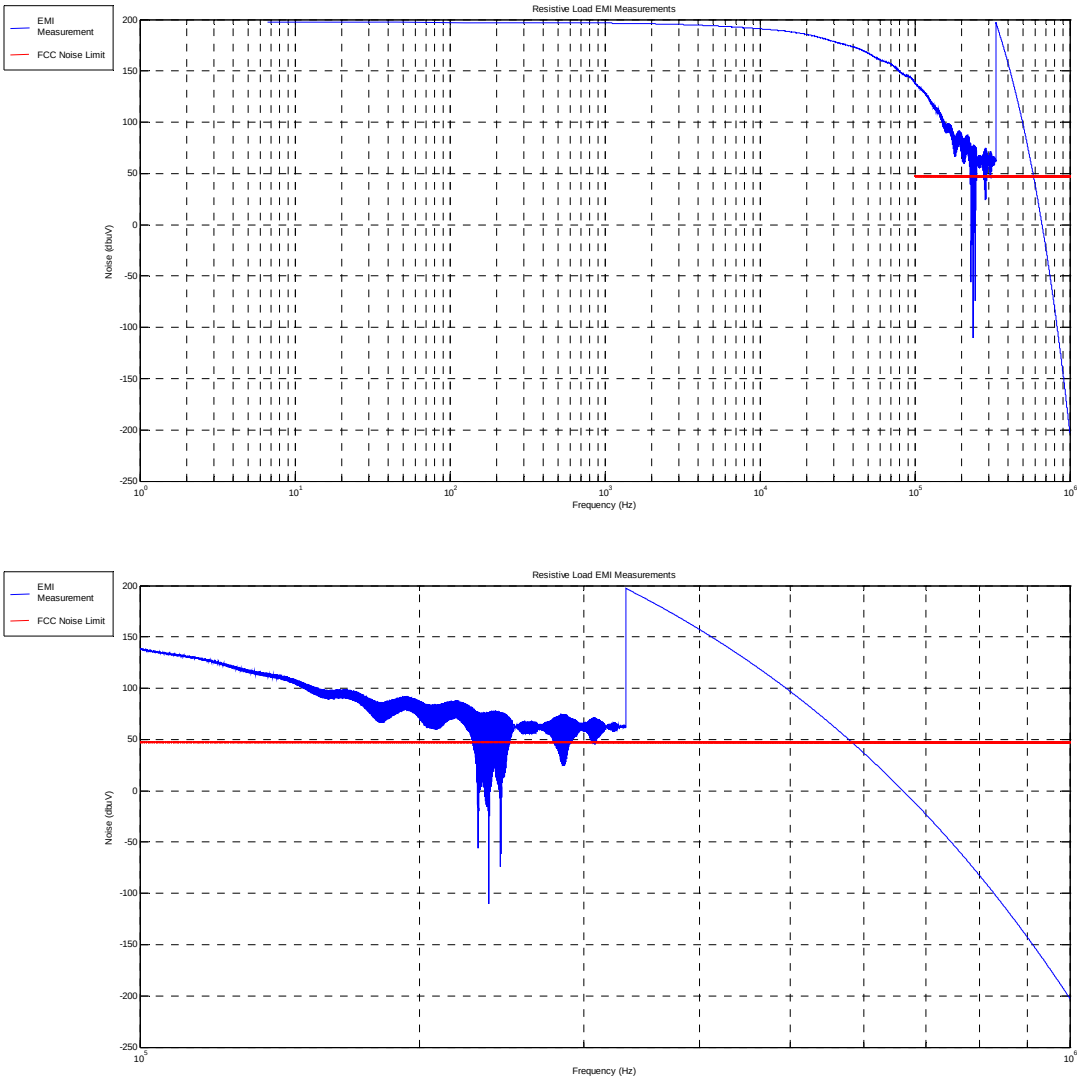

Figure 103. Resistive Load EMI measurement.

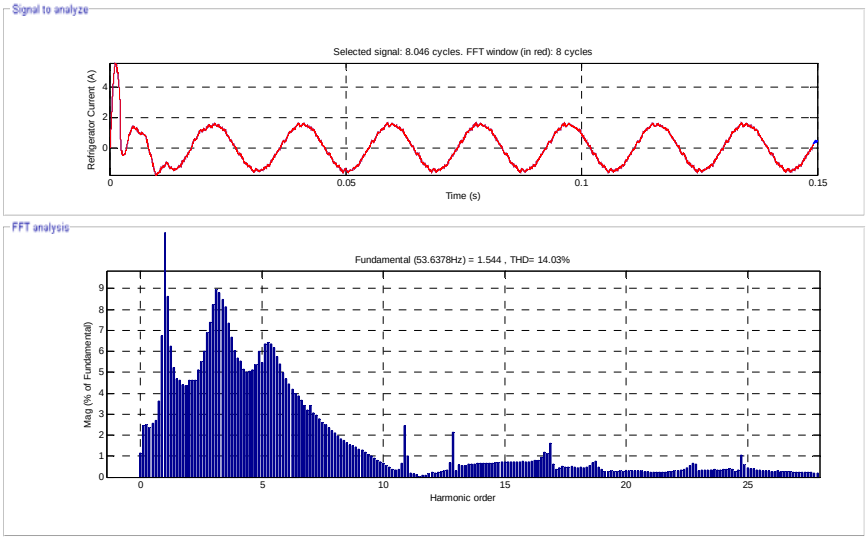

Figure 104. Refrigerator Current Harmonic Analysis.

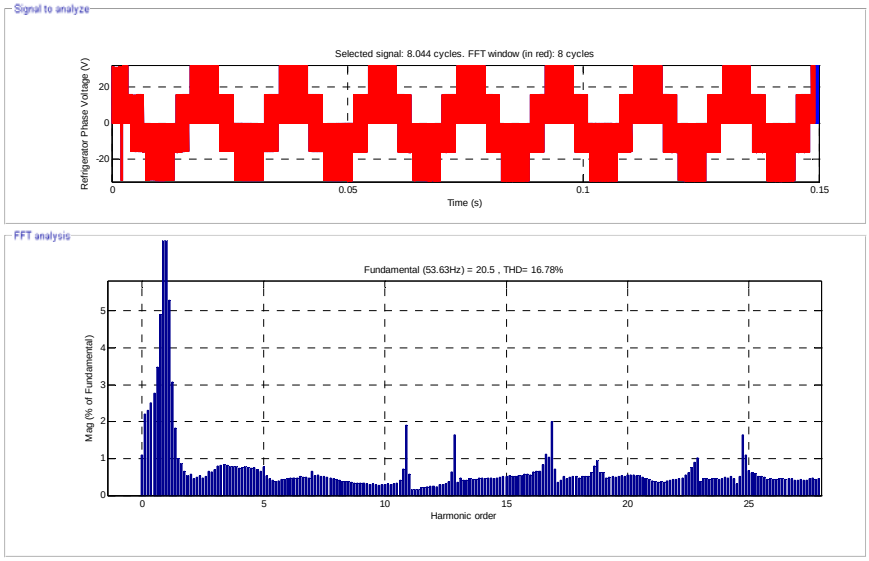

Figure 105. Refrigerator Voltage Harmonic Analysis.

Case III (Steady State):

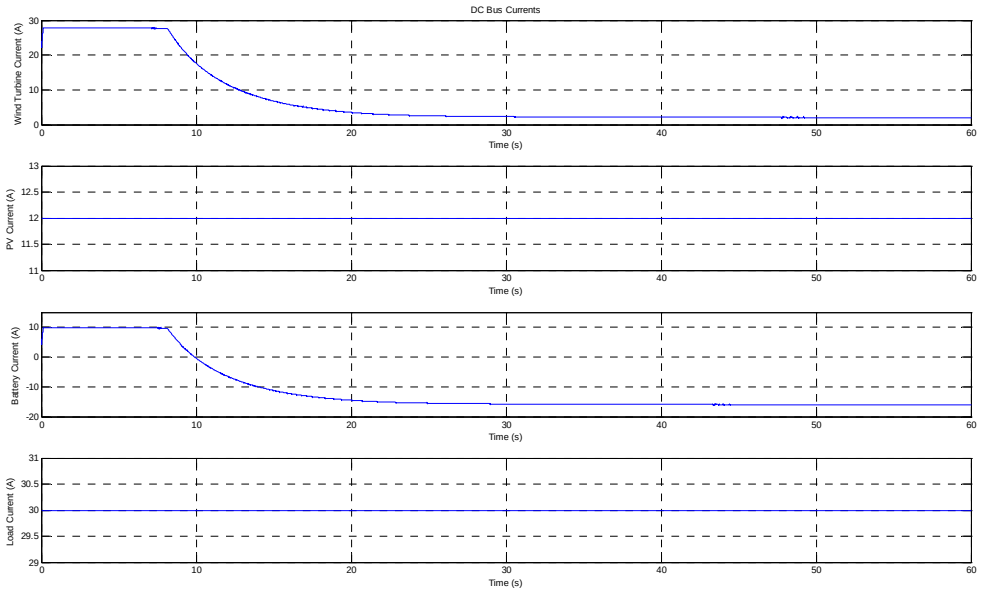

Figure 106. DC Bus Currents, for Case III in Steady State.

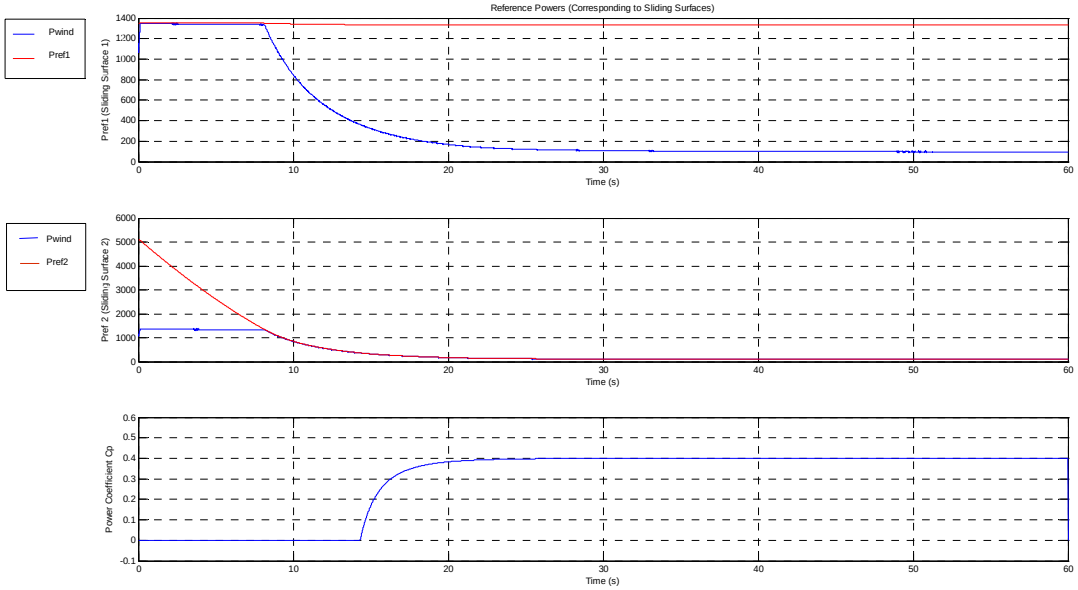

Figure 107. Power References and Power Coefficient for the WECS, Case III.

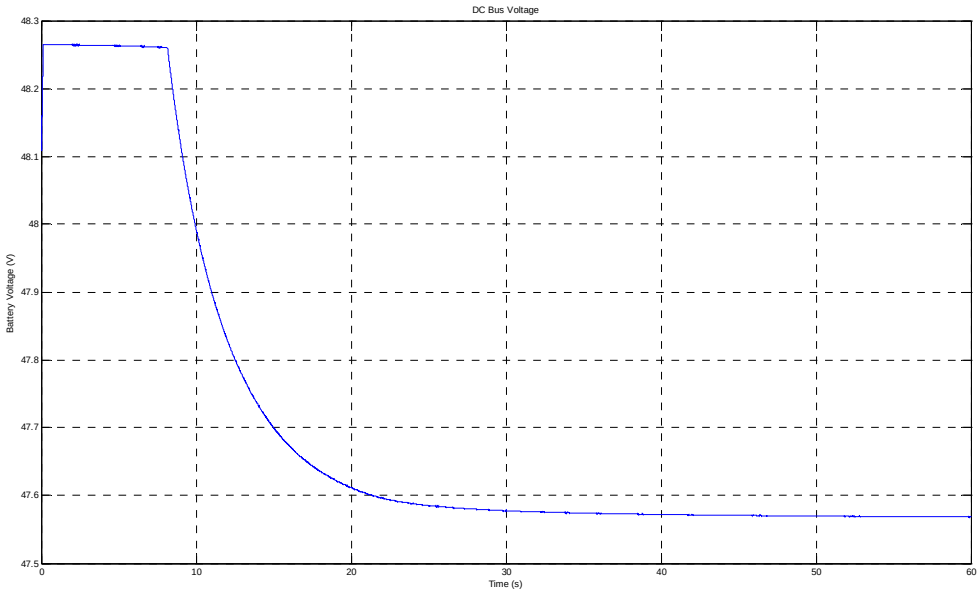

Figure 108. Battery Voltage for Case III, Steady State.